DESIGN AND ANALYSIS OF HIGH-EFFICIENCY L-BAND POWER AMPLIFIERS

Thesis by

Feiyu Wang

In Partial Fulfillment of the Requirements for the

Degree of

Doctor of Philosophy

CALIFORNIA INSTITUTE OF TECHNOLOGY

Pasadena, California

2006

(Defended December 19, 2005)

ACKNOWLEDGEMENTS

First of all, I would like to acknowledge the guidance, support and patience from my advisor Prof. David Rutledge. His knowledge and wisdom have guided me in my research; his continuous support and encouragement have helped me through many challenging situations. I appreciate this wonderful opportunity to study and work in the MMIC group at Caltech.

I would also like to thank Dr. Sander Weinreb for helpful advice during the past four years. I have learned many different aspects of microwave and millimeter-wave engineering from him. I am equally grateful for Prof. Almudena Suarez's guidance in the study of the stability analysis. It would not be possible to tackle such a difficult topic without her advice and energy.

Special appreciation goes to Dale Yee, "my advisor of everything else." With her kind advice, I saved much time in everyday life, so I can focus my attention on research.

It was a great pleasure to work with the following individuals from the Jet Propulsion Laboratory (JPL), Pasadena, CA: Wendy Edelstein, Dr. Alina Moussessian, and Constantine Andricos. Their support and encouragement are appreciated.

Sanggeon Jeon deserves special acknowledgement for numerous helpful conversations and discussions during the past three years. He has been a wonderful friend, colleague, and teacher.

I would like to thank Kent Potter and some former students in the group: Dr. Ichiro Aoki, Dr. Lawrence Cheung, Dr. Scott Kee, Dr. Dai Lu, and Dr. Matthew Morgan. I appreciate the time and patience they have spent to teach me many different aspects of microwave and power amplifier designs.

I would also like to thank the following individuals for helpful discussions: Joe Bardin, Patrick Cesorano, Dr. Younkyu Chung, Glenn Jones, Prof. Bumman Kim, Dr. Seungwoo

Kim, Sébestien Lasfargues, Min Park, Ann Shen, Edwin Soedarmadji, Yulung Tang, Takahiro Taniguchi, and Nikalas Wadefalk.

I would like to thank Prof. Ali Hajimiri and former and current students in his group for helpful discussions. They are Dr. Xiang Guan, Dr. Roberto Aparicio, Prof. Hui Wu, Dr. Chris White, Dr. Behnam Analui, Prof. Donhee Ham, Prof. Hossein Hashemi, Ehsan Afshari, Arun Natarajan, and Abbas Komijani.

I would like to acknowledge the members of the candidacy exam committee: Prof. John Doyle, Dr. Alina Moussessian, Prof. David Rutledge, Prof. Kerry Vahala, and Prof. Changhuei Yang. I am equally grateful to the members of the thesis defense exam committee: Prof. William Bridges, Dr. Alina Moussessian, Prof. David Rutledge, Prof. Kerry Vahala, and Dr. Sander Weinreb.

I would like to thank Carol Sosnowski, Linda Dosza, Heather Hein, Patama Taweesup, and Lyn Hein, and other staff members in the Department of Electrical Engineering, for their contribution has made my work much easier.

I want to thank the Caltech institution for providing me with an opportunity to pursue my M.S. and Ph.D. degrees. I want to acknowledge the financial support from Caltech, Lee Center, and JPL.

To my parents, who have shown great love and continuous support in every step of my life, I appreciate everything they have done for me.

To Ms. Margaret Wong, my advisor at Breck School, Minneapolis, MN, I would never have come to this stage of academic career without her generous help. To my undergraduate research advisor, Prof. William Jemison, I would like to thank him for introducing me to the world of microwave engineering.

Most of all, I would like to thank my wife, Jia Fan. Beyond a supporter, she is a comrade, who continuously fights alongside with me. Her love, effort, and sacrifices are most deeply appreciated.

ABSTRACT

Discrete solid-state high-power amplifiers are among the important circuit components in today's wireless communications and remote-sensing applications. As the device technologies continue to improve, there are new opportunities and new challenges presented to power amplifier designers. This thesis presents novel techniques in the design and the analysis of L-band high-efficiency power amplifiers, which may be used in many communications and radar applications.

In this work, high-efficiency power amplifier topologies are discussed and implemented. The goal is to push the boundary of output power, operating frequency, efficiency and bandwidth. Also, the design of a key passive component, a balanced-to-unbalanced transformer (balun) is discussed in detail. Some new designs of the baluns are shown, and the results show advantages of these baluns over some of the traditional work at L-band.

The stability analysis of power amplifiers is one of the most critical and the most challenging aspects of power amplifier design. This work shows an analysis technique, which accurately predicts the oscillations in power amplifiers. Using the technique, different stabilization techniques and circuits are designed and implemented.

TABLE OF CONTENTS

LIST OF FIGURES

Chapter 4.

Chapter 5.

Chapter 6.

LIST OF TABLES

Chapter 1

Applications of High-Efficiency L-Band Amplifiers

The growth in wireless communications and radar applications has put greater demand on the performance of power amplifiers (PAs). In the recent years, lower microwave frequency, from 800 MHz to 2.5 GHz, has dominated the commercial wireless market. Figure 1.1 shows only some of the main applications in this frequency band. The rapid growth in device technologies and processing technologies presents new opportunities to power amplifier designers. In today's technology, a commercially available package of a push-pull pair of two transistors can output over 200 W at 2 GHz for base station applications [1][2][3]. Newer applications, such as WiMax, are also emerging and high power amplifiers are needed in the hundred watt level beyond 2.5 GHz. This opens up possibilities to achieve wireless communications for longer range and for better quality.

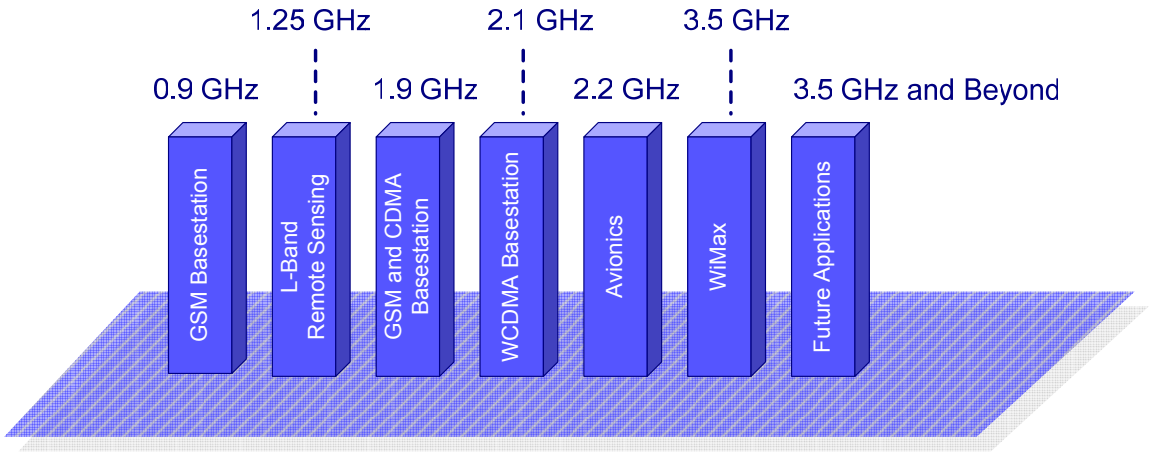

Figure 1.1. Applications of power amplifiers in low microwave frequency.

As the technology pushes for higher output power at higher operating frequency, there are also many challenges presented to PA designers. One of the fundamental problems in today's wireless technologies is the limitation of energy resource. For cellular handsets, we

want to have high efficiency to conserve battery energy. In satellite applications, high-efficiency transmitters reduce high energy cost. On laptop computers, high-efficiency transmitters can save energy while using wireless internet. In these wireless transceivers, power amplifiers are the most power-consuming components. The efficiency of the power amplifier directly determines the energy consumption of the transceiver.

Furthermore, in high power amplifiers, heat dissipation has become a limiting factor when devices are operating in higher and higher power. Properly designed high-efficiency amplifiers reduce heat dissipation, thereby improving the reliability of amplifiers and reducing the need for bulky and heavy heat sinks.

We will discuss the applications of high-efficiency high-power amplifiers in two areas: cellular base station and remote-sensing radar. Since the amplifiers discussed in the dissertation are used for remote-sensing applications, the emphasis will be on L-band radar applications.

1.1 Cellular Applications

There is no need to emphasize the importance of cellular phones in everyday life today. The cellular phone market has grown tremendously over the past decade. Cellular applications typically cover several low microwave frequency bands, including 800 MHz, 900 MHz, 1800 MHz, 1900 MHz, and 2100 MHz. The handset PAs typically have maximum output power ranges from one watt to a few watts. Most of the handset PAs are built on chip as integrated circuits with a few off-chip components. There are even PAs fully integrated on chip [4][5]. These amplifiers, due to their different power level, different processing technology and different set of optimization parameters, are beyond the scope of this dissertation. The base station power amplifiers have output power of tens or hundreds of watts, and in today's technology, they have to be implemented with discrete or hybrid technologies.

For wireless communication applications, the most important requirement is linearity. This requirement puts constraints on the design of power amplifiers. Most base station amplifiers are operated in linear or weakly nonlinear mode. The efficiency of these

amplifiers is low compared to an amplifier driven well into saturation. However, in the recent years, envelope tracking, Doherty, and several digital pre-distortion methods have shown promises to use strongly nonlinear amplifiers to be used in linear wireless applications such as EDGE and WCDMA.

1.2 Radar Applications

Radar remote sensing plays an important role in deriving unique measurements that address fundamental questions in the National Aeronautic and Space Administration (NASA) Earth Science Enterprise (ESE) strategic plan. Synthetic aperture radar (SAR) can provide measurements key to the water cycle (e.g. soil moisture and water level), global ecosystem (biomass estimation, land cover change), and ocean circulation and ice mass (ice motion). L-band radar provides the ability to make these measurements under a variety of topographic and land cover conditions, day or night, with wide coverage at fine resolution and with minimal temporal decorrelation [6][7].

L-band repeat-pass interferometric SAR (InSAR) techniques can provide very accurate and systematic measurements of surface deformation and surface strain accumulation due to seismic and volcanic activity. The dynamics of the solid Earth motion are complex and there are vigorous efforts to model, understand and eventually predict earthquakes using InSAR data. L-band InSAR is also useful for natural hazard monitoring, assessment and disaster response.

L-band SAR technologies developed for NASA also have national security application. For example, these techniques could provide observations that are complementary to the traditional high-resolution imagery of the intelligence community. L-band SAR can provide information on vehicle and troop movements, and building damage. Significant contributions are also possible in providing detailed surface characteristics, such as the measurement of surface soil moisture and sub-pixel roughness for trafficability, which could have dual-use science and military application. Furthermore, L-band radar technologies could also have application to future DoD space-based radar (SBR) for airborne moving target indication (AMTI) and ground moving target indication (GMTI).

1.3 Organization of Thesis

This thesis focuses on the design and implementation of L-band compact, high-efficiency power amplifiers. These amplifiers are used in the L-band radar T/R modules described above. The chapters are organized as followings:

Chapter 2 reviews some of the most typical classes of power amplifiers. The use of these classes in high-power and high-efficiency application at UHF and low microwave frequency bands are discussed. The chapter focuses on the techniques and circuit topologies that improve the efficiency of power amplifiers. The implementations of these techniques in L-band are presented.

Chapter 3 discusses a key component of the amplifier: balanced-to-unbalanced transformers or baluns. Different balun topologies are presented from HF, VHF and UHF frequencies to microwave frequencies. A novel balun is presented, and the balun has good performance along with important features such as impedance-transformation and harmonic tuning.

Chapter 4 presents the simulated and measured results of several different versions of amplifiers. The chapter demonstrates the improvements in iterations of amplifiers. The final results are compared with the state-of-the-art amplifiers.

Chapter 5 discusses one of the important aspects of power amplifier design: stability analysis. The chapter describes the limitations of the current stability analysis techniques. It introduces a series of techniques based on the nonlinear bifurcation analysis. The analysis includes oscillation detection and pole-zero analysis. Conversion matrix technique and auxiliary generator technique are also presented. Several different stabilization techniques are discussed and compared. The power amplifier is stabilized, and the performance is shown.

Chapter 6 leads to the future work of L-band power amplifier design. In particular, current and new transistor technologies are reviewed. SiC and GaN devices are introduced. Preliminary results using SiC transistors are presented. In order to properly use the newer

device technologies, improvement in the area of device modeling has to be made. There are discussions on the limitations of the current modeling approaches and newer approaches in modeling active devices. Finally, the chapter discusses the possible implementation of discrete Distributed Active Transformer in L-band to improve the output power.

This dissertation is based on the following published work:

Feiyu Wang, Almudena Suarez, David B. Rutledge, "Bifurcation analysis of stabilization circuits in an L-band LDMOS 60-W power amplifier," *IEEE Microwave Wireless Compon. Lett.*, vol. 15, no. 10, pp. 712–714, Oct., 2005.

Feiyu Wang and David B. Rutledge, "A 60-W L-Band Class-E/$F_{odd,2}$ LDMOS power amplifier using compact multilayered baluns," *IEEE Topical Workshop on Power Amplifiers for Wireless Comm. Tech. Dig.*, Sep. 2004.

Wendy N. Edelstein, Constantine Andricos, **Feiyu Wang**, David B. Rutledge, "High-efficiency L-band T/R module: development results," *NASA 2005 Earth-Sun Syst. Tech. Conf.*, Adelphi, Maryland.

Wendy N. Edelstein, Constantine Andricos, Soren Madson, **Feiyu Wang**, David B. Rutledge, "Current status of the high-efficiency L-band transmit/receive module Development for SAR Systems," *NASA 2003 Earth-Sun Syst. Tech. Conf.*, Adelphi, Maryland.

Wendy N. Edelstein, Constantine Andricos, Alina Moussessian, **Feiyu Wang**, David B. Rutledge. "High-efficiency L-band transmit/receive module for synthetic aperture radar." *Proc. 2003 IEEE Radar Conf.*, pp. 238–243, May, 2003.

Chapter 2

High-Efficiency Design Techniques

Power amplifiers are widely used in wireless communication applications and radar applications. Due to the variety of applications, there is a great variety of requirements for power amplifiers. Some of the most basic requirements in power amplifier design include *frequency of operation*, *output power level*, *bandwidth*, *efficiency*, *gain*, *linearity*, *size*, and *cost*. It is almost never possible to simultaneously maximize all design criteria at the same time. Thereby tradeoffs must be made, and only a subset of the requirements can be satisfied. Some of the classic tradeoffs include: gain vs. bandwidth, operating frequency vs. output power, and linearity vs. efficiency.

A typical attempt to optimize a subset of design criteria is the introduction of different classes of power amplifiers. It is worth noting that there are a lot of confusion and debates over the classification of power amplifiers. Some classes overlap others; some classes can be thought of as a limiting case of other amplifiers. Nevertheless, the current classification gives a good starting point for basic understanding of these amplifiers.

As knowledge of power amplifiers accumulates, many different classes of power amplifiers have evolved over the years. Generally speaking, power amplifiers are divided into two types: transconductance amplifiers and switching-mode amplifiers. Conventional transconductance amplifiers include Class-A, Class-AB, Class-B, and Class-C amplifiers. Conventional switching-mode amplifiers include Class-D, Class-E, and Class-F amplifiers. Each of the power amplifier classes optimizes a certain subset of design criteria. While some classes of amplifiers have advantages over other classes, they also have disadvantages. Several classes of amplifiers attempt to combine advantages of two different classes. These classes are typically denoted as “Class-XY” amplifiers. Some examples of these intermediate classes of amplifiers include: Class-BD [8], Class-CE [9], and Class-DE [10]. Another class of amplifiers combines the advantages of Class-E and Class-F^{-1}

amplifiers, and it is called the Class-E/F amplifiers. This particular class was invented by Scott Kee at Caltech [11].

The classic tradeoff between the transconductance amplifiers and switching-mode amplifiers are linearity and efficiency. While Class-A amplifiers are the most linear power amplifiers, they can achieve a maximum efficiency of 50%. Switching-mode amplifiers can achieve an ideal efficiency of 100%, but they are strongly nonlinear amplifiers. Class-AB, Class-B, and Class-C amplifiers are compromises in between as shown in Figure 2.1.

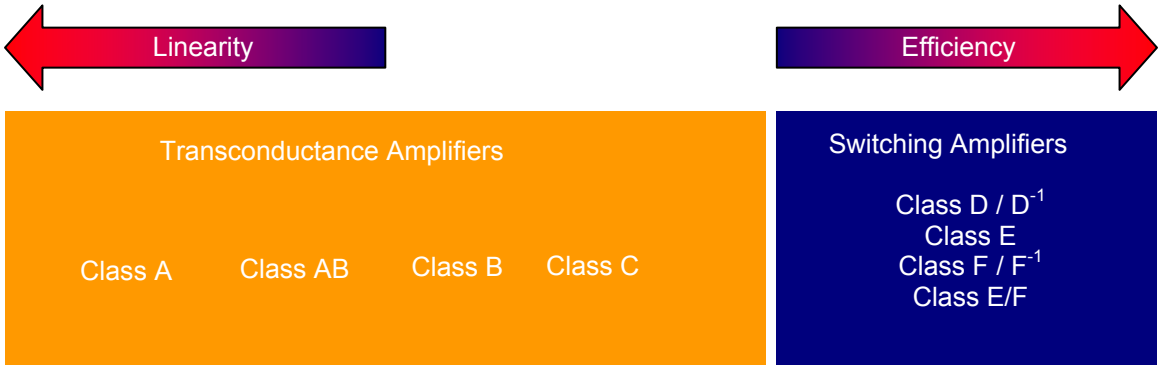

Figure 2.1. The linearity-efficiency tradeoff between transconductance amplifiers and switching-mode amplifiers.

The problem is that many applications require that high linearity and high efficiency be achieved at the same time. Naturally, some PA designers choose to start from the left side of Figure 2.1 and use a Class-A or a Class-AB amplifier as the starting point, and then try to find a solution to improve efficiency without compromising the linearity. Some other PA designers choose to start from a switching-mode topology of the amplifier with high efficiency, and then investigate complicated linearization techniques. These techniques include Envelope Elimination and Restoration (EER) technique [12][13][14][15], Doherty [16][17], Chireix [18][19][20] and even digital pre- or post-distortion techniques [21][22][23]. These techniques are beyond the scope of the thesis. Since the power amplifiers described in the thesis will be used in applications where highly nonlinear effects can be tolerated, we will only focus on the techniques that improve the efficiency of the amplifiers.

Two of the most noteworthy schools of high-efficiency PA design are: (1) voltage and current waveform shaping using time-domain techniques, as in Class-E amplifiers; (2) voltage and current waveform shaping using frequency-domain or harmonic-tuning techniques as in Class-F amplifiers. It is important to look beyond the class nomenclature, and often it is easier to understand the newer techniques based on these two theories. In this chapter, several typical classes of power amplifiers are reviewed. Discussions emphasize on high-efficiency design techniques used in switching-mode amplifiers. In this thesis, only common-source or common-emitter configurations are considered.

2.1 Transconductance Amplifiers

Transconductance power amplifiers are extensions from linear transconductance amplifiers. These amplifiers use active transistors as controlled current sources. Class-A, Class-AB, Class-B, and Class-C amplifiers are conventional transconductance amplifiers. They are widely used in today's wireless transmitters, and they have been discussed in detail in several books [24][25][26].

Figure 2.2 shows a simplest circuit diagram of Class-A, Class-AB, Class-B, Class-C amplifiers. The circuit is single ended, and we assume that the RF choke, DC-coupling capacitor and the filter are all ideal.

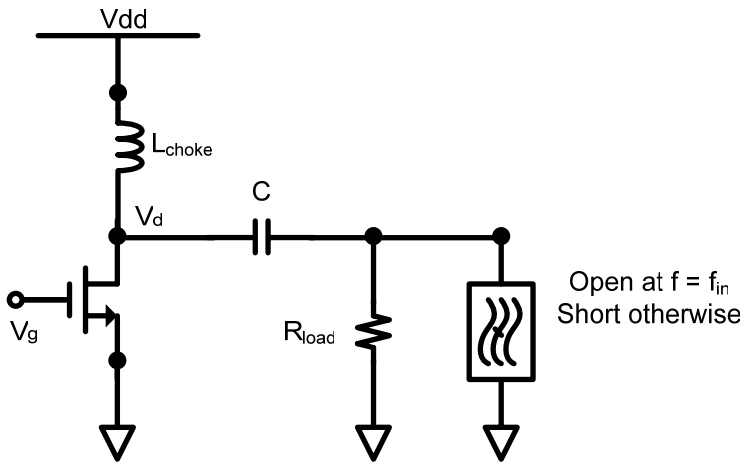

Figure 2.2. Simple circuit diagram of Class-A, Class-AB, Class-B, and Class-C amplifiers.

2.1.1 Class-A Amplifiers

The most simplistic way to distinguish these classical transconductance amplifiers is the conduction angle. Class-A amplifiers have a conduction angle of $\theta_C = 2\pi$; Class-AB amplifiers have a conduction angle of $\pi < \theta_C < 2\pi$; Class-B amplifiers have a conduction angle of π ; Class-C amplifiers have a conduction angle of $0 < \theta_C < \pi$. Figure 2.3 shows the voltage and waveforms of a Class-A amplifier. The Class-A amplifier is the most linear and the most "well-behaved" amplifier.

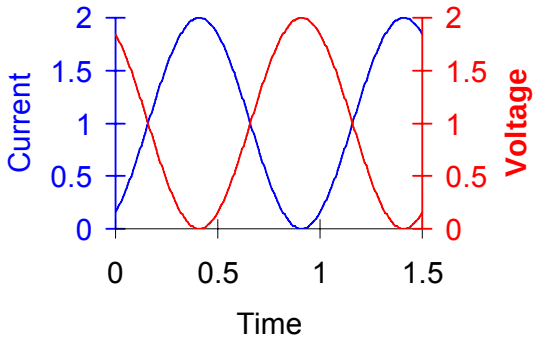

Figure 2.3. Class-A voltage and current waveforms.

However, the biggest drawback of the Class-A amplifier is the ideal maximum efficiency of 50%. This efficiency number, in practice, is reduced significantly to about 35% for L-band applications. Let us take 33% drain efficiency as an example. If the output power of the amplifier is 100 W, the total power consumption of the power amplifier is 300 W, and 200 W is dissipated power. This number is usually well beyond the heat-handling capability of a common-source transistor package. This is the reason why Class-A amplifiers are not suitable for L-band high-power amplifiers.

In today's technology, the use of Class-A amplifiers is only popular at high microwave frequency beyond 5 GHz up to millimeter-wave territory. The advantage of the Class-A amplifier at higher frequency range is that it requires considerably less drive power and has higher gain than other classes of power amplifiers. Since at higher frequency, the power gain is usually the limiting factor in PA design, Class-A is much more suitable.

2.1.2 Class-AB, Class-B, and Class-C Amplifiers

The voltage and the current waveforms of a Class-AB amplifier are shown in Figure 2.4. Since the gate bias level is reduced from Class-A amplifier, the current clipping occurs. Although current clipping generates harmonics and nonlinear effects, Class-AB amplifiers are popular candidates for L-band power amplifiers. Higher efficiency than Class-A amplifiers can be obtained without much compromise in the power gain and the linearity. Many PA designers use Class-AB amplifiers as a starting point, and apply harmonic control techniques to improve efficiency. These techniques are discussed in the later part of the chapter.

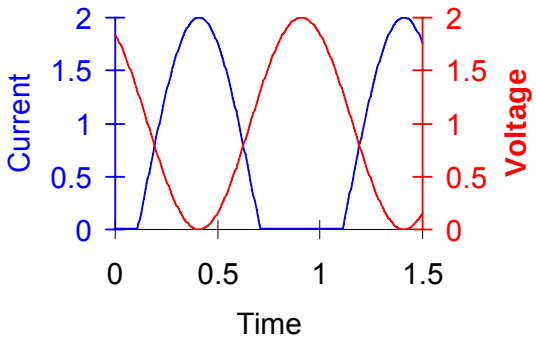

Figure 2.4. Class-AB voltage and current waveforms.

We can look at a Class-B amplifier as a transition between a Class-AB and a Class-C amplifier. The ideal maximum drain efficiency of a Class-B amplifier is 78.5%, which is significantly higher than the Class-A amplifier. Practically, an L-band high-power Class-B amplifier can achieve a drain efficiency of 60%. If we take the same case as before, we see that for an output power of 100W, a practical Class-B amplifier only dissipates about 60W of power. We can easily see that is a great reduction from 200W in the Class-A case.

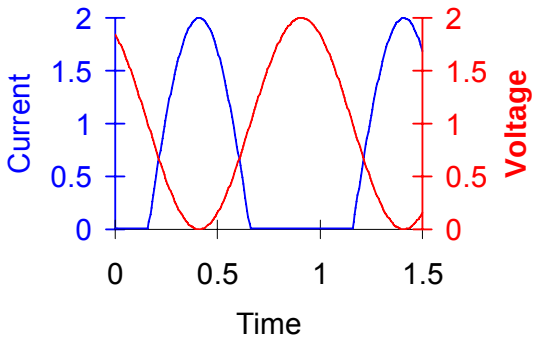

Figure 2.5. Class-B voltage and current waveforms.

Class-C amplifiers are high-efficiency amplifiers, with an ideal efficiency of 100%. However, there are several problems for an L-band Class-C implementation. The first drawback of this amplifier is the efficiency comes at the expense of the power gain. In fact, in the classic definition of Class-C amplifier, the output power approaches to zero, as the efficiency approaches to 100%. At microwave frequency, this approach is typically not desired, since high power gain is difficult to obtain. The second drawback is that the amplifier is highly nonlinear, so it can be used only in applications that can tolerate a high degree of nonlinearity, or it has to be used with linearization techniques.

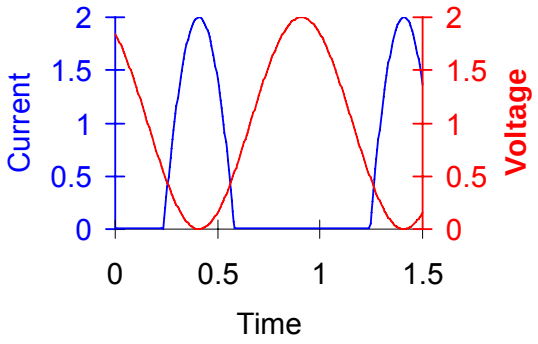

Figure 2.6. Class-C voltage and current waveforms.

2.2 Switching Amplifiers

Switching-mode power amplifiers use active transistors as switches. That is, the active device is ideally fully on (short-circuit) or fully off (open-circuit). These circuits are commonly found in switching power supplies, but only recently have they been exploited

as RF amplifiers due to the availability of transistors with substantial gain and power at microwave frequencies. The theoretical efficiency for Class-E and Class-E/F amplifiers is 100%; practical efficiencies of 70-90% have been demonstrated at VHF and UHF frequencies [27][28][29].

In ideal switching-mode amplifiers, the transition between the on-state and the off-state can be achieved instantaneously. The switching-mode amplifiers differ from the traditional classes of amplifiers, which use the active devices as controlled current sources. Since ideally the device is either fully on or fully off, the voltage and the current will never be nonzero simultaneously as shown in Figure 2.7. Therefore, ideally no power is dissipated, and the efficiency is 100%. This theoretical number is significantly higher than the traditional Class-A and Class-AB amplifiers. To optimize the efficiency, we need to reduce the overlap between the voltage and the current. In fact, we see that from the transconductance amplifiers already. If we compare the voltage and the current waveforms from the four different transconductance classes discussed in the previous section, we see that in Class-A amplifier, the current and the voltage are both non-zero at all time, and the Class-A amplifier has the lowest efficiency; Class-C amplifier has the highest efficiency due to the least overlap between nonzero voltage and current region.

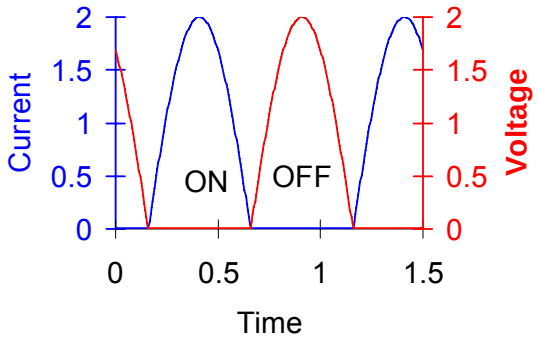

Figure 2.7. Sample voltage and current waveforms for an ideal switching-mode amplifier. Note that the current and the voltage do not overlap.

To see how to achieve no overlapping between the voltage and the current, we will start from one of the simpler approaches of switching-mode amplifiers: Class-D and Class-D^{-1} amplifiers.

2.2.1 Class-D and Class-D^{-1} Amplifiers

Class-D and Class-D^{-1} (also called inverse Class-D or current-mode Class-D) amplifiers use two active devices driven as switches at 180^{o} out of phase (in a push-pull configuration). The load circuit consists of a band-pass or a band-stop filter. Class-D amplifier's band-pass filter has a short circuit at the fundamental frequency and an open circuit at other frequencies. The voltage waveform is a square wave, while the current waveform is sinusoidal.

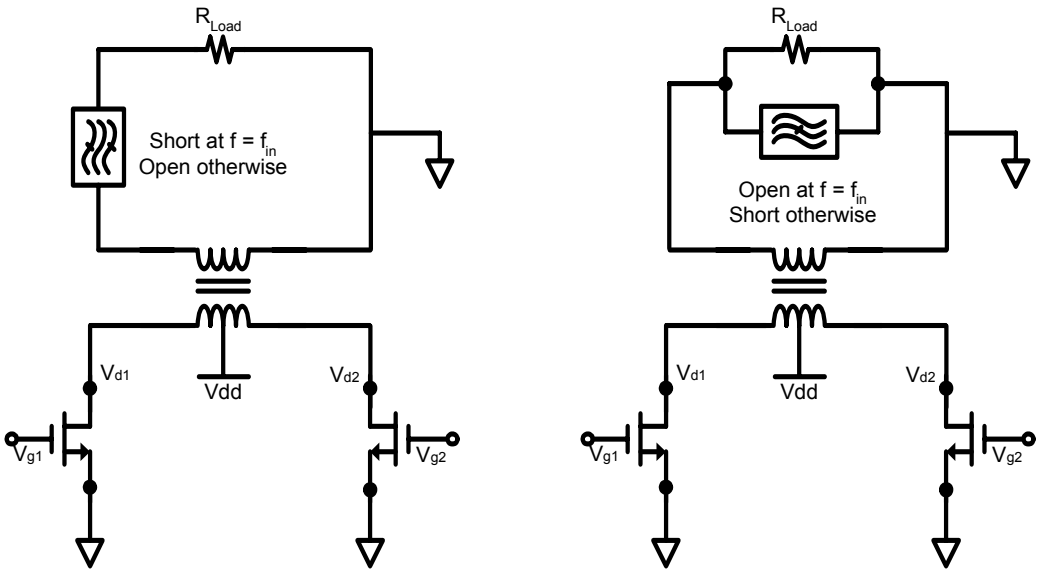

Figure 2.8. Schematics of Class-D (left) and Class-D^{-1} (right) amplifiers.

Class-D^{-1} amplifier's band-pass filter has an open circuit at the fundamental frequency and a short circuit at other frequencies. The current waveform is a square wave, and the voltage waveform is sinusoidal. The waveforms of Class-D and Class-D^{-1} are shown in Figure 2.9.

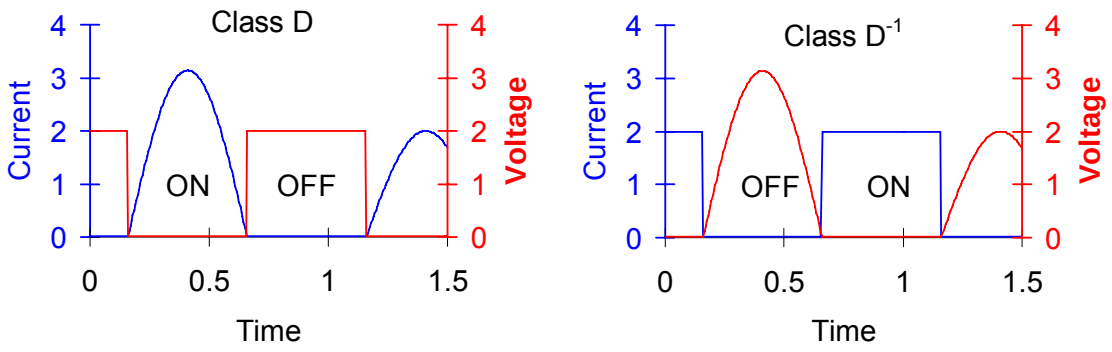

Figure 2.9. Voltage and current waveforms of Class-D and Class-D^{-1} amplifiers.

Under ideal conditions, Class-D and Class-D^{-1} can achieve 100% efficiency. However, one of the assumptions of Class-D and Class-D^{-1} amplifiers is that the transistors have zero output capacitance. In high-power amplifiers, the devices are typically large in size, and thereby having a large output capacitance. The susceptance of the output capacitance also increases with frequency, so at UHF and microwave frequencies, the effect by the output capacitance cannot be ignored. In Class-D configuration, the loss due to large output capacitance can be very large in microwave frequency, thereby the use of this type of power amplifiers are mostly limited to audio amplifiers.

In Class-D^{-1} amplifier, the effect of the output capacitance is not the same. If we look carefully at the schematic in Figure 2.8, we see that the output capacitances of the devices are in parallel with the parallel resonance circuit. If this capacitance is not too large, we can in fact use this capacitance as a part of the parallel resonance circuit. Therefore, we can still achieve ideal efficiency of 100%. This is commonly referred as the output capacitance is "absorbed" in the tuning circuit. We will discuss this point further in the later sections.

It is also assumed that in Class-D and Class-D^{-1} amplifiers, the transistors behave as switches, which can be toggled between ON state and OFF state instantaneously. This is certainly not the case in microwave transistors. Within the finite turn-on and turn-off time, the voltage and the current waveforms overlap, and increase the transistor loss. This drawback is addressed in the time-domain design and analysis in Class-E amplifiers.

2.2.2 Class-E Amplifiers

The Class-E amplifiers were invented by N. O. Sokal and A. D. Sokal [30][31]. The Class-E amplifier consists of a single-ended transistor as a switch with an output load circuit. The output load circuit has a series resonant circuit at the fundamental frequency along with load impedance which is tuned slightly inductive. This basic circuit is shown in Figure 2.10.

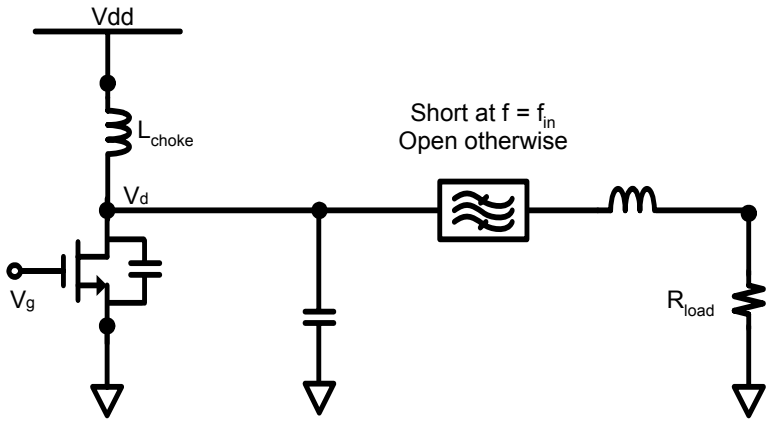

Figure 2.10. Circuit schematic of a Class-E amplifier.

The main advantages of Class-E amplifiers are: (1) "soft-switching" to reduce loss, (2) "absorption of output capacitor" in the output circuit, (3) relatively simple circuit compared to Class-F amplifier.

Since the switching time of the transistors is not instantaneous, a Class-D amplifier suffers power loss due to the voltage and the current are simultaneously nonzero. At microwave frequency, the switching time may be a significant fraction of the cycle, and the loss may be too great to tolerate. This adverse effect can be significantly reduced in Class-E tuning, when the inventors include an inductive load. From the time-domain waveform of the voltage, Class-E tuning reduces the slope of the voltage waveform before the switch turns on. This feature, sometimes referred to as soft-switching or zero-voltage-derivative-switching (ZdVS), minimizes the level of the voltage during the turn-on of the switch.

Another beauty of Class-E amplifier is the relatively simple circuit topology for an easy implementation. Also, unlike Class-D amplifiers, which assume a zero output capacitance

of the active device, Class-E amplifier design equations take into account the output capacitance.

The Class-E amplifier is not quite the perfect solution for high-efficiency PA. The amplifier suffers from relatively high peak voltage and high rms current compared to the ideal Class-D^{-1} amplifier. Also the efficiency of the amplifier reduces significantly as the output capacitance of the transistor becomes large.

2.2.3 Class-F and Class-F^{-1} Amplifiers

Class F and Class-F^{-1} are power amplifiers based on waveform shaping using multiple harmonic resonators. To the first order, this is a frequency-domain technique compared to the time-domain technique of Class-E amplifiers. The amplifiers achieve high efficiency by shaping the drain voltage or drain current waveforms using these harmonic open or short circuits shown in Figure 2.11.

The ideal waveforms of a Class-F and Class-F^{-1} amplifier are very similar to those of a Class-D and Class-D^{-1} amplifier shown in Figure 2.9. If we take the Class-F^{-1} as an example, it has low peak voltage, so the amplifier can be operated in a higher bias voltage without exceeding the breakdown voltage of the transistor. This improves the output power level of the amplifier. The current waveform has a lower rms value, which reduces the resistive loss of the transistor, and in turn improves the efficiency.

We can look at Class-D^{-1} amplifiers as a special implementation of the Class-F^{-1} amplifiers. The reason for this similarity is symmetric topology of Class-D^{-1} design. At the line of symmetry, the switch is terminated with virtual short circuits for odd harmonics, and the switch is terminated with a virtual open circuit for even harmonics. In practice, the output capacitance of the transistor cannot be omitted. In this case, the even harmonics are being terminated with the output capacitance. This causes undesired effects, which will be discussed in the next section.

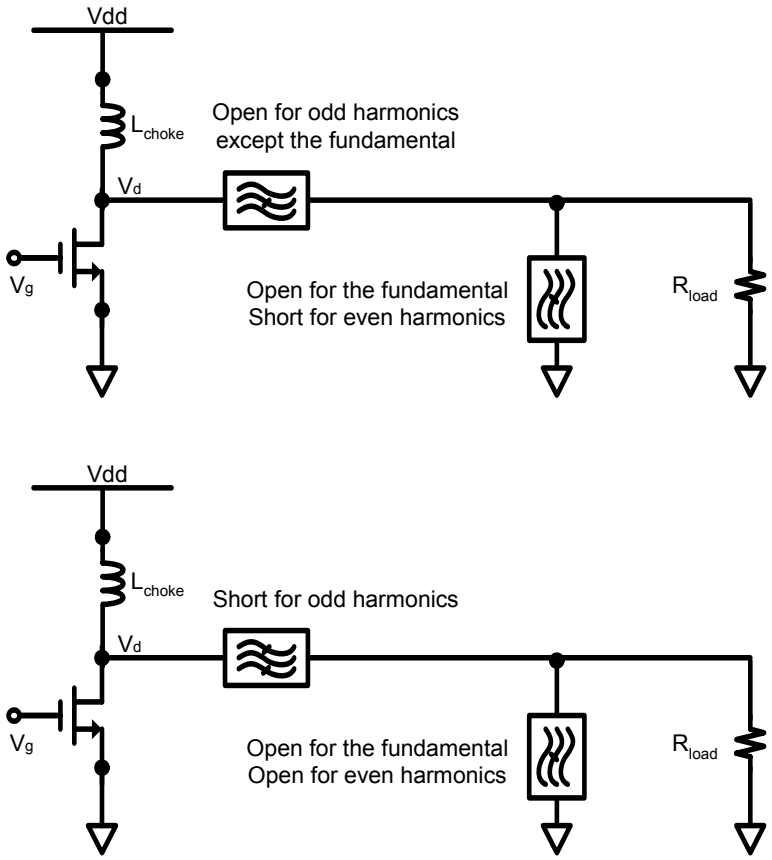

Figure 2.11. The circuit schematics of Class-F (top) and Class-F^{-1} (bottom) amplifiers.

It is also clear from the schematic in Figure 2.11 that the circuit requires infinite number of harmonic-control circuits to achieve the ideal Class-F tuning. In practice, it translates into a complex circuit, which is difficult to implement. A solution to achieve desired harmonic tuning with simple circuits like Class-D and Class-E amplifiers is in the next section.

2.2.4 Class-E/F Family

After we have looked carefully at two different waveform shaping techniques through Class-E and Class-F design, we can take a close look at the Class-E/F family of power amplifiers, which was invented by Scott Kee and Ichiro Aoki at Caltech [11][33][34]. Class-E/F amplifiers combine the advantages of Class-E and Class-F^{-1} amplifiers. The switch is terminated like the Class-F^{-1} amplifiers. The load is tuned inductive to achieve soft switching. A push-pull Class-E/F topology is relatively simple as Class-D^{-1} and Class-E amplifiers.

To reduce the complexity of the circuit, only selected number of harmonics are controlled like Class-F^{-1}. A Class-E/F amplifier which has a Class-F^{-1}-like terminations at x, y, z-th harmonics are denoted as Class-E/$F_{x,y,z}$ amplifier. If all the odd harmonics of are terminated with short circuits, the notation becomes Class-E/F_{odd} amplifier. Some of the examples of the notation are shown in Table 2.1.

Table 2.1. Harmonic Terminations of Different Classes of Power Amplifiers

	f_0	2 f_0	3 f_0	4 f_0	5 f_0	6 f_0	7 f_0	8 f_0
Class E	R+L	C	C	C	C	C	C	C
Class F^{-1}	R	open	short	open	short	open	Short	open
Class E/$F_{2,3}$	R+L	open	short	C	C	C	C	C
Class E/F_{odd}	R+L	C	short	C	short	C	Short	C
Class E/$F_{odd,2}$	R+L	open	short	C	short	C	Short	C

Figure 2.12 shows the schematic of a subset of Class-E/F amplifier—a push-pull Class-E/F_{odd} power amplifier. The amplifier uses a pair of transistors as switches. The transistors are driven 180^o out of phase. The odd harmonics are shorted by the virtual ground at the line of symmetry. Also by symmetry of the push-pull configuration, the amplifier suppresses the even harmonics of the operating frequency, thereby achieving higher efficiency. Also by examining the topology carefully, we can see that the output capacitance can be used as a part of the resonance circuit between the drains of the transistor. This reduces the undesired effects of the output capacitance.

The circuit topology is almost identical to Class-D^{-1} shown in Figure 2.8 with two minor differences: the output capacitances of the transistors are considered; the load is tuned slightly inductive like Class-E amplifier to achieve soft switching. Overall, we can say that the Class-E/F_{odd} amplifier reduces to a Class-D^{-1} amplifier, if the output capacitance of the transistor is low. But we will see that in addition to odd harmonic tuning, the Class-E/F design may also tune critical even harmonics to significantly improve the efficiency of the amplifier.

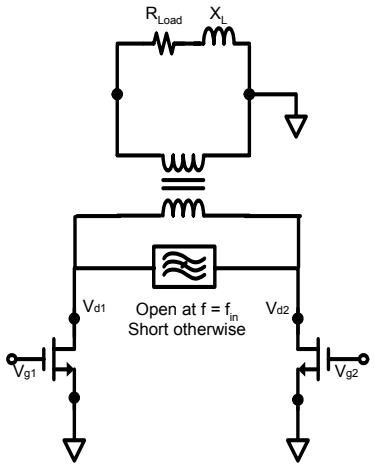

Figure 2.12. A schematic of push-pull Class-E/F_{odd} amplifier.

2.3 L-Band Implementation of Class-E/F Amplifiers

At microwave frequencies, the output power is limited; the active transistors are not perfect; the passive elements are lossy and non-ideal; the bandwidth is limited; power gain over 10 dB is a luxury. It is no surprise that for a given transistor technology, we want to push its limit in frequency and output power at the same time. If the goal is to increase the output power and the operating frequency while still maintaining high efficiency, the output capacitance is the limiting factor of the performance.

2.3.1 Transistor Output Capacitance and the Second Harmonic Trap

The power transistors in UHF and microwave frequency bands have improved in the past several decades, but high-power devices still have large input and output capacitances. Since the classic Class-D^{-1} amplifier analysis does not take into account the output capacitance, it has ideal voltage and current waveforms. If we include the output capacitance in the model, the current waveforms are shown in Figure 2.13. The current waveform starts from a square wave in the case of zero output capacitance. As the output capacitance increases, a sinusoidal component at the fundamental frequency is added to the square wave. The current waveform is not desired because the rms current increases.

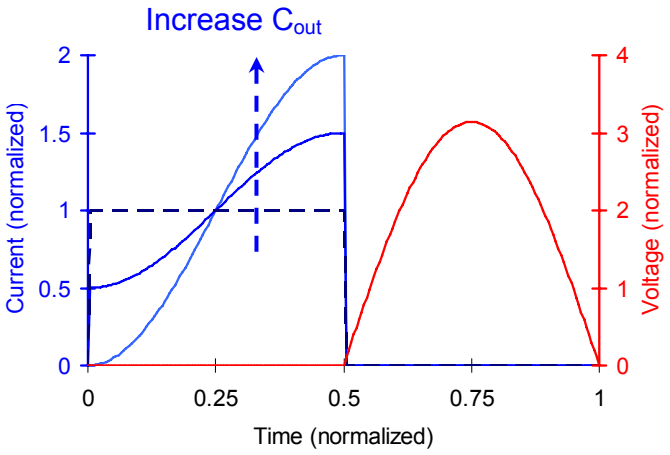

Figure 2.13. The change of current waveform due to the change in output capacitance of the transistors in Class-E/F_{odd} amplifiers.

To achieve better efficiency, a second-harmonic trap is introduced. Effectively, we add a negative capacitance at the second harmonic in parallel with the output capacitance. Using the harmonic trap, the switch is terminated with an open circuit, instead of a capacitive load as shown in Figure 2.14.

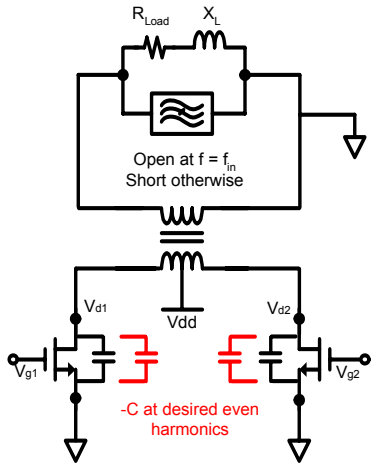

Figure 2.14. A schematic of push-pull Class-E/F_{odd} amplifier also tuned at an even harmonic or even harmonics.

The improved current waveform is shown in Figure 2.15, and the efficiency is improved by up to 5%.

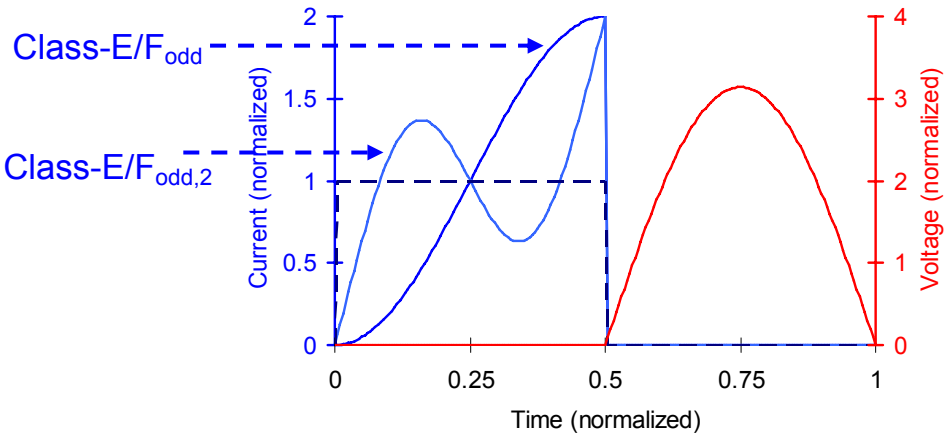

Figure 2.15. A comparison between the current waveform of Class-E/F$_{odd}$ and Class-E/F$_{odd,2}$ amplifiers in the case of large output capacitance in the transistors.

2.3.2 Loss Mechanisms in Power Amplifiers

The design of high-efficiency microwave power amplifiers requires proper trade-off between different types of power losses. These power losses can be divided into losses due to active devices and losses due to passive elements. The primary loss mechanisms due to active devices include conduction loss, discharge loss and matching loss. Active device losses for switch-mode amplifiers occur mainly during transitions from one switch state to another. By using a high-Q resonant output network, Class-E and Class-E/F amplifiers minimize this switching loss. At L-band, the high-power active devices are typically large in size, have large on-resistance, large output capacitance, and very low input and output impedances; all these factors contribute to the different types of losses.

The primary loss mechanisms due to passive structures include metal resistive loss and dielectric loss. The design of a low loss passive network also presents technical challenges. Due to the topology of the push-pull amplifier, a balun is used to convert the single-ended signal to a double-ended signal at the input and vice versa at the output. This balun must be small and planar with a flexible geometry for easy integration into the amplifier circuit. Proper modeling of parasitic capacitance and inductance is also another important challenge to ensure the circuit can be properly designed and reproduced to the given requirements.

Chapter 3

Transformers, Baluns, and Power-Combining Technologies

In this chapter, HF, VHF, UHF, and microwave transformers and baluns are reviewed. Several new compact and planar baluns are introduced. The new baluns are able to handle high power with low loss. These baluns are capable of impedance transformation, which are ideal for power amplifier's low-impedance environment. Extra features, such as centered-tapped DC feed and harmonic tuning, are also included in the baluns. Finally, different baluns are compared in terms of bandwidth, size, losses, impedance and power-handling capability. This comparison provides a guide to select a proper balun structure for a specific application.

3.1 Baluns in Power Amplifiers

Transformers are critical passive components in power amplifiers. Since high-power amplifiers require large devices, which have very low input and output impedances, proper impedance transformation to 50Ω connectors is critical in the design of power amplifiers. These impedance-transforming circuits need to be low-loss and meet the bandwidth requirement of the application.

The topology of push-pull amplifiers shown in Chapter 2 requires a special type of balanced-to-unbalanced transformer, or balun, at the input and output of the amplifier to convert the unbalanced signal to balanced signal and vice versa. Both input and output baluns need to achieve the following desired characteristics. The balun has three ports. One port is the unbalanced port, and the other two ports are the balanced ports. The balance implies that the magnitudes of the signals are the same, and the phases of the signals are 180^{o} out of phase. The insertion loss is kept to a minimum. The insertion loss may include

the metal loss, the dielectric loss, and the loss due to other on-board components, such as chip capacitors.

A typical block diagram of a discrete L-band push-pull amplifier is shown in Figure 3.1. At the input and the output of the amplifier, there are two 50 Ω stand-alone baluns. These baluns have port impedances of 50 Ω at all three ports. Between the active devices and the baluns, there are input and output matching networks, which typically consist of transmission lines and discrete inductors and capacitors. The DC-bias lines at this frequency also consist of high value discrete inductors, or quarter-wave transmission lines. For high-efficiency applications, there are also harmonic-tuning circuits at the output of the amplifier.

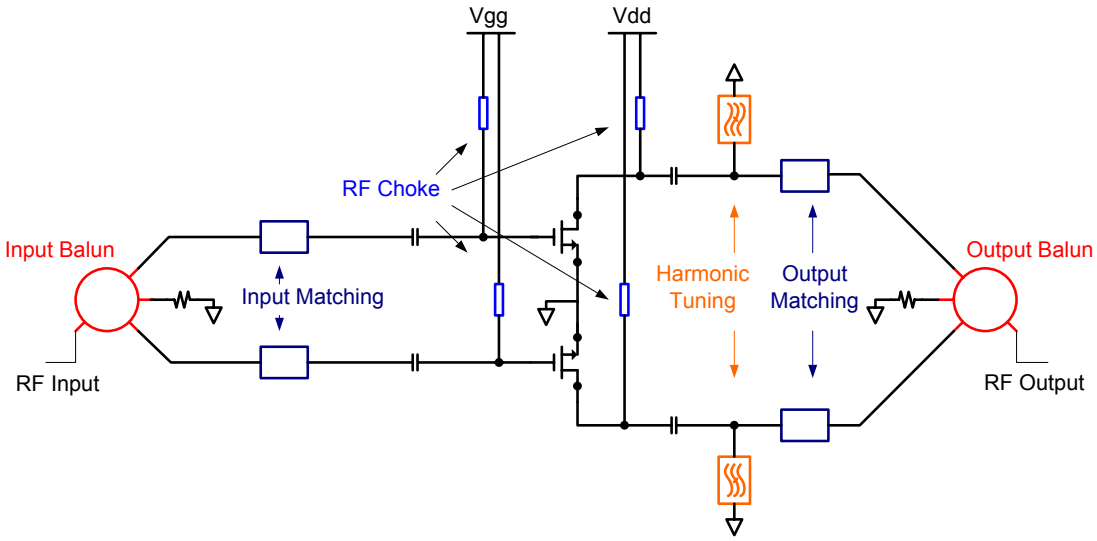

Figure 3.1. A typical push-pull power amplifier topology.

The 50 Ω baluns in the block diagram are easy to measure and useful for a variety of applications. In fact, two identical 50 Ω baluns may be used at the input and the output of the amplifier. However, these baluns are not optimized for the purpose of power amplifiers for several reasons.

First, using 50 Ω baluns is not an efficient use of impedance transformation in power amplifiers. It is important to realize that 50 Ω baluns are not 1:1 baluns. Since 50 Ω impedances at the balanced ports are effectively in series, 50 Ω baluns actually transform the impedance from 100 Ω to 50 Ω. That means that we need to up-convert low

impedances at the gate and the drain of the transistors to 100 Ω and then down-convert to 50 Ω. This significantly reduces the bandwidth of the amplifier. One obvious improvement to this approach is to design 50 Ω to 25 Ω baluns, which take advantage of the nice feature of push-pull amplifiers that the gates and drains are in series. This is demonstrated in Figure 3.2. But even this approach does not take into account the second disadvantage of this type of balun.

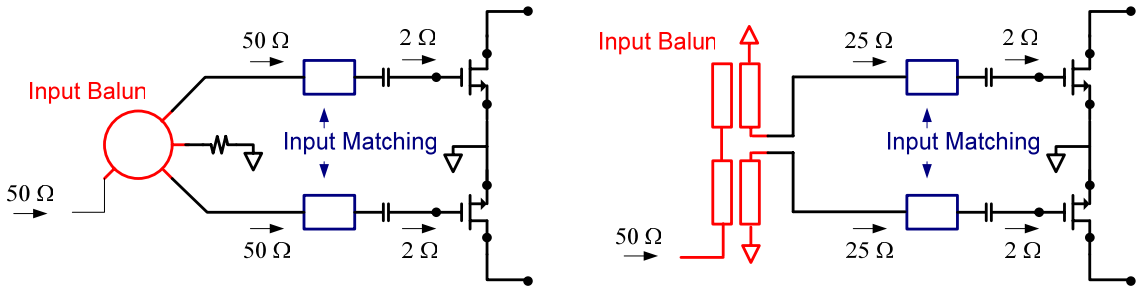

Figure 3.2. Comparison between a balun with 50 Ω terminations at all ports and a balun with 50 Ω termination at unbalanced port and 25 Ω terminations at balanced ports.

Second, 50 Ω baluns do not efficiently combine the capacitive device impedance and the inductive transformer impedance. Most active transistors do not have resistive input and output impedances. In fact, most power transistors have large input and output capacitances. Many transformers, on the other hand, are inherently inductive due the transmission lines and inductances. The extra inductance of the transformer often tunes the capacitive device impedance, which makes simpler matching circuit with lower loss and better bandwidth, as shown in Figure 3.3.

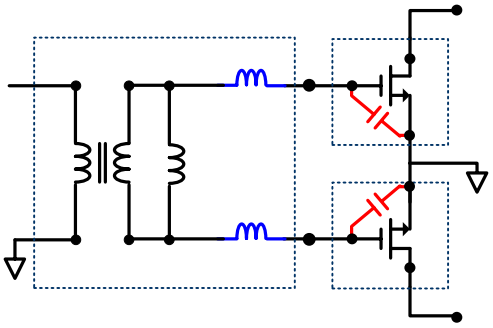

Figure 3.3. Impedance matching using the gate capacitance of the transistor and the leakage inductance of the balun.

Third, the input and output baluns should be optimized separately for their own purposes. In power amplifiers, while the input and the output baluns share many similarities, some of the goals are different, so the design approach is also very different. For the input balun, the goal is to match the low impedance at the gate to the 50 Ω source. The approach is similar to the standard S-parameter input matching technique. Once the small-signal matching network is finished, a large-signal matching optimization can be done if the large signal model of the device is provided.

The output balun design is slightly different. The goal is to present the desired load impedances at the fundamental frequency as well as the harmonics. For example, for a Class-E/$F_{odd,2}$ tuning, the switches of transistors should be presented with a load impedance of R_L at the fundamental frequency, a short circuit at odd harmonics, and an open circuit at the 2nd harmonic. This is shown in Figure 3.4. It is clear that a balun may not satisfy the requirement of both the input and the output baluns because of different purposes for these baluns.

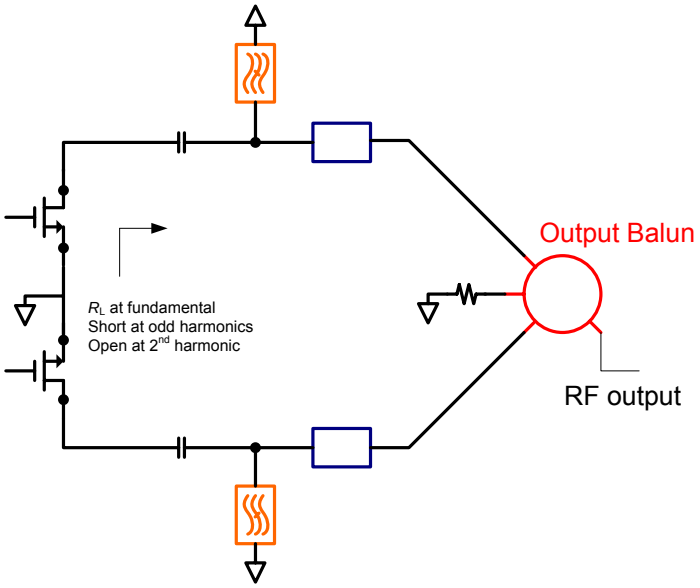

Figure 3.4. Optimization goal for power amplifier's output balun.

There are many different varieties of microwave baluns. However, at 1–2 GHz, the traditional microwave baluns, such as a hybrid ring, are not practical due to their large sizes. Coil transformers are often used at lower frequencies, but we were concerned that it would be difficult to make one at this frequency that would handle the large output power.

Since most high-frequency power devices have low input and output impedances, impedance matching at the input and the output of the amplifier is very important. Most of the published baluns are 50 Ω baluns. This document presents a low-loss, compact microstrip balun that performs impedance-transformation as well as balanced-to-unbalanced signal conversion. Also, at L-band, the RF chokes are typically large in size. The balun in this design has a center-tapped choke, which can be made much smaller than the conventional RF chokes.

3.2 Examples of Transformers and Baluns

3.2.1 HF, VHF, and UHF Transformers

In this section, two types of low-frequency transformers are introduced.

3.2.1.1 Coil Transformers

The coil transformer is one form of the traditional transformers. The impedance transformation of the transformer is N^2. This transformer can make high ratio of impedance transformation with relatively high bandwidth. It is therefore an ideal transformer for power amplifiers, which have very low input and output impedances. The second advantage of coil transformer is the complete isolation between DC and RF signals. Finally, the configuration can be used as a center-tapped balun, as shown in Figure 3.5.

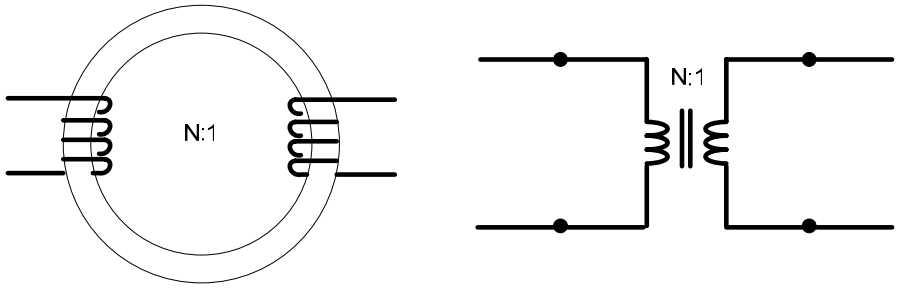

Figure 3.5. A coil transformer using a ferrite core (left). The equivalent circuit model of a center-tapped coil transformer balun (right).

For L-band applications, the length of the coils needs to be much less than a quarter wavelength, which would be too small at L-band. The power handling capability is reduced. Also, the ferrite cores used in the low-frequency transformers are too lossy at microwave frequencies.

3.2.1.2 Transmission-Line Transformers

Transmission-line transformers are popular choices in VHF and UHF applications [35]. The Guanella 4:1 transformer balun is shown Figure 3.6. The key advantage of the transmission-line transformer is broadband impedance transformation. At L-band, the manufacturing of these transformers are difficult, and the performance may be compromised.

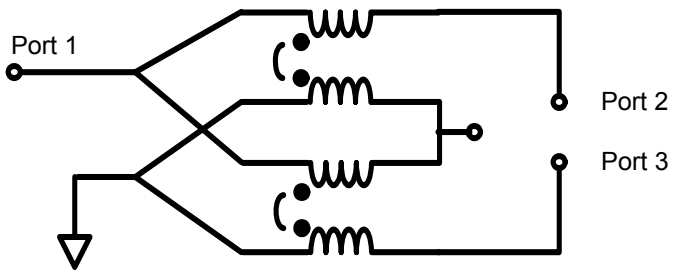

Figure 3.6. Simplified schematic of a 4:1 Guanella balun.

An alternative to Guanella transformer balun is the Ruthroff transformer balun. Compared to the coil transformer and Guanella transformer, there is no symmetry point in the Ruthroff transformer to be used as a center-tapped DC feed. Also the DC and the RF signals are not separated, so additional DC-coupling capacitors need to be used. Large RF chokes are also required for this balun transformer.

3.2.2 Microwave Baluns and Transformers

At microwave frequencies, there are also many different types of baluns [37]. Three of the baluns are briefly introduced. Figure 3.7 shows a typical hybrid-ring coupler. The coupler is a four-port device, and the device can be used as a balun, with the fourth port terminated with a 50 Ω load. The detailed analysis of the balun can be found in [37]. The advantage of the balun is that it can achieve balanced outputs with a relatively easy implementation for an octave bandwidth.

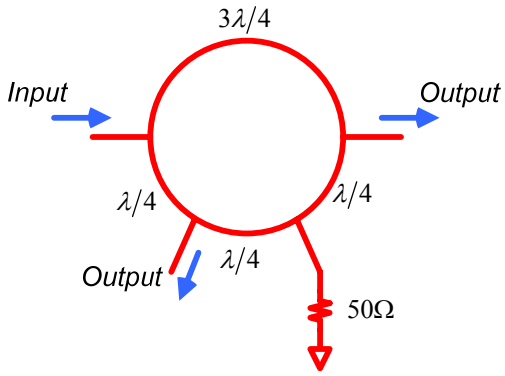

Figure 3.7. Schematic of hybrid-ring balun.

A quarter-wavelength coaxial balun is shown in Figure 3.8. This balun can also achieve an octave bandwidth.

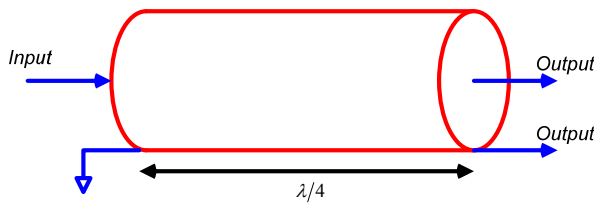

Figure 3.8. Quarter-wave coaxial transmission line balun.

Another classic microwave balun is a Marchand balun shown in Figure 3.9. The balun is typically realized in microstrip or coaxial cable forms. The bandwidth of these baluns can be as high as a decade.

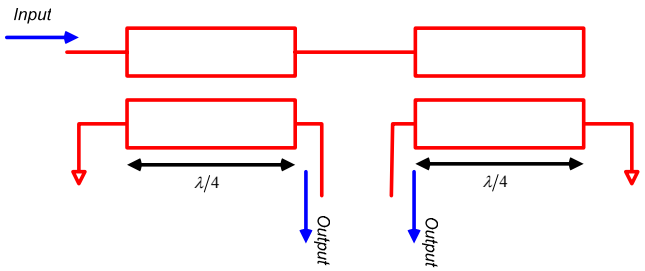

Figure 3.9. Microstrip implementation of Marchand balun.

While all microwave baluns shown can be implemented in L-band discrete power amplifiers, the size of the baluns is too large for this frequency band. Since all these configurations require quarter-wave length transmission lines, the design of a compact power amplifier at this frequency will require more compact baluns.

3.2.3 Distributed Active Transformer (DAT)

The Distributed Active Transformer (DAT) was invented by Ichiro Aoki at California Institute of Technology [4][5][34]. The transformer is capable of combining up to four push-pull pairs of transistors (eight transistors) in a single circular configuration. While DAT has been implemented successfully in L-band Si integrated power amplifiers and HF discrete power amplifiers, it is difficult to implement the same structure in an L-band discrete high-power amplifier. The challenges and potential opportunities are discussed in Chapter 6.

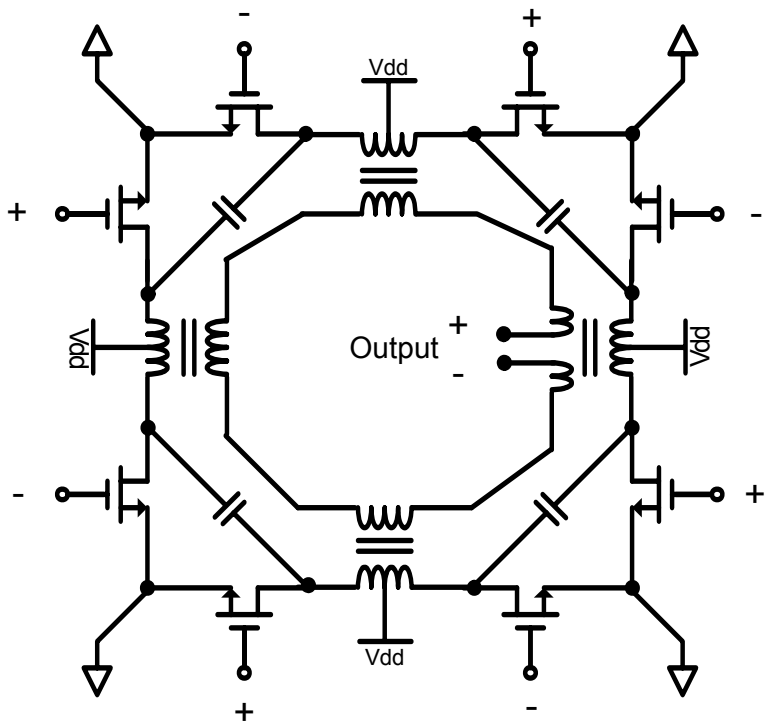

Figure 3.10. Schematic of the output circuit of a power amplifier with a Distributed Active Transformer.

3.3 Compact L-Band Baluns

The baluns reviewed in the previous sections are too large and do not meet the design specification, because the L-band radar requires very compact T/R modules. Furthermore, some of the structures, such as coaxial cables, are not planar and require manual soldiering. This is not suitable for production in large quantity, as in an L-band phase array.

A microstrip balun (Figure 3.12) is designed using two small sections of magnetically coupled metals as the balun [38]. The structure of this balun is represented by Figure 3.11. The size of each microstrip has to be much less than one quarter wavelength. At L-band, this balun is smaller than the conventional microwave baluns. It is planar, and it has a flexible geometry. However, the drawback of the balun is the low coupling coefficient between the primary and the secondary inductors. The low coupling coefficient decreases the impedance transformation ratio of the balun, making the input and output matching of

the power amplifier difficult. The balun shown in Figure 3.12 is also a 50 Ω balun, which does not optimize the impedance transformation in power amplifiers.

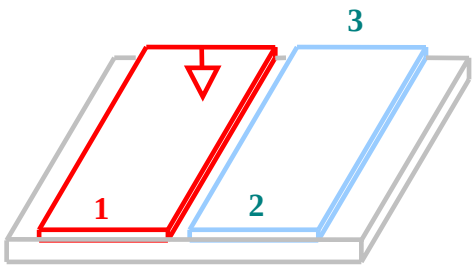

Figure 3.11. A compact side-coupled microstrip balun on a dielectric substrate.

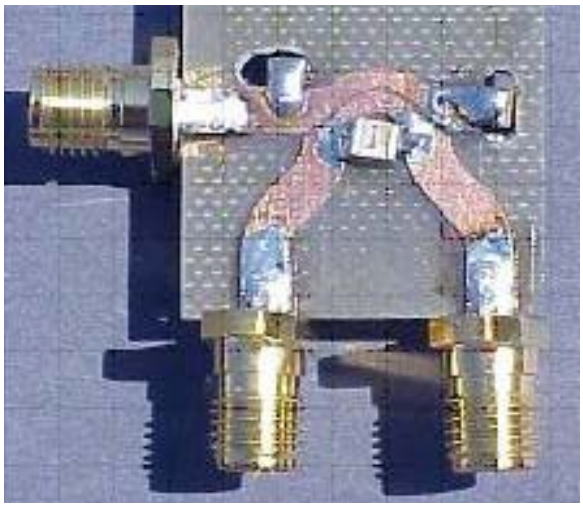

Figure 3.12. A compact magnetic-coupled 50 Ω balun built on FR4 board.

3.3.1 Lumped-Element Model

The magnetically coupled microstrip lines can be modeled by the equivalent circuit model in Figure 3.13. The short microstrip lines are modeled as inductors L_1 and L_2. The magnetic coupling is represented by the coupling coefficient k. The capacitive coupling between the inductors is represented by the capacitors between the inductors. And the capacitive coupling between the microstrip lines and the ground plane is represented by capacitors to ground.

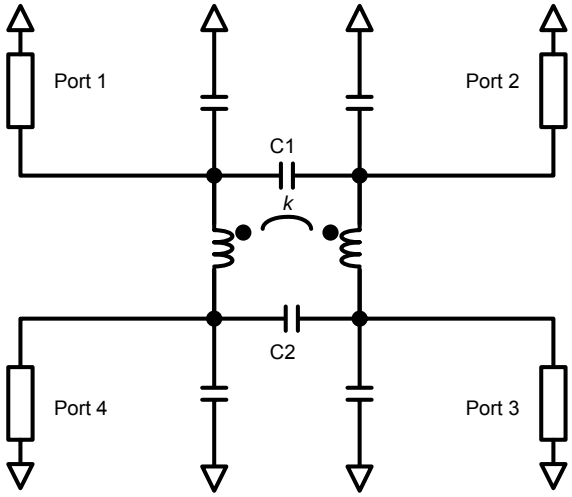

Figure 3.13. A four-port equivalent circuit model for coupled microstrip lines.

3.3.2 Tight-Coupling Microstrip Lines

It is common in microwave circuits to achieve tight coupling between two coupled microstrip lines. The tight coupling often increases the bandwidth in microwave filters, couplers, and transformers. It is important to note that high coupling coefficient can be easily achieved in microwave and RF integrated circuits, due to the smaller size and spacing. Similar kinds of high coupling coefficients can also be achieved in low-frequency circuits using magnetic materials and coaxial lines. For discrete L-band high-power applications, coupling coefficients over 0.9 are extremely difficult to achieve even using the best PCB technologies. More often, parallel microstrip lines as shown in Figure 3.12 have a coupling coefficient of 0.35, which is not nearly enough for matching and impedance transformation. Two types of topologies are introduced next to improve the coupling between the coupling lines: interdigitated lines and broadside-coupling lines.

In interdigitated configuration, the primary and secondary strip inductors are split into two or more strips. Primary and secondary strips are placed alternately, and the equivalent terminals are connected using small metal strips or bond wires shown in Figure 3.14. Using this method, the magnetic field is more confined inside the structure, which increases the magnetic coupling between the primary and the secondary inductors.

An alternative to the balun is using two strip inductors stacked up together as shown in Figure 3.15. The metal strips are separated by a thin dielectric layer. With the current multilayer printed circuit board (PCB) technology, the thickness of the dielectric layer may be as low as 125 μm.

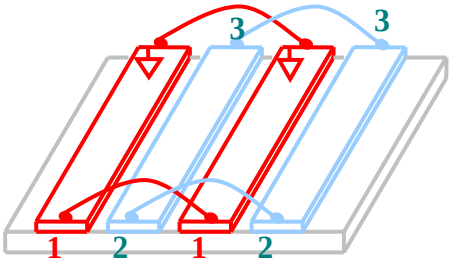

Figure 3.14. Interdigitated balun with coupled inductors connected by wire bonds.

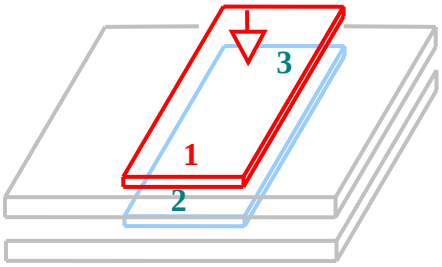

Figure 3.15. Broadside coupling balun with coupled inductors in a multilayered board.

The baluns are simulated as 4-port terminals, and fitted in the model shown in Figure 3.13. Figure 3.16 and Figure 3.17 show the simulated coupling coefficients for side-coupled and broadside-coupled microstrip baluns. Simulated side-coupled and broadside-coupled microstrip baluns have coupling coefficients over 0.55 and 0.85, respectively. In practice, the coupling coefficient may be somewhat lower due to the constraint of circuit layout.

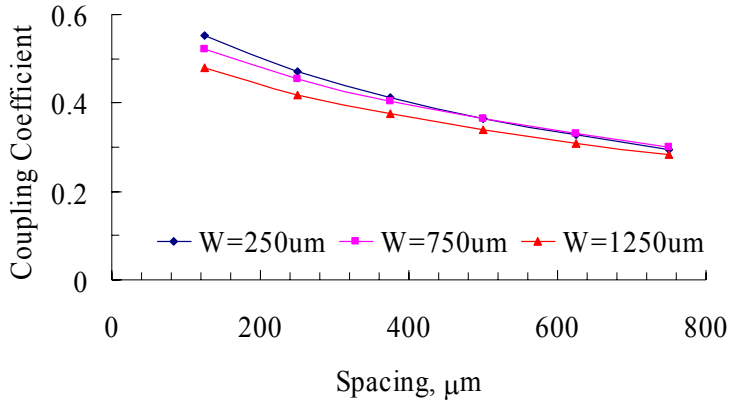

Figure 3.16. Simulated coupling coefficient of ideal interdigitated inductors.

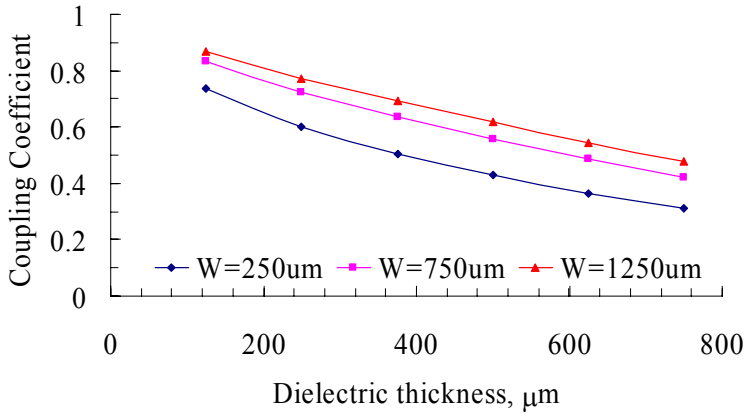

Figure 3.17. Simulated coupling coefficient of ideal broadside-coupling inductors.

3.3.3 Balance Optimization

Since one end of the inductor shown in Figure 3.13 is grounded (in this case, let port 4 be grounded), the equivalent circuit is modified as Figure 3.18. Ideally, port 2 and port 3 should be balanced. However, from the circuit in Figure 3.18, unbalance clearly exists theoretically, because one of coupling capacitors C_1 is connected between port 2 and port 1, the other coupling capacitor C_2 is now connected between port 3 and ground.

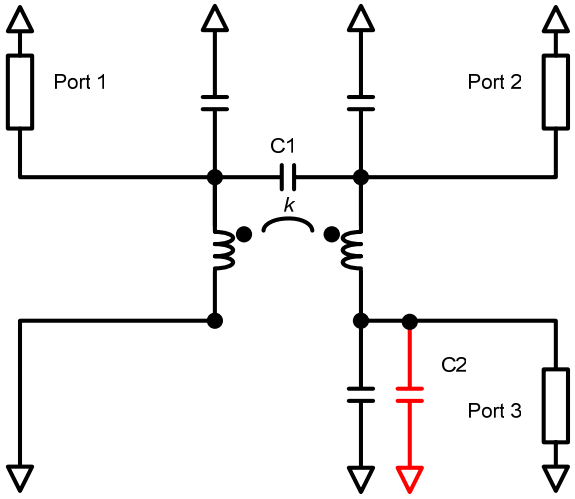

Figure 3.18. Coupled inductors with one port grounded showing asymmetry.

Port 2 and Port 3 shown in Figure 3.18 would be perfectly balanced if capacitors C_1 and C_2 do not exist. To minimize the unbalanced effect, we need to minimize the effects of those two capacitances. Based on the simple assumption of a parallel-plate capacitance (3.1), we can optimize one or more of the variables in the equation.

$$C = \varepsilon_r \varepsilon_0 \frac{A}{d} \tag{3.1}$$

1. Lower the capacitive coupling between the two microstrip lines by increasing the dielectric thickness between the microstrip lines. The reduction in the capacitance between the microstrip lines reduces the unbalanced effect as well. However, the problem with this approach is that increasing spacing also reduces the magnetic coupling between the microstrip lines. In most cases, a high magnetic coupling is desired for impedance transformation and bandwidth. So unless there is too much magnetic coupling involved, this method is not helpful.

2. Use narrower microstrip lines to reduce the capacitance. Effectively, this approach decreases the area, and then reduces in capacitance and the unbalanced effect. This method works well for broadside-coupled baluns, where there may be a lot of capacitive coupling due to the large area of the microstrip baluns. By reducing the width of the microstrip, the self inductance of the microstrip line increases, which may or may not be a desired effect in the circuit design.

3. Use a lower dielectric constant. This is another effective approach. Typical dielectric constant of a Duroid material ranges from 2 to 10. Using lower dielectric constant can reduce the coupling capacitance significantly.

In power amplifier applications, the most effect approach may be to reduce the load resistance of the balun. Since the load resistance of the balun is in parallel with the capacitance, lowering the load resistance effectively shorts out the capacitance of the balun, which in turn reduces the unbalanced effect. There is another advantage of this method. Since RF power devices typically have low input and output impedances, the balanced-to-unbalanced conversion can take place at low impedance levels, rather than high impedance levels. It is recommended to calculate the reactance of the capacitances C_1 and C_2. If the load resistance is much smaller than the reactance, better balance can be achieved.

Figure 3.19 shows the amplitude and the phase balance as functions of load resistance and dielectric constant. It is clear that the amplitude and the phase are well balanced for lower dielectric constant and lower load resistance. For a load resistance less than 10Ω, the amplitude balance is less than 0.25 dB and the phase unbalance is no more than 5^o.

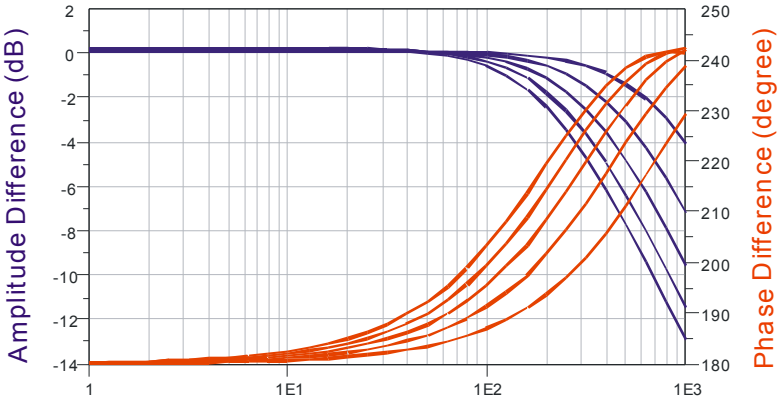

Figure 3.19. Amplitude and phase differences for different load resistances and dielectric constants.

3.3.4 Input Impedance Transformation

Since the input and the output of the RF power devices typically have low impedances, impedance matching is critical. Most of the published baluns are 50Ω baluns, which do not perform impedance transformation. If a 50Ω balun is used, a matching circuit is required

for each gate of the devices as shown in Figure 3.1. The bandwidth is optimized individually for the balun and the input matching network. Therefore, it is difficult to achieve an input matching network that is optimized for the overall input circuit.

We propose an impedance-transforming balun, which can be used for impedance matching as well as balanced-to-unbalanced conversion. The design of the impedance-transforming balun is based on the simplified equivalent circuit model of the balun shown in Figure 3.13. For this simplified approach, we are going to ignore the effect the capacitance to ground and the capacitive coupling between the inductors.

The mutual inductance of L_1 and L_2 is given by

$$M = k\sqrt{L_1 L_2} \tag{3.2}$$

There are many different equivalent circuit models of Fig. 4a, such as T-model and Pi-model. Here the analysis is based on a model with an ideal transformer shown in Fig 5(a) and (b).

$$L' = \frac{1-k^2}{k^2} L_1 \tag{3.3}$$

$$N = \frac{M}{L_1} \tag{3.4}$$

$$C' = C_2 \cdot N^2 \tag{3.5}$$

The input matching circuit can be simplified to the schematic in Figure 3.20. The circuit is effectively a 2nd-order band-pass filter with LC matching. It is also clear from this equivalent circuit that the coupling coefficient k plays a very important role in the impedance transformation. In the ideal transformer shown in blue, the impedance multiplied by k^2. For example, if the coupling coefficient is 0.35, as in the case of side-coupling lines, the impedance is reduced by a factor of 10. If the coupling coefficient is 0.5, as in the case of interdigitated balun, the impedance is reduced by a factor of 4.

This circuit can be used to optimize the input matching performance. The detailed analysis is described in [39]. However, simulation tools can also be used to optimize the values of the inductances and the capacitances.

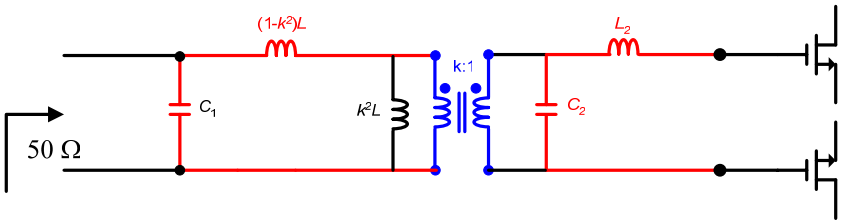

Figure 3.20. Input matching optimization for the input balun.

Figure 3.21 shows an example of a 3rd-order matching circuit from 7.5 Ω to 50 Ω using this topology. The simulation shows nearly octave bandwidth impedance transformation, while performing well in magnitude and the phase balance.

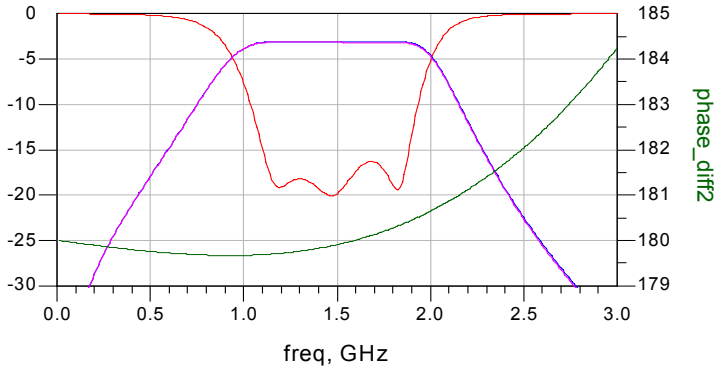

Figure 3.21. Simulated results for a 7.5 Ω to 50 Ω balun with a 3rd-order band-pass filter. The left vertical axis is for the input return loss and the output magnitude in dB. The right vertical axis is for the phase difference at the balanced ports.

3.3.5 Output Impedance Transformation

The output impedance transformation is critical for the output power as well as the efficiency. A simplified output circuit is shown in Figure 3.22. The transistor is assumed to be a switch in parallel with an output capacitance, and in series with a package inductance. The output balun is substituted by two coupled inductors. A key component, C_2, is introduced in parallel with the load resistance.

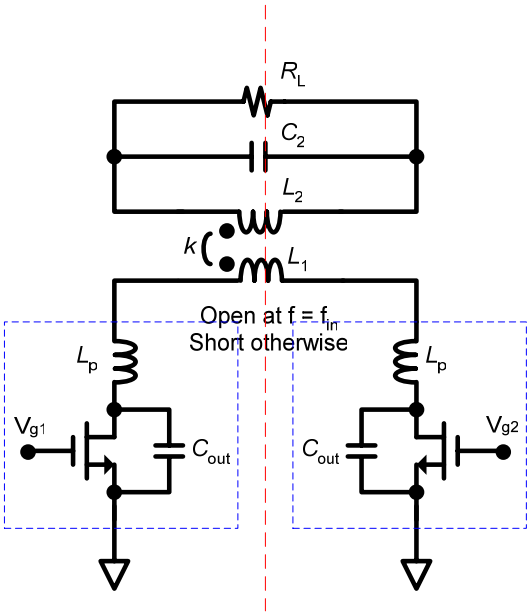

Figure 3.22. A simplified output transistor and balun model for the output balun analysis.

From Figure 3.4, we see that we need to optimize the impedance looking away from the switch. For the push-pull amplifier, we can use the half-circuit analysis shown in Figure 3.23. For Class-E/F_{odd} topology, the switch should see a high-impedance resonance at the fundamental frequency of operation. Here in the figure, the switch actually sees two high-impedance resonances, indicated in the figure. Traditionally, the resonance on the left has been used for the fundamental frequency. However, for a transistor with a high output capacitance, the susceptance increases with high output capacitance as well as high frequency of operation. The package inductance also plays a significant role, as the operating frequency increases. As a result, the resonance frequency of the resonant circuit on the left is far below the desired operating frequency. The second resonance (on the right) becomes significant as the frequency increases. The advantage is that the capacitance C_2 is an arbitrary capacitor, not related to the output capacitance of the transistor. The resonance frequency, in the ideal case, can be also arbitrarily high. Using this capacitance, the output circuit becomes not as dependent on the transistor output capacitance as before.

Note that good bandwidth and desired operating frequency can be achieve only when tight coupling is achieved between the primary and the secondary inductors of the output balun.

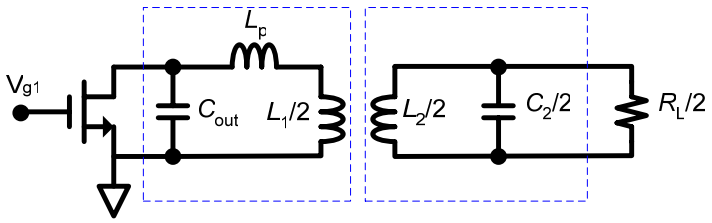

Figure 3.23. A half circuit of the transistor and the balun.

Potential applications with this topology are: broadband amplifiers and dual-band amplifiers. For example, if the two resonance circuits in Figure 3.23 are close to each other, it is possible to combine the two resonances to design a broadband amplifier. Also, we can tune both resonance impedances at two different bands to realize a dual-band amplifier. One example would be a 900 MHz/1900 MHz GSM power amplifier.

3.3.6 Center-Tapped DC Feed and 2nd Harmonic Trap

An RF choke is important to separate the DC bias from the RF signal in the amplifier. Typically in frequencies below microwave frequency, a large inductor is used for the RF choke. In higher frequency, a quarter-wavelength microstrip is used for RF choke. In both of these options, the RF choke is very large in size.

In the low-frequency power amplifiers, it is common to feed the DC power for a push-pull amplifier at a symmetry point of the amplifier as shown in Figure 3.24. The center-tapped DC feed takes the advantage of the push-pull symmetry and the virtual ground, and there is no need for a very high-impedance inductor for RF choke. Sometimes, only a relatively short microstrip line and bypass capacitors are sufficient to separate DC and RF signals. Furthermore, the harmonics of the amplifier are not likely to get into the DC power supply for a center-tapped DC feed.

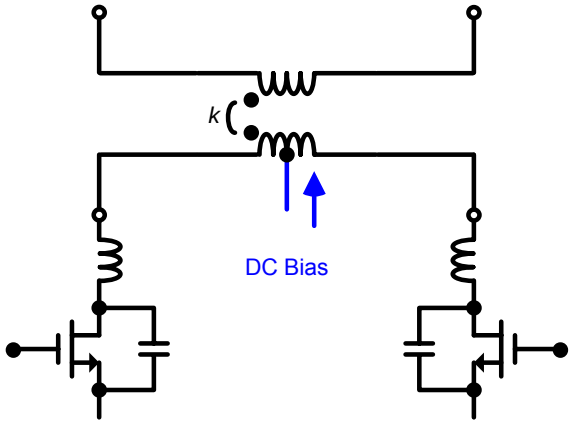

Figure 3.24. Schematic of center-tapped DC bias line.

At microwave frequencies, while many different balun topologies do not allow a center-tapped DC bias line, this topology has a natural symmetry point at the center of the primary inductor, which is suitable for the DC feed.

As discussed in Chapter 2, for Class-E/F amplifiers with high output capacitances, it is desired to improve the current waveform using a second harmonic trap. The topology is then called a Class-E/$F_{odd.2}$ amplifier. One convenient way to implement the second harmonic trap is on the center-feed bias line. One way to design such second harmonic tank is to use the network shown in Figure 3.25. It is a T-network with two inductors and a capacitor. A bypass capacitor provides an RF ground.

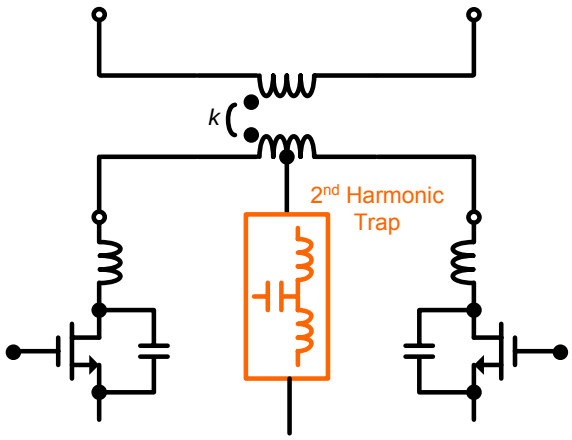

Figure 3.25. Schematic of 2nd harmonic trap on the DC bias line.

The impedance at the second harmonic from the switch is shown in Figure 3.26. From the Smith chart, the second harmonic (at 2.5 GHz) sees an open circuit. In Figure 3.27, we see a comparison of the simulated output spectrum before and after the implementation of the second harmonic trap. The second harmonic in the second graph is suppressed by 20 dB due to the second harmonic trap. The simulated efficiency is improved by 5%.

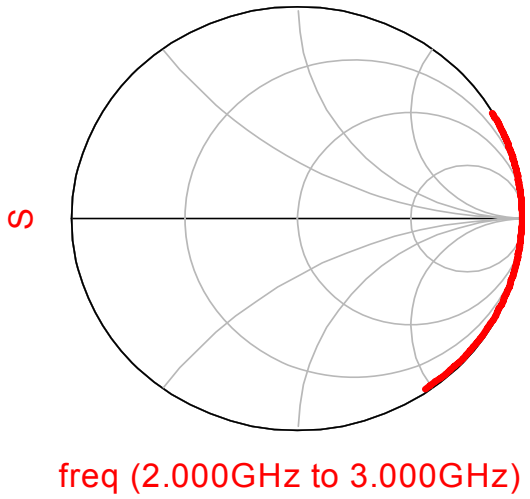

Figure 3.26. Simulation of the 2nd harmonic trap in the Smith chart showing an open circuit for the 2nd harmonic.

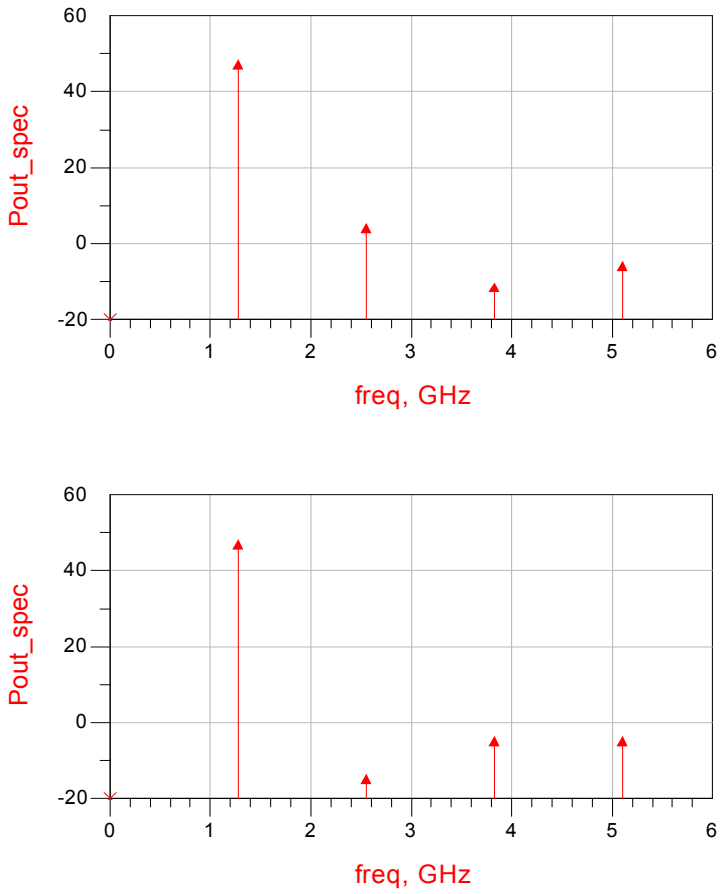

Figure 3.27. Simulated output spectrum without (top) and with (bottom) the second harmonic tank. The simulated efficiency improves by 5%.

The output balun presents a load resistance at the fundamental frequency and high impedance at the second harmonic. The switch voltage and the switch current waveforms are shown in Figure 3.28. The desired voltage waveform is nearly sinusoidal, and the desired current waveform has a waveform similar to a square waveform. This reduces the rms current as discussed in Chapter 2.

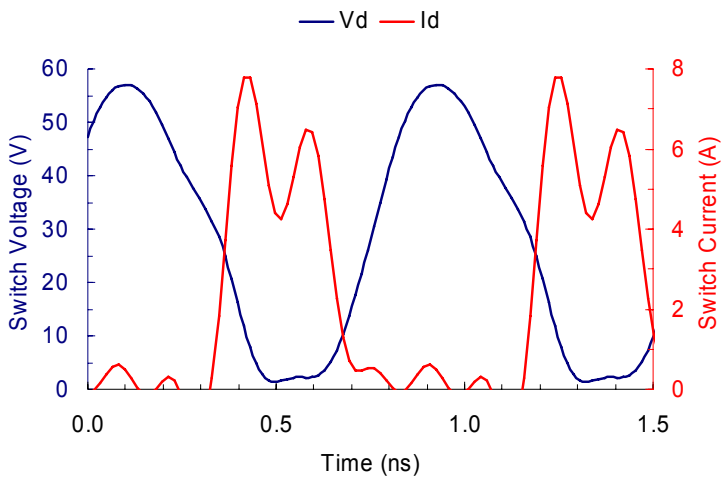

Figure 3.28. The switching voltage and current waveforms. Switch current is near zero when the switch voltage is high. Switch voltage is near zero when the switch current is high. Low RMS current and low peak voltage.

SONNET, an EM simulator mostly for planar structures, is used for all electromagnetic simulation. For the most part of the design, a full 3-D electromagnetic simulation is not necessary. The only true 3-D structures in the circuits are the vias and air bridges for the interdigitated baluns. The via structure and the air bridges in SONNET are sufficient to model these structures.

3.4 Balun Selection

In this chapter, many different baluns were reviewed, and a new balun was introduced. The question presented to power amplifier designers then is how to choose the balun that fits the need of a particular application. Here are several factors that need to be considered when searching for a proper balun.

3.4.1 Bandwidth

Someone may say that it is better to have a balun with the broadest bandwidth. In high-efficiency power amplifier design, this is not always the case. In narrowband applications, a narrowband balun typically serves as a natural low-pass filter, which gives low harmonic levels, which is beneficial. In a push-pull power amplifier, it is often a good idea to have a balun which has good balance up to twice the fundamental operating frequency. This way,

the second harmonic of the amplifier is suppressed due to the symmetry of the amplifier; the third harmonic can be tuned by a harmonic trap, and higher harmonics are filtered by the balun. Most conventional microwave baluns have relatively narrow bandwidth up to an octave.

Of course, there are many applications, which require multioctave- or even decade-bandwidth. In this case, wideband baluns must be used, and harmonic tuning is very difficult. Coil transformers and transmission-line transformers are some of the broadest bandwidth baluns, which can be used this type of applications.

3.4.2 Size

As amplifier designers, we typically would like to have compact baluns to reduce the overall size of the amplifier. From this perspective, most baluns belong to one of the following two cases: (1) the size of the balun is much less than a quarter wavelength, and (2) the size is comparable to quarter wavelength. In the first case, baluns typically use inductive coupling as a means of transformation. Such baluns include coil-transformers, transmission-line transformers, and the new baluns introduced in this chapter, as well as the coupling structure used in Discrete Active Transformer. In these baluns, the lengths of the transmission lines are much less than a quarter wavelength (typically less than one-sixth of a quarter wavelength), and thereby can be assumed as coupled inductors. The amplifier and phase balances are compromised as the assumption is violated. Good balance may be achieved sometimes, but only in very limited bandwidth. Conventional microwave baluns, such as Marchand baluns and hybrid rings, have approximately the size of a quarter wavelength. These baluns typically have good performance as long as they are close to a quarter wavelength.

It is then quite clear that selecting a compact balun structure depends on the operating frequency and the process technology. For example, in applications lower than GHz level, it is very difficult to implement a compact balun using conventional microwave balun structures. In applications above 30 GHz, inductive-coupling balun structures are difficult due to the process technologies.

It should be noted that with advanced processing technologies, many HF, VHF and UHF baluns are rediscovered to be useful at frequencies up to a few gigahertz. Basically, these transformers are scaled down in size and up in frequency.

3.4.3 Impedance Level and Impedance Transformation

For power amplifier applications, the impedance level is typically low, between a few Ohms. It is important to consider impedance level of the components, realizable in a particularly processing technology. For example, if a coaxial cable is used as a part of the balun, and the impedance of the transistor is 10 Ω, the characteristic impedance of the coaxial cable should be between 10 Ω and 50 Ω. For the same transistor technology, if coupled inductors are used in the balun, the reactance of the inductor should be between 10 Ω and 50 Ω. For most processing technologies, it is relatively easy to make a transmission line with characteristic impedance between 10 Ω and 50 Ω.

Chapter 4

Implementation of Power Amplifiers

In this chapter, the implementation of four generations of power amplifiers and the measurement results are presented. Two types of baluns are implemented in the power amplifiers: interdigitated baluns and broadside-coupling baluns. As different improvements are implemented in the different generations, the measurement results improve as well. At the end of the chapter, the results of different versions of amplifiers are compared. There is also a comparison between the measurement results with the best published results.

The specifications of the L-Band high-efficiency power amplifier are listed in Table 4.1. The combination of output power, bandwidth, and efficiency requirements make this amplifier difficult to design.

Table 4.1 Amplifier Specifications

Parameter	*Value*
Operating frequency	1220 –1300 MHz
Output power	30 W
Efficiency	70%
Gain	10 dB

Since most of the transistors in L-band are pre-matched for wireless base station applications at 1.8-1.9 GHz, there are not many choices for proper devices. Freescale MRF284 LDMOS devices are chosen as the active devices of the amplifier. These devices are unmatched. Some key specifications are listed in Table 4.2.

Table 4.2 Specifications of Freescale MRF 284

Maximum Drain-Source Voltage	65 V
Maximum Gate-Source Voltage	±20 V
Total Device Dissipation	87.5 W
Gate Threshold Voltage	3 V
Output Capacitance (Vds=26 V f=1 MHz)	23 pF
Output Power	30 W

4.1 Implementation and Measurement

4.1.1 800 MHz Power Amplifier Using Interdigitated Baluns

Figure 4.1 shows a picture of the first design of the Class-E/F power amplifier. Two LDMOS transistors are placed side-by-side as close as possible. This way the inductance between the drains of the amplifiers can be reduced. Interdigitated baluns are used. The primary inductance has four fingers, while the secondary inductance has three fingers. The width of the fingers is 20 mils while the spacing between the fingers is 5 mils. The baluns are gold plated, so the fingers are connected using wire bonds. The 5 mil spacing is the smallest that can be fabricated, and the close spacing is used to maximize the coupling between the fingers. The balun structure is modeled using the equivalent circuit model discussed in Chapter 3. The model is verified using the electromagnetic simulator, SONNET. The amplifier is built on FR4 board with a dielectric constant of 4.3.

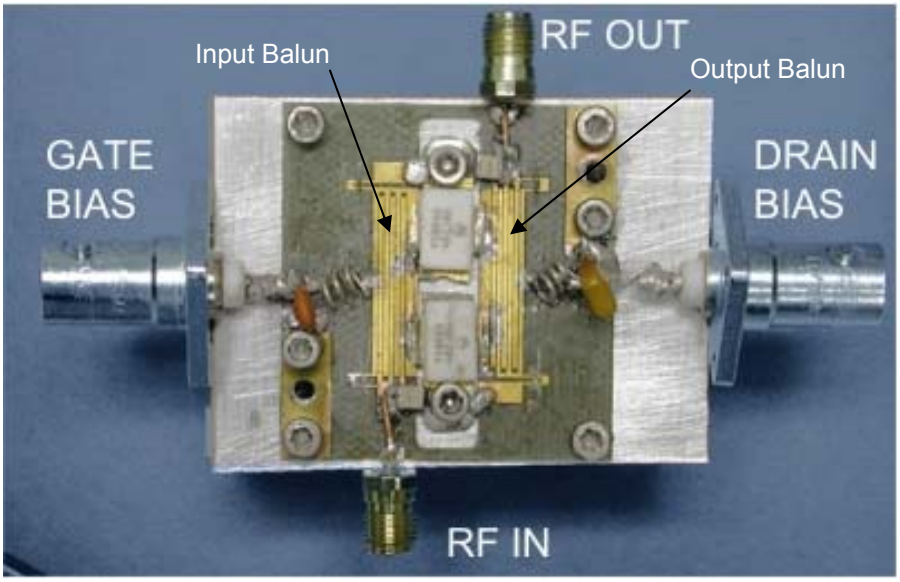

Figure 4.1. 800 MHz Class-E/F power amplifier with interdigitated baluns.

The measurement block diagram is shown in Figure 4.2, and a photo of the measurement setup is shown in Figure 4.3. The output power and drain efficiency are measured and shown in Figure 4.4. The power measurement was performed using a Bird power meter. Amplifier Research model is used as the driver amplifier. The measurement was performed

at 800 MHz. At 30 W output power level, 12 dB gain and 64% drain efficiency are achieved.

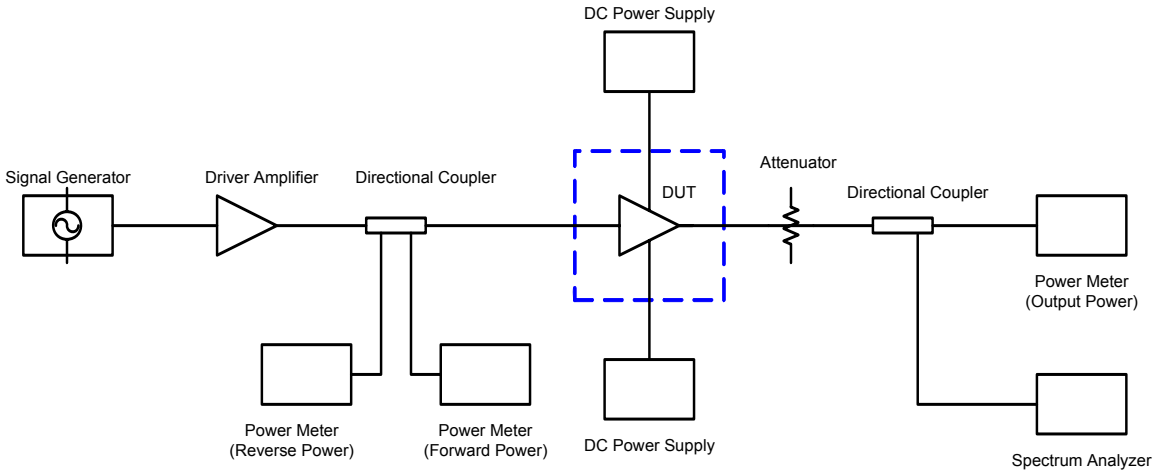

Figure 4.2. Block diagram of the measurement setup.

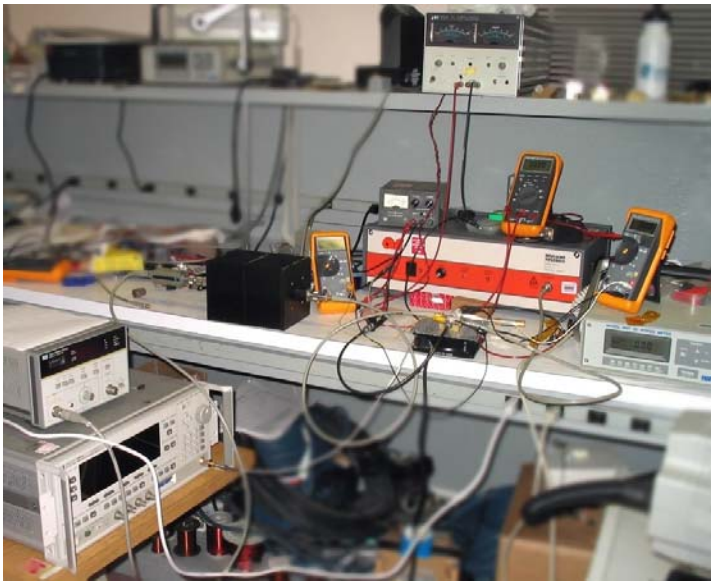

Figure 4.3. A typical measurement setup for the power amplifier.

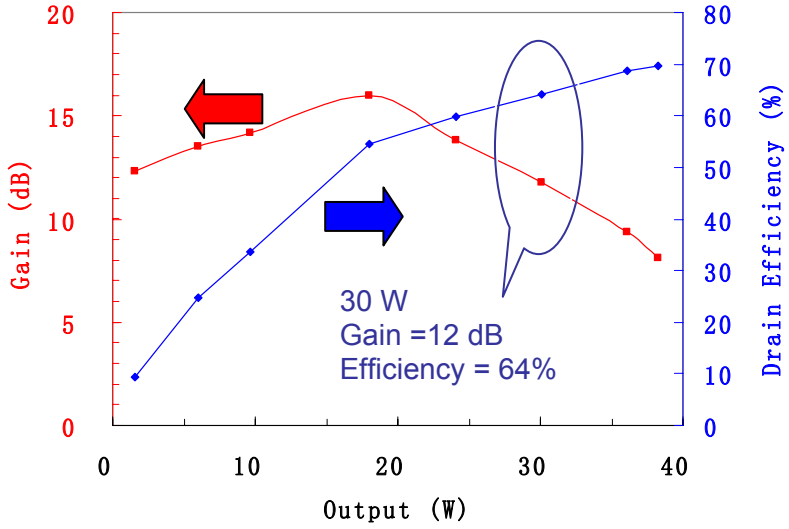

Figure 4.4. Gain and PAE vs. output power for 800 MHz PA.

The operating frequency is less than the target 1220–1300 GHz. The reason is the high output capacitance of the transistors, because the operating frequency is inversely proportional to the square root of the capacitance. One way to increase the operating frequency is to reduce the self-inductance of the output balun. However, in this configuration, the lengths of the fingers of the baluns are limited by the size of the transistors. In order to reduce the length of the balun, another configuration of the amplifier is designed to have the drains of the transistor facing each other. This configuration is discussed in the next section.

There are a few other issues with the design. The lengths of the baluns are not much smaller than a quarter-wave length. This introduces unbalance due to the capacitance between the fingers and the capacitance to ground. The unbalance causes reduction in output power, gain and efficiency. The input matching circuit is also not optimized. Some of these issues are addressed in the second version of the amplifier.

4.1.2 900 MHz PA Using Interdigitated Baluns

In this version of design, several significant changes are made to the amplifier. The picture of the amplifier is shown in Figure 4.5. The amplifier is fabricated on FR4 material. The

width of the balun fingers are 25 mils, and the spacing between the fingers is 5 mils. Copper wire bonds are used to connect the interdigitated fingers of the baluns.

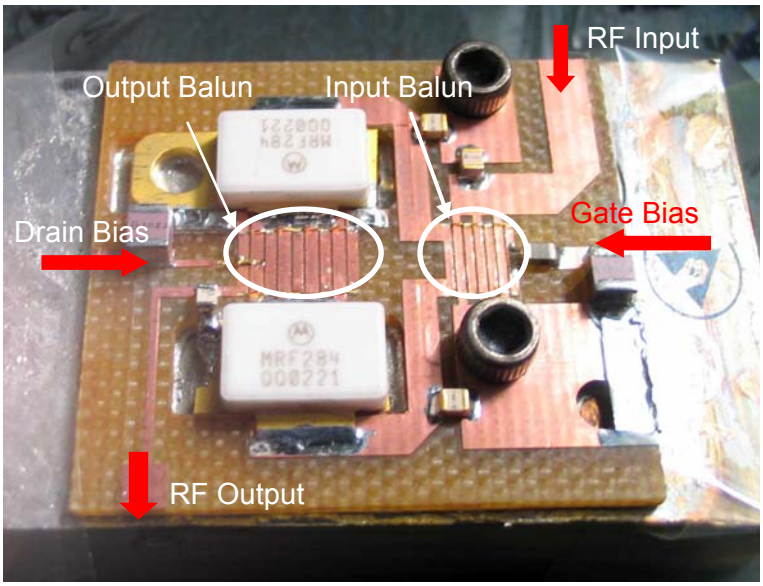

Figure 4.5. 900 MHz Class-E/F power amplifier with interdigitated baluns.

The first change of the amplifier is to have the drains of the transistors facing each other. Using this layout, the lengths of the baluns are reduced significantly from the previous design. This change, in theory, increases the operating frequency of the amplifier, and improves the balance of the balun. However, the amplifier suffers from a low-frequency oscillation, which is not identified using theoretical models. A ferrite bead is used on the gate bias line to reduce to the oscillation. It is partially effective.

Another significant change is to have a much shorter input balun compared to the previous version. This also helps improve the balance of the push-pull amplifier, which is critical for the power, gain and efficiency. In addition to the input balun, more input matching circuits are included.

The amplifier had a similar performance to the previous version. In this case, the operating frequency increases slightly to 900 MHz. The output power, gain and efficiency are similar. The reduced length of the output balun did not improve the operating frequency as expected because of the significant package inductance of the transistors, which is in series with the output balun.

Another key problem with this design, as described in Chapter 3, is the poor coupling coefficient between the primary and the secondary of the input and output balun. From Figure 4.5, we can see that the RF output has a long, narrow transmission line to increase the impedance at the secondary of the output balun. In order to improve the coupling, multilayered board is used to implement broadside-coupling baluns in the next version.

4.1.3 1200 MHz PA Using Broadside-Coupling Baluns on FR4

Broadside-coupling baluns are used in this version of power amplifier. The main reason is to improve the coupling coefficient between the primary and the secondary inductors. The multilayer configuration is enabled by the multilayer PCB technology. The amplifier is built on a three-layer PCB using FR4 material shown in Figure 4.6, which has a dielectric constant of 4.3. Since we want to minimize the separation of between the primary and the secondary inductors in order to improve the coupling coefficient, we use the minimum separation between two layers, which is 5 mils. This minimum thickness limits the coupling coefficient between the layers. The dielectric layer between the first and the second metal layer is a 5 mil core of FR4 material. The vias between the first and the second metal layer are made. The second dielectric is a 62 mil core and its vias are built. Then the two boards on connected together for the final multilayered board.

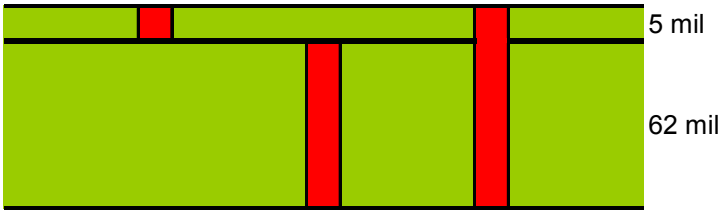

Figure 4.6. Cross-sectional view of the multilayer PCB built on FR4. The vias are shown in red.

The layout and the photo of the amplifier are shown in Figure 4.7 and Figure 4.8. The size of the amplifier is 3 cm by 3 cm. As in the previous version, the drains of the transistors face each other, while the gates are away from each other. The output balun connects between the leads of the drains of the transistors. The primary inductor is on the top layer of PCB, and the secondary inductor is on the second level of PCB, directly below the primary inductor.

One advantage of this wide balun is that the impedance of the transmission line is low, which is very suitable for impedance transformation at low impedance level. This also reduces the self-inductance of the output balun. Compared to the interdigitated version, the overall width of the balun is increased by a factor of 2.5. The second advantage of the wide baluns is reduced loss. The simulated loss of the output balun is 5%, using SONNET. The power amplifier is simulated in Agilent ADS.

Again, a center-tapped DC bias line is used in the balun. For the output matching, only one output capacitor is used as the output matching element, along with the output balun. This simple output transformation structure is compact and low loss.

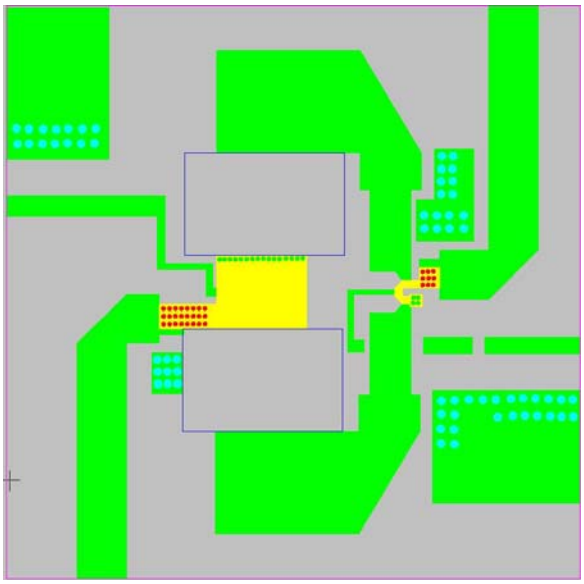

Figure 4.7. Layout of 1200 MHz Class-E/F power amplifier with broadside-coupling baluns.

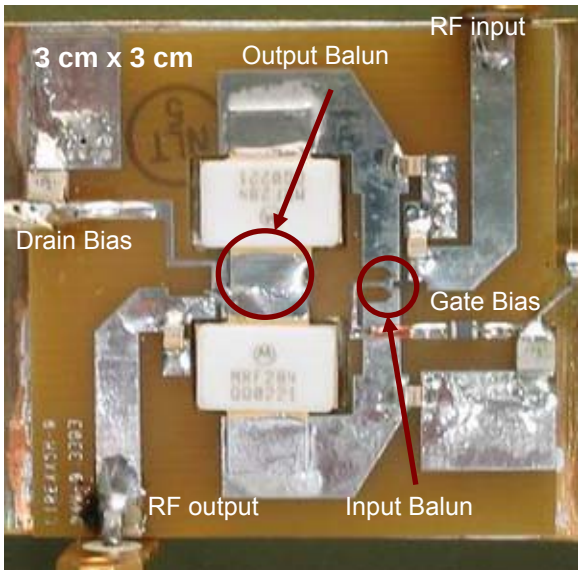

Figure 4.8. 1200 MHz Class-E/F power amplifier with broadside-coupling baluns on FR4.

On the input side, wide lines are used for input matching due to the low-impedance level at the gate of the transistor. The input baluns have reduced size in order to improve the input magnitude and phase balance. A centered-tapped DC feed is used for the input balun with a series ferrite bead as an RF choke. The lossy nature of the ferrite bead is used to eliminate oscillation.

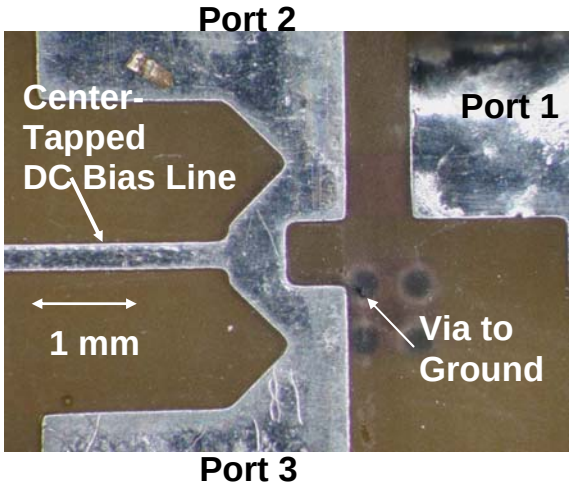

Figure 4.9. Photo of the center-tapped input balun. The primary inductor in the second layer is directly below the secondary inductor.

The performance of the amplifier is shown in Figure 4.10 and Figure 4.11. All measurements were performed with a continuous wave (CW) input signal. The simulated loss of the output balun is 5%, using SONNET. The power amplifier is simulated in Agilent ADS. Figure 4.10 shows that at 1075 MHz, output power is 44 W while the gain is 12 dB and PAE is 60%. Figure 4.11 shows the frequency response of the power amplifier. The 3 dB bandwidth is 45 MHz. The bandwidth is limited by the input matching.

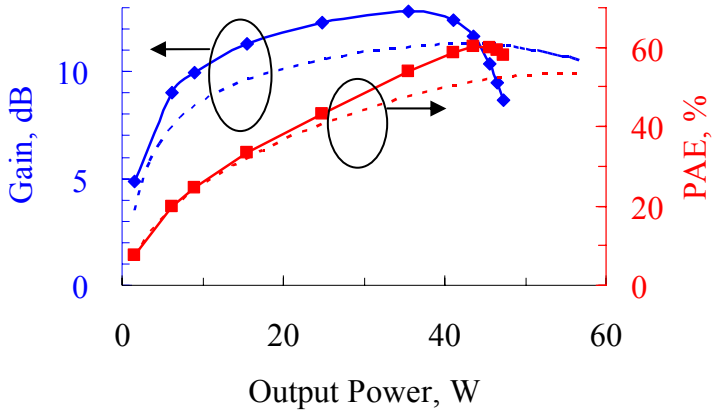

Figure 4.10. Gain and efficiency vs. output Power at 1075 MHz.

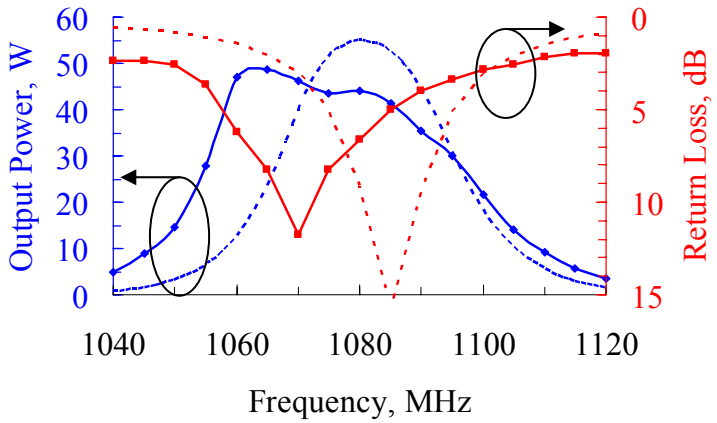

Figure 4.11. Output power and return loss vs. frequency.

Figure 4.12 shows the output frequency spectrum of the amplifier. The output power spectrum of the amplifier shows excellent suppression of harmonics of the fundamental frequency. The 2nd harmonic is 45 dB below the fundamental, and the 3rd harmonic is also

45 dB below the fundamental. The push-pull configuration reduces the level of the even harmonics. In addition, the narrow-band nature of the output balun helps suppress both even and odd harmonics.

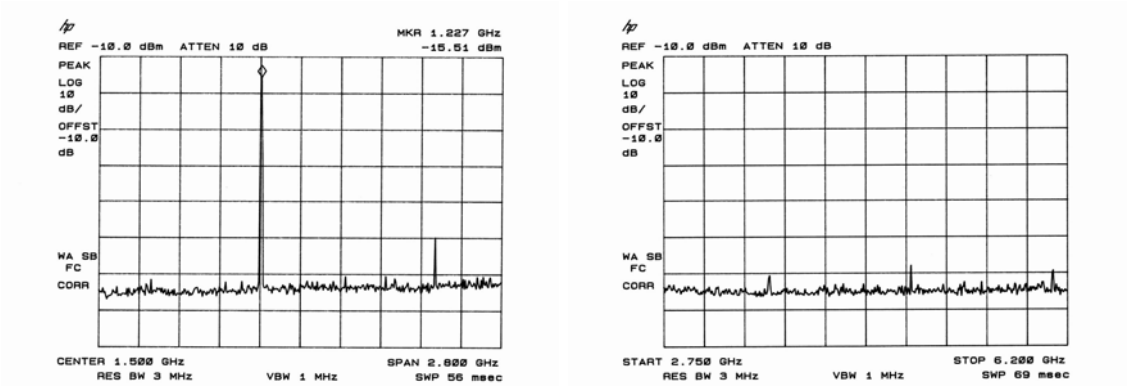

Figure 4.12. Frequency spectrum of fundamental and harmonics

4.1.4 1100 MHz PA Using Broadside-Coupled Baluns on Duroid

The multi-layered boards are manufactured on Rogers RT/Duroid 5880. The dielectric constant is 2.2. This board is chosen because it has lower dielectric loss than FR4 board, and it has a lower dielectric constant, which improves the balance of the baluns.

The cross-sectional view of the multilayered board is shown in Figure 4.13. The duroid material is softer than FR4 material; the building process is also more difficult. Dielectric between the top and the second metal layer is 5 mils of RF 5880 plus 2 mils of bonding film which is made of a low-loss dielectric with a dielectric constant of 2.6 [40]. Dielectric between the second and the bottom metal layer is 62 mils. Effectively, the separation between the first and the second metal layer is 7 mils. The coupling coefficient between the layers is thereby less than the previous version.

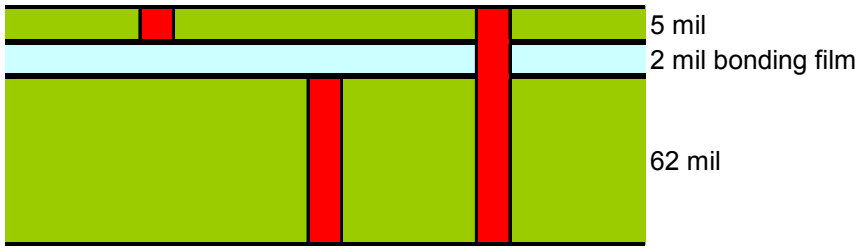

Figure 4.13. Cross-sectional view of the multilayer PCB built on FR4.

The matching circuit is significantly improved from the previous version in order to extend the bandwidth of the amplifier. The circuit schematic is shown in Figure 4.14, and the photo of the amplifier is shown in Figure 4.15.

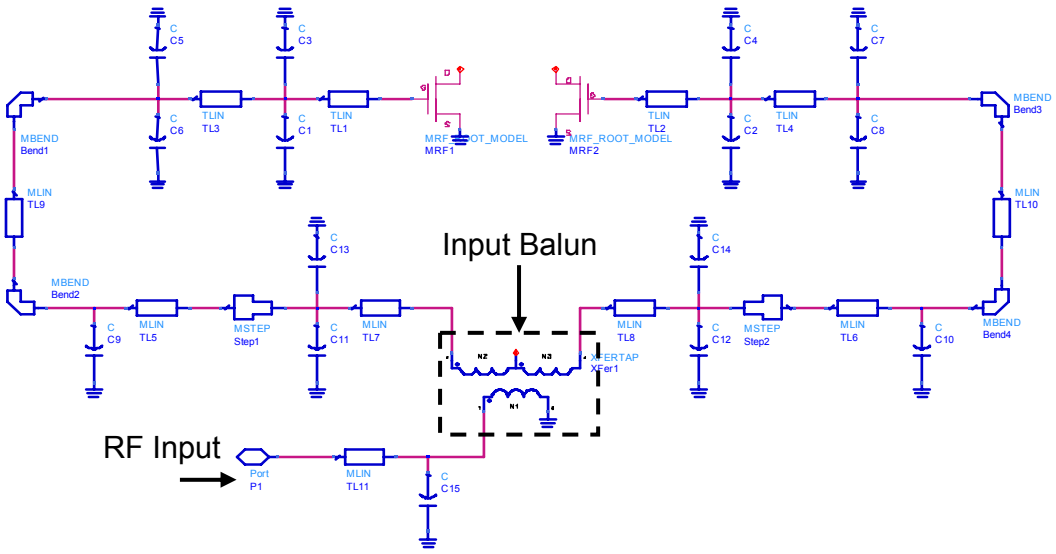

Figure 4.14. Input matching network of the L-band power amplifier.

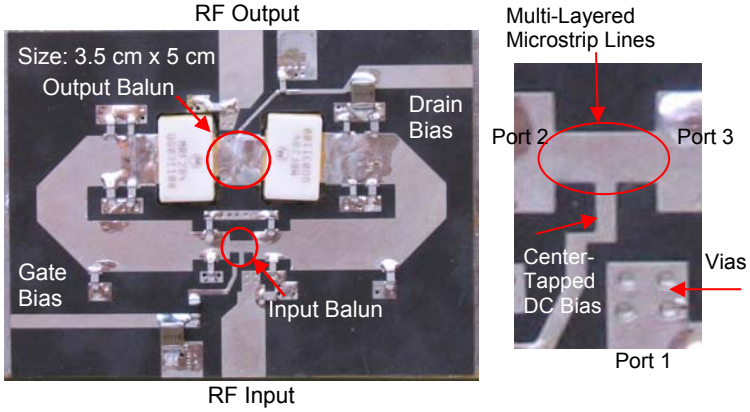

Figure 4.15. 1200 MHz Class-E/F power amplifier with broadside-coupling baluns on Duroid.

Figure 4.16 and Figure 4.17 show the measured performance. At 1.1 GHz, the peak output power is 60 W with a drain bias of 32 V. The peak power-added efficiency is 65%. Also shown on Figure 4.16 for comparison are the gain and PAE predicted by an ADS harmonic-balance simulation. The measured PAE is quite close, but the measured gains are 2 dB to 3 dB low. This suggests that it may be possible to improve the gain. The 3-dB

bandwidth is 150 MHz. Figure 4.19 shows the measured output power spectrum. The largest harmonic components are the 3rd and 5th, at –40 dBc.

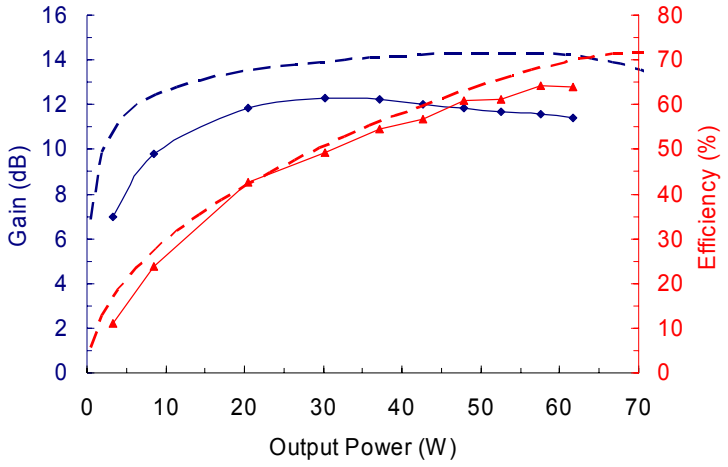

Figure 4.16. Gain and PAE vs. output power. The dash lines are simulated results, and the solid lines are measured results.

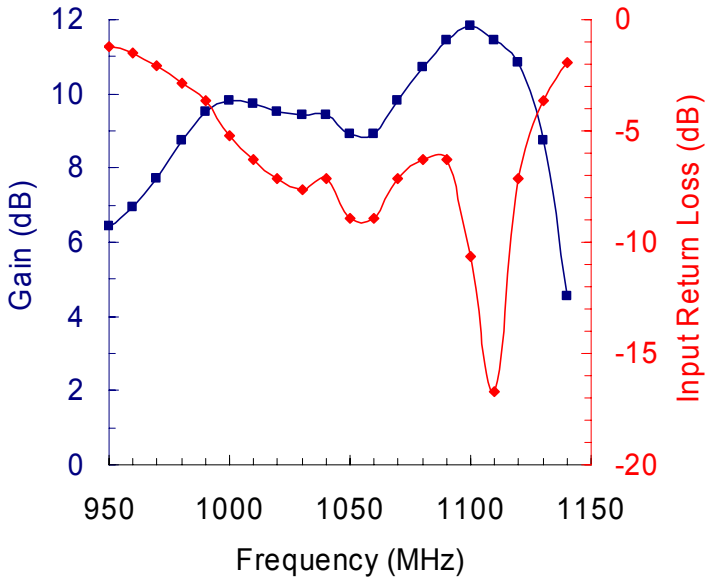

Figure 4.17. Gain and input return loss vs. frequency.

The simulated waveforms from ADS are shown in Figure 4.18. The voltage waveform is nearly a half sinusoid. This reduces the peak voltage compared with a Class-E amplifier. The current waveform has a relatively square shape, reducing the rms current compared to

a Class-E amplifier. This helps to reduce the on-resistance loss in the amplifier. The simulated loss of the output balun is 5.2%, with half the loss in the metal, and half the loss in the capacitors. The loss of the Duroid coupling layer was negligible.

The switching-amplifiers can be used for wireless communications applications which can tolerate strongly nonlinear effects of the amplifiers. Constant envelope signals, such as MSK, can be faithfully reproduced. Using the digital signal analyzer, the MSK signal is generated to feed the power amplifier, and the output is measured by the analyzer. The eye diagram and the phase trellis are shown in Figure 4.20.

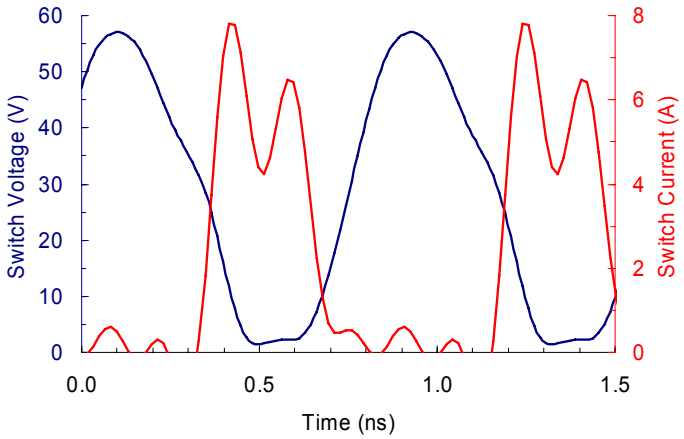

Figure 4.18. Simulated waveform of Class-E/F amplifier.

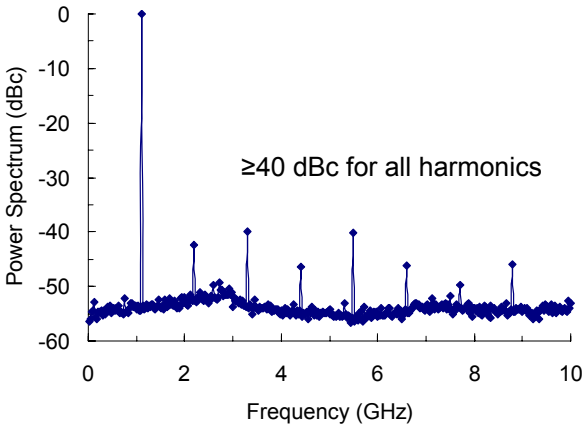

Figure 4.19. Output power spectrum.

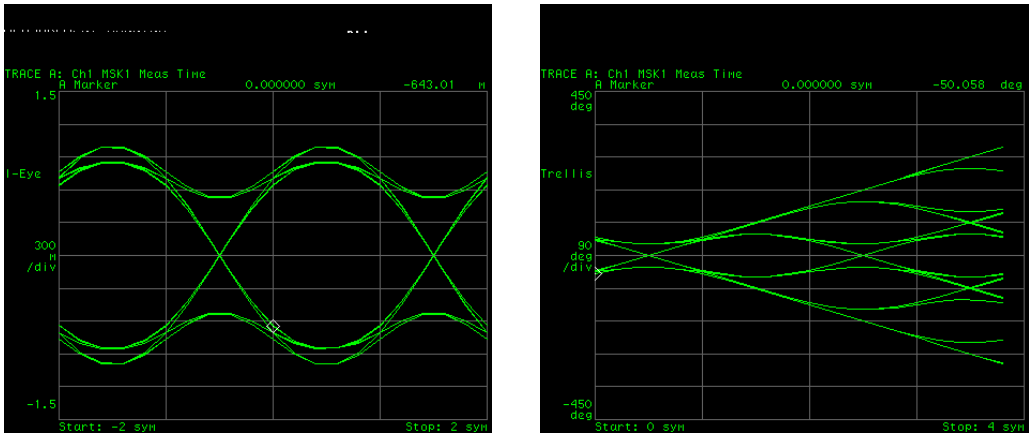

Figure 4.20. Measured eye-diagram and phase trellis using an MSK signal.

4.1.5 1200 MHz PA Using Broadside-Coupled Baluns on Duroid

The previous amplifier is tuned with better capacitor models with series inductance, and vias are properly modeled. The improved measurement results are shown in Figure 4.21 and Figure 4.22. The peak measured output power is 74 W with a peak PAE of 67%. The 1 dB bandwidth is 170 MHz.

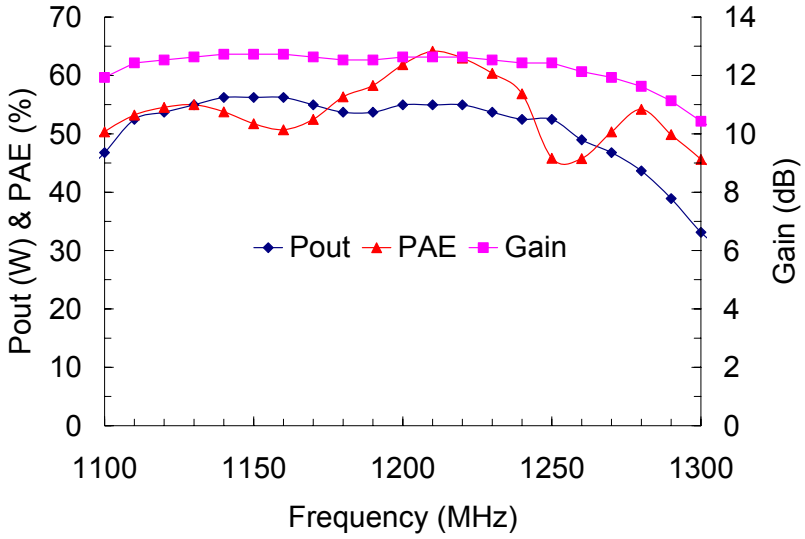

Figure 4.21. Output power, gain and PAE vs. frequency.

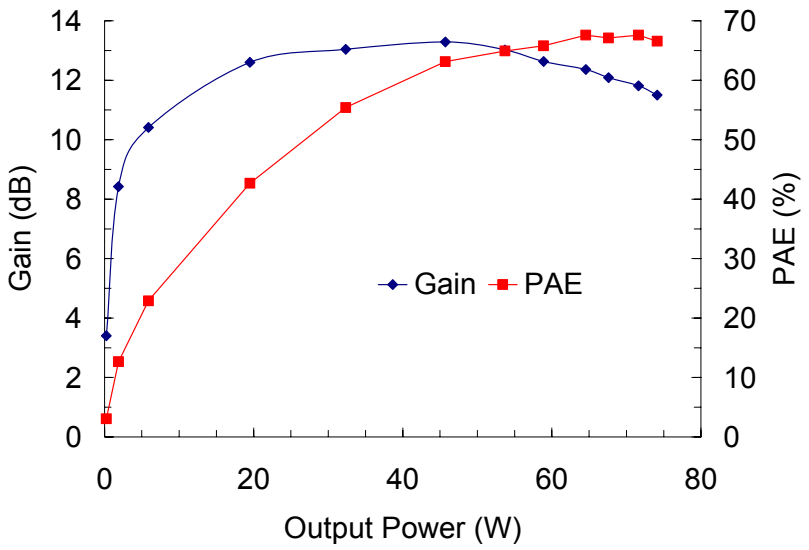

Figure 4.22. Gain and PAE vs. output power at 1220 MHz.

4.2 Performance Comparison

The following table summarizes the performance of the amplifiers during different iterations.

Table 4.3 Performance Summary of Different Versions of Amplifiers

Ver.	*Freq*	*Power*	*Eff.*	*BW*	*Comment*
1	800 MHz	30 W	56%	N/A	Poor coupling coefficient
2	900 MHz	30 W	52%	N/A	Package inductance is significant
3	1220 MHz	35 W	63%	80 MHz (3 dB)	Stronger coupling coefficient Insufficient input matching
4	1100 MHz	60 W	65%	>150 MHz (3 dB)	Lower frequency due to passive component modeling
5	1210 MHz	74 W	67%	170 MHz (1 dB)	Better performance than previous versions

The final table compares the performance of this power amplifier to comparable recently reported amplifiers. Our amplifier has an output power five times larger than the other

amplifiers, with an area five times smaller. The bandwidth of the amplifier is also significantly higher than the other amplifiers.

Table 4.4 Comparison of Performance with Published Results

	This Work	*Long* et al. [41]	*Le Gallou* et al. [42]	*Adahl* et al. [43]
Power	74 W	13 W	10 W	10 W
Gain	11 dB	14 dB	13 dB	13 dB
PAE	67%	58%	66%	66%
BW	150 MHz (1 dB)	N/A	>50 MHz (3 dB)	50 MHz (1 dB)
Class	Class E/$F_{odd,2}$	Class D^{-1}	Class F^{-1}	Class E
Freq.	1.21 GHz	1.0 GHz	1.5 GHz	1.0 GHz
Device	Motorola Si LDMOS MRF 284	Ericsson Si LDMOS PTF 10135	UMS Custom GaAs HBT	Motorola Si LDMOS MRF 282
Size	5 cm x 3.5 cm	6 cm x 20 cm	Confidential	10 cm x 10 cm

Chapter 5

Bifurcation Stability Analysis of L-Band Power Amplifier

Power amplifiers are likely to exhibit instabilities, leading to oscillations at sub-harmonic or incommensurate frequencies. Oscillations may degrade the gain and the efficiency of the power amplifiers, cause interference with other applications, and even destroy the active devices in the power amplifiers as well as other elements in the transmitters and receivers. Since oscillations are common phenomena in power amplifiers, effective and accurate theoretical prediction of these oscillations is a critical part of power amplifier design.

When designing power amplifiers, designers often follow a set of general guidelines based on previous experiences and intuition. These guidelines are frequently helpful in reducing the probability of oscillations. However, in many other situations, spurious oscillations occur due to many reasons and are not easy to predict due to the complexity of the circuits. When oscillations occur, the process of determining the causes of oscillation may be lengthy. Trial-and-error is a common approach to stabilize the amplifier. This approach may take much iteration without eliminating the oscillations. Sometimes, eliminating one oscillation leads to the onset of another. Stabilization of power amplifiers can be one of the most frustrating parts of the design of power amplifiers.

The theme of this chapter is to introduce the nonlinear bifurcation stability analysis of power amplifiers. Taking into account of strong nonlinearity in power amplifiers, this theoretical approach effectively detects the oscillation in the amplifier, and predicts the behaviors of the oscillations. Based on the information provided by the analysis, effective stabilization techniques can be designed to ensure globally stable amplifiers. In particular, the technique is applied to the L-band power amplifier discussed in previous chapters. Based on the results of the stability analysis, three different stabilization circuits are introduced to effectively eliminate the oscillations in the amplifier.

5.1 Introduction to Stability Analysis

There are many causes of instabilities in power amplifiers. Some of the common causes include linear gain and feedback, resonant tanks in bias networks, interaction with DC power supplies, parametric oscillations due to nonlinear capacitances, and thermal feedback. The oscillations may exhibit different behaviors such as mixer-type oscillations, sub-harmonic oscillations, hysteresis and even chaotic behaviors [44][45]. Push-pull amplifiers may have common-mode oscillations and differential-mode oscillations [46][47].

Some of the causes of oscillations can be solved by simple experimental methods. For example, the bias network needs careful placement of bypass capacitors and chokes inductors. Addition of resistive elements such as ferrite beads can be helpful in providing damping effect on oscillations. These measures often eliminate low frequency oscillations due to bias networks and DC power supplies.

Other oscillations may be detected by linear stability techniques based on the *k* factor. This is particularly true for linear and weakly nonlinear power amplifiers operating in Class-A and Class-AB modes. In some nonlinear power amplifiers, the onset of an oscillation does not require an RF drive. In such cases, the *k*-factor may also be used to detect the potential oscillation.

The most difficult situations deal with situations beyond small-signal or linear analysis. Since most high-efficiency amplifiers are driven deep into saturation and are highly nonlinear, the oscillations often occur from a certain level of input power or nonlinear capacitances of the active devices. These oscillations cannot be detected with conventional techniques based on the *k* factor. Their detection requires a large-signal stability analysis of the steady-state solution. Furthermore, the linear techniques are limited only to the detection of the oscillations, but do not describe the behaviors of the oscillation described previously. In the case of push-pull amplifiers, the linear techniques do not give information about the amplitude and the phase of the oscillation.

In this section, the linear stability techniques are reviewed, and a new bifurcation analysis technique based on harmonic balance (HB) is introduced. This technique takes into account the nonlinear elements in the power amplifiers, and accurately predicts the conditions of the onset of oscillations. It also provides information describing the behavior of the oscillation, which is valuable to devising stabilization techniques.

5.1.1 Methods in Stability Analysis

5.1.1.1 Stability Analysis Based on Linear S-Parameter

The most common stability analysis in microwave amplifiers is performed based on two-port S-parameters. The detailed derivation of the method can be found in [48] and [49]. With the two-port small-signal S-parameters at a particular frequency and a particular bias condition, the input and output stability circles can be derived. The stability circles can be graphically represented on the Smith chart. These circles provide a set of source and load impedance such that the magnitudes of the input and the output reflection coefficients are less than one. The radii and the centers of the stability circles are given in (5.1) – (5.4).

Input stability circle:

$$r_S = \left| \frac{S_{12}S_{21}}{|S_{11}|^2 - |\Delta|^2} \right| \tag{5.1}$$

$$C_S = \left| \frac{\left(S_{11} - \Delta S_{22}^*\right)^*}{|S_{11}|^2 - |\Delta|^2} \right| \tag{5.2}$$

Output stability circle:

$$r_L = \left| \frac{S_{12}S_{21}}{|S_{22}|^2 - |\Delta|^2} \right| \tag{5.3}$$

$$C_L = \frac{\left(S_{22} - \Delta S_{11}^*\right)}{|S_{22}|^2 - |\Delta|^2} \tag{5.4}$$

where

$$\Delta = S_{11}S_{22} - S_{12}S_{21} \tag{5.5}$$

The stability circles focus on the interaction of the source and load impedances with the input and output impedances of the amplifier. When the result of the interaction shows negative resistance, the amplifier is potentially unstable. Practically, an array of stability circles can be drawn by sweeping the frequency and the bias conditions of the amplifier.

For the unconditionally stable condition, the *k*-factor analysis is often used. Again, the condition is only valid at one frequency and bias condition; the input signal is small signal. The unconditionally stable criteria are given in (5.6) – (5.7).

$$k > 1 \tag{5.6}$$

and

$$|\Delta| < 1 \tag{5.7}$$

where

$$k = \frac{1 - |S_{11}|^2 - |S_{22}|^2 + |\Delta|^2}{2|S_{12}S_{21}|} \tag{5.8}$$

and

$$\Delta = S_{11}S_{22} - S_{12}S_{21} \tag{5.9}$$

While the *k* factor and the stability circles are helpful tools for stability analysis of linear amplifiers, they have many limitations when used in stability analysis of nonlinear power amplifiers. First, the linear analysis technique does not account for the instability caused by the nonlinear elements in the transistor. This is particularly true for the variable capacitances in power amplifiers. As the voltage at the gate and the drain of the transistors change, the capacitances of the transistors show strong nonlinearity. As a result, the oscillation may occur due to the nonlinearity of the capacitors.

Second, the linear analysis technique does not provide the onset condition of oscillation, such as the drive frequency and the input power. While some power amplifiers exhibit self-biasing oscillations, many power amplifiers do not exhibit oscillation, unless they are driven by an external RF input source. For some power amplifiers, even if the *k* factor is below 1, no oscillations are observed. For other power amplifiers, the *k* factor may be below 1 for a range of frequencies, but only one oscillating frequency is observed. Furthermore, some power amplifiers exhibit chaotic behavior, and the *k* factor does not predict it.

Thirdly, the *k*-factor analysis does not provide information about the nature of the oscillation. There is no prediction of the amplitude and the phase of the oscillation. The amplitude and the phase of the oscillation provide useful information about the nature of the oscillation. They are therefore important to devise effective stabilization techniques. We will discuss other analysis tools to obtain these pieces of information.

As the final words in this section, *k*-factor analysis does have several practical advantages. It is very simple to calculate, and it takes very little time on today's computers. The analysis is available in many commercial microwave circuit simulation packages. The analysis does not require accurate nonlinear models of the active devices, which are often difficult to find. Instead, it only requires one set of S-parameter measurement data. If a quick and simple analysis is needed, *k*-factor may still be a nice choice.

5.1.1.2 Local Linear Stability Analysis

The purpose of this section is to give a brief overview for the linear stability analysis technique. The information is used to interpret the simulation results of the actual power amplifiers. The detailed mathematical derivations can be found in [44].

In the local linear stability analysis, a set of linear ordinary differential equations (ODEs) are used to state variables such as voltages and currents in the circuits. In general, a linear circuit can be represented by the following differential equation with initial conditions,

$$\frac{d\bar{x}}{dt} = f(\bar{x}, t)$$
$$\bar{x}(0) = \bar{x}_0 \tag{5.10}$$

where $\bar{x}$ are the state variables such as node voltages and branch currents.

In the simplest case, in which a circuit contains only passive lumped elements, stability conditions can be discussed using the solutions of the following differential equation.

$$\mathbf{C}\frac{d\bar{x}(t)}{dt} + \mathbf{G}\bar{x}(t) + \bar{u}(t) = 0$$
$$\bar{x}(0) = \bar{x}_0 \tag{5.11}$$

where $\bar{x}(t)$ represents the vector of node voltages, $\bar{u}(t)$ represents the vector of independent sources, **C** represents the generalized capacitance matrix, **G** represents the generalized conductance matrix.

While solving the differential equations in the time domain is difficult, it is possible to solve the differential equation in the frequency domain using Laplace transform. The solution in the frequency domain is then converted back to the time domain using inverse Laplace transform. The result of the analysis shows that the lumped circuit is stable if all non-zero eigenvalues (λ) of the matrix ($\mathbf{A} = -\mathbf{G}^{-1}\mathbf{C}$) have a negative real part.

$$\mathrm{Re}\{\lambda_j\} < 0 \tag{5.12}$$

This result is equivalent to all poles (s), real or complex, of the transfer function given by

$$s_j = \frac{1}{\lambda_j} \tag{5.13}$$

have a negative real part.

$$\mathrm{Re}\{s_j\} < 0 \tag{5.14}$$

The stability analysis of microwave distributed circuit requires frequency-domain analysis and the use of Nyquist criterion. We use a modified equation from the previous lumped element analysis,

$$\mathbf{C}\frac{d\bar{x}(t)}{dt}+\mathbf{G}\bar{x}(t)+\int_{-\infty}^{t}\mathbf{y}(t-\tau)\bar{x}(\tau)d\tau+\bar{u}(t)=0 \tag{5.15}$$

where $\mathbf{y}(t)$ is a matrix made up of the time-domain impulse responses of the linear distributed elements.

We take the Laplace transform of (5.15) and solve for the state variables in the frequency domain. By carefully examining the state variable $\bar{X}(s)$, it can be represented by the ratio of two functions of *s*. For zero-input case ($\bar{u}(t)=0$), if $\bar{X}(s)$ have no poles with a positive real part, the circuit is stable.

The stability conditions of a microwave distributed circuit can be represented conveniently using the Nyquist plot.

Since power amplifiers are nonlinear circuits, the stability analysis cannot be restricted to the linear case. In the next section, we will expand the theory to accommodate the nonlinearities in the power amplifiers.

5.1.1.3 Nonlinear Stability Analysis

Nonlinear bifurcation analysis extends the techniques described in the previous section to nonlinear regime. The general microwave nonlinear circuit is represented by

$$\frac{d\bar{q}(\bar{x}(t))}{dt}+\bar{f}(\bar{x}(t))+\int_{-\infty}^{t}\mathbf{y}(t-\tau)\bar{x}(\tau)d\tau+\bar{u}(t)=0 \tag{5.16}$$

Obtain the solution of the nonlinear differential equation (5.16).

Introduce a small perturbation $\delta\bar{x}(t)$

Take the linearization of the differential equation, and get the perturbation equation (5.17).

$$\frac{d}{dt}\left[\mathbf{C}\left(\bar{x}(t)\right)\delta\bar{x}(t)\right]+\mathbf{G}\left(\bar{x}(t)\right)\delta\bar{x}(t)+\int_{-\infty}^{t}\mathbf{y}(t-\tau)\delta\bar{x}(\tau)d\tau=0 \tag{5.17}$$

where

$$\mathbf{C}\left(\bar{x}(t)\right)=\left[\frac{\partial\bar{q}}{\partial\bar{x}}\right]\Bigg|_{\bar{x}=\bar{x}_0(t)} \text{ and } \mathbf{G}\left(\bar{x}(t)\right)=\left[\frac{\partial\bar{f}}{\partial\bar{x}}\right]\Bigg|_{\bar{x}=\bar{x}_0(t)} \tag{5.18}$$

Condition for local stability: a nonlinear circuit is locally stable around the steady-state solution $\bar{x}_0(t)$ if the solution $\delta\bar{x}(t)$ of the perturbed system goes to zero as t goes to infinity.

Generally, two conditions are considered. The first condition corresponds to an equilibrium point of the circuit, or the DC solution of the circuit. The second condition corresponds to the time-varying operating condition of the circuit. One special case of the second condition is considered. It is when the operating condition is a periodic in time.

5.2 Nonlinear Bifurcation Analysis

Many nonlinear analysis techniques require complex mathematical derivations. Often these mathematical approaches are relatively easy to understand as a concept, but difficult to implement in practical situations. The key advantage of the methods described here is that they can be quickly implemented in a commercial circuit simulator.

The bifurcation analysis studies the qualitative change in the behavior of a system as a function of system variables. In the case of power amplifiers, the bifurcation analysis is used to analyze the dramatic changes of behavior of the amplifier due to changing variables, such as the input power, drive frequency, bias voltages, and circuit elements (capacitors, inductors, and resistors). Qualitative changes of behavior may include the onset of an oscillation from an amplifier operation, the onset of a second oscillation from the first oscillation, and the onset of a chaotic spectrum from an oscillation. The bifurcation points are defined as the boundary points between two different types of behaviors in the power amplifier.

Since the oscillations start at the bifurcation points, the goal of this work is to detect the complete set of these bifurcation points (or bifurcation boundary), and effectively eliminate these bifurcation points.

5.2.1 Oscillation Detection Using Small-Signal Generator

The nonlinear bifurcation analysis considered in this chapter is based on Harmonic Balance (HB) simulations [50]. Harmonic Balance is widely implemented in commercial circuit simulators to simulate the large-signal or the nonlinear behavior of the power amplifiers. Let us consider the general nonlinear circuit used in HB with three kinds of elements: state variables x_n with $1 \le n \le Q$, nonlinear elements y_m with $1 \le m \le P$, and independent generators g_l with $1 \le l \le S$. The vectors of the state variables, the nonlinear elements and the independent generators are represented by

$$\begin{aligned} \bar{x}(t) &= \left(x_1(t), x_2(t), ..., x_Q(t)\right)^T \\ \bar{y}(t) &= \left(y_1(t), y_2(t), ..., y_P(t)\right)^T \\ \bar{g}(t) &= \left(g_1(t), g_2(t), ..., g_S(t)\right)^T \end{aligned} \tag{5.19}$$

In HB analysis, the set of frequencies must be chosen beforehand. It is important to realize that choosing the initial frequency basis is critical to HB simulation, because only the linear combinations of frequencies $f_1, ..., f_k$ are considered in the HB simulation. In other words, all potential oscillation frequencies in the power amplifier must be chosen prior to HB simulation. If any of the oscillation frequencies is missing, HB will not be able to analyze it. Once the frequency basis of *k* frequencies is chosen, the state variables, nonlinear components, and the independent generator can be represented by Fourier series

$$\begin{aligned} \bar{x}(t) &= \sum_{m_1=-\infty}^{\infty} \cdots \sum_{m_k=-\infty}^{\infty} \bar{X}_{m_1 \ldots m_k} e^{j(m_1\omega_1 + \ldots + m_k\omega_k)t} \\ \bar{y}(t) &= \sum_{m_1=-\infty}^{\infty} \cdots \sum_{m_k=-\infty}^{\infty} \bar{Y}_{m_1 \ldots m_k} e^{j(m_1\omega_1 + \ldots + m_k\omega_k)t} \\ \bar{g}(t) &= \sum_{m_1=-\infty}^{\infty} \cdots \sum_{m_k=-\infty}^{\infty} \bar{G}_{m_1 \ldots m_k} e^{j(m_1\omega_1 + \ldots + m_k\omega_k)t} \end{aligned} \tag{5.20}$$

Again, we see that only discrete frequency values are represented in the Fourier series representation. In order to pick a complete set of frequencies for the HB, a small-signal current source is inserted at one node of the amplifier shown in Figure 5.1. This approach is referred as the conversion matrix or large-signal/small-signal approach [50]. Under the large-signal operation determined by HB, the system is linearized, and the small-signal response of the system is calculated. The small-signal source cannot disturb the large-signal operation of the power amplifier. Depending on the complexity of the circuit, the small-signal current source may be inserted at different nodes of the circuit to detect the complete set of oscillation frequencies. In complicated circuits, such as distributed active transformer (DAT) or multi-stage power amplifiers, the current source needs to be inserted at all critical points of the amplifier. Common choices for such nodes are the gate and the drain of the transistors.

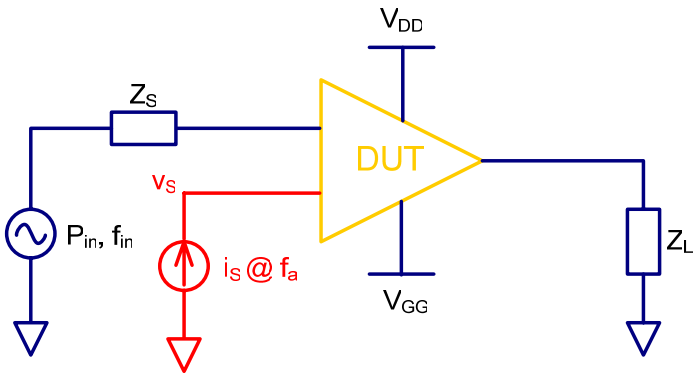

Figure 5.1. Conversion matrix approach to detect oscillations using a small-signal current source inserted at one node of the power amplifier.

After defining the current source i_s, we can also determine the voltage at the node of the amplifier v_s. We can then define an impedance function and an admittance function shown in (5.21) and (5.22).

$$Z = \frac{v_s}{i_s} \tag{5.21}$$

$$Y = \frac{i_s}{v_s} \tag{5.22}$$

Using commercial simulation tools such as ADS, Z and Y can be calculated easily while sweeping the frequency of the small-signal current generator. All frequencies f_a for $0 < f_a < f_{in}$ need to be examined carefully, where f_{in} is the drive frequency of the amplifier. Since operation of power amplifier needs to be analyzed using nonlinear simulation and the current source is a small-signal source, we need to use HB simulation with small-signal simulation option activated to perform this simulation. Once the impedance function Z and the admittance function Y is calculated, three different methods are introduced here to detect potential oscillation.

5.2.1.1 Pole-Zero Identification Technique

The poles and the zeros of the impedance function Z can be plotted on the complex plane. The poles with positive real parts are on the right-hand side of the complex planes. These poles are unstable poles. There may be unstable zeros with positive real parts appearing in the right-hand side of the complex plane. In some cases, these unstable zeros lie exactly on top of the unstable poles. In those cases, the pole-zero cancellation occurs, and no oscillation is observed. Figure 5.2 and Figure 5.3 illustrate two of the possible cases in power amplifiers. The values of the poles and zeros are listed in Table 5.1 and Table 5.2, respectively. In Figure 5.2, an L-band power amplifier is stable under a particular set of operating conditions. There are two sets of unstable poles. However, both sets of unstable poles are canceled by the two sets of unstable zeros of the admittance function. The stability performance is thereby dominated by the set of stable poles represented by the green crosses in the figure. Notice that this set of stable poles are at 208 MHz.

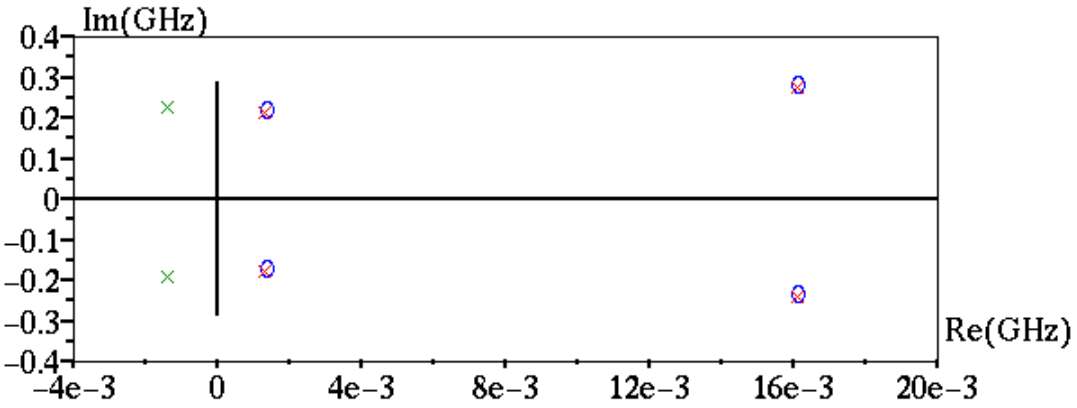

Figure 5.2. Poles and zeros of an L-band power amplifier operating in a stable condition. The green crosses represent the stable poles, pink crosses represent unstable poles, and blue circles represent zeros. There are two sets of complex-conjugate unstable poles and one set of stable poles. However, the unstable poles and unstable zeros cancel each other.

Table 5.1. Poles and Zeros of an L-Band Power Amplifier in a Stable Condition

Poles	Real ($x10^6$)	Imaginary (MHz)
	1.14	±194
	−1.53	± 208
	15.9	± 259
Zeros		
	1.14	±194
	15.9	± 259

In Figure 5.3, the same amplifier operates under an unstable condition. Now one set of previously unstable poles have moved to the left-hand side of the complex plane, so as one set of previously unstable zeros. The previously stable poles at 208 MHz, however, have moved to the right-hand side, making the poles unstable. This creates an oscillation at 208 MHz, which is verified experimentally.

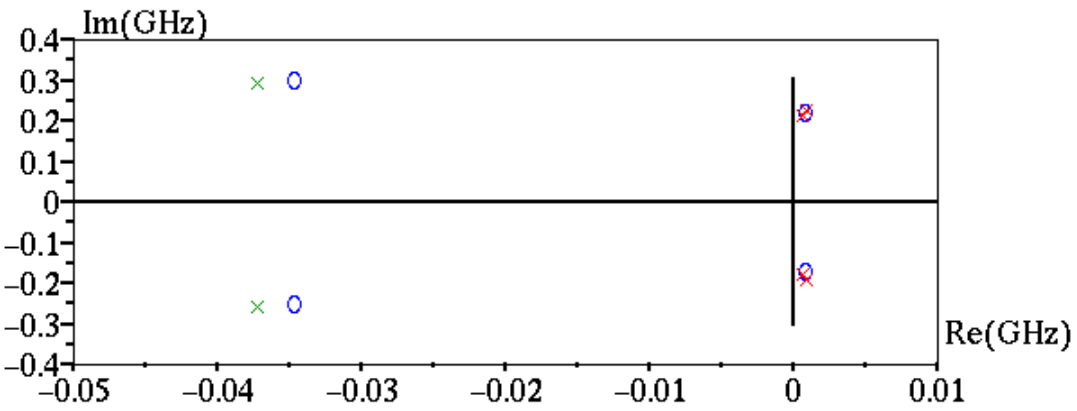

Figure 5.3. Poles and zeros of an L-band power amplifier operating in an unstable condition. There are two sets of complex-conjugate unstable poles and one set of stable poles. Only one set of unstable poles are canceled. Therefore, the amplifier is unstable due to the other set of unstable poles.

Table 5.2. Poles and Zeros of an L-Band Power Amplifier in an Unstable Condition

	Real ($\times 10^6$)	Imaginary (MHz)
Poles		
	0.255	±196
	0.537	±208
	−37.6	±274
Zeros		
	0.255	±196
	−35.2	±274

5.2.1.2 Kurokawa's Condition

Another start-up condition for oscillation is demonstrated by Kurokawa [51]. When plotting the real part (the conductance) and the imaginary part (the susceptance) vs. generator frequency, the oscillation condition is obtained for negative conductance and the zero-crossing of susceptance with a positive slope. Figure 5.5 demonstrates the use of this condition to determine stable and unstable conditions of the amplifier. Note that Figure 5.4 and Figure 5.5 correspond directly to the pole-zero analysis in Figure 5.2 and Figure 5.3. In Figure 5.4, as the susceptance crosses the real axis at 208 MHz, the conductance is positive, which indicates stable operating condition. In Figure 5.5, as the susceptance crosses the real axis at 208 MHz, the conductance is positive, indicating unstable operation.

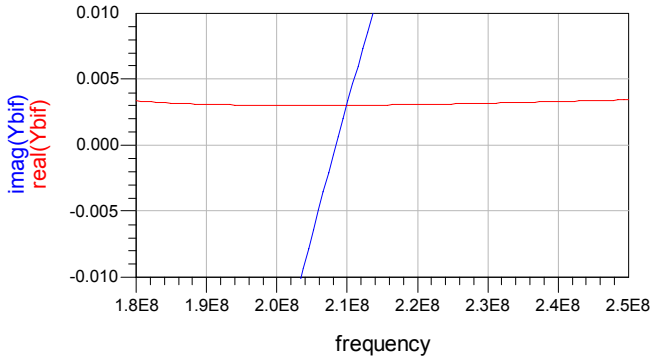

Figure 5.4. Plot of the real and imaginary parts of the admittance function vs. frequency demonstrate the use of Kurokawa's condition to determine the stability conditions. Power amplifier operating in a stable condition.

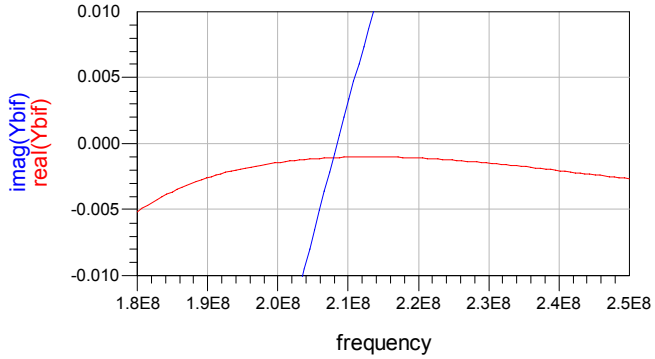

Figure 5.5. Plots of the real and imaginary parts of the admittance function vs. frequency demonstrate the use of Kurokawa's condition to determine the stability conditions. Power amplifier operating in an unstable condition.

5.2.1.3 Admittance Plot

The third tool for detecting oscillations is to plot the imaginary part of the admittance vs. the real part of the admittance, while sweeping current generator frequency. The analysis is analogous to Nyquist criterion. If the graph crosses the real axis with a negative admittance, the oscillation is likely to start. Figure 5.6 shows that the power amplifier operates in a stable condition, while Figure 5.7 shows that the amplifier operates in an unstable condition. Again these cases correspond to the stable and the unstable conditions in sections 5.2.1.1 and 5.2.1.2.

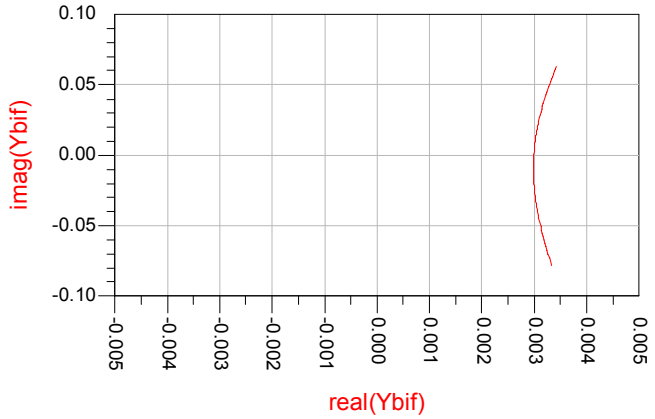

Figure 5.6. Admittance plots showing stable conditions of the amplifier.

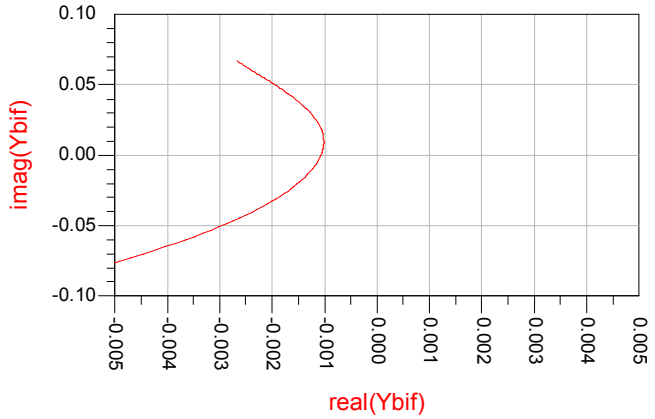

Figure 5.7. Admittance plots showing unstable conditions of the amplifier.

It is important to note that the Kurokawa's condition and the admittance plot techniques are essentially the same techniques, which always lead to the same conclusion. The pole-zero identification technique is an independent technique, which can be used to verify the results of the other two techniques. Also the same procedures need to be repeated for the circuit operating in other bias conditions, drive frequency and input power. It is a critical step because the mistakes in formation of frequency basis will lead to errors in the conclusions of the stability analysis.

5.2.2 Determination of Stability Contour

Different techniques [44][45][46][47][48], based on harmonic balance (HB), have been proposed for this analysis. In case of variation of circuit parameters, the boundary between

stable and unstable operation can be efficiently determined through bifurcation detection on HB [44][45]. Using the conversion matrix approach described in the previous section, the small-signal admittance matrix is calculated based on large-signal operation. To determine the boundary between the stable and the unstable regions, the non-perturbation, $Y = 0$, must be satisfied. Since the admittance function is complex, both the real part and the imaginary part of *Y* are set to zero. Using the two equations $\mathrm{Re}\{Y\} = 0$ and $\mathrm{Im}\{Y\} = 0$, two circuit variables can be solved simultaneously.

In general, the amplifier will operate under different values of bias voltages and different input frequency and input power, so the bifurcation analysis should be carried out in terms of all significant operation parameters. This global analysis will be applied here to a push-pull power amplifier, in the band from 1.1 GHz to 1.3 GHz. The results are shown in the later part of this chapter.

5.2.3 Bifurcation Analysis Using Auxiliary Generator

Auxiliary generator (AG) is another useful technique to analyze the behavior of the power amplifier and other nonlinear circuits. The use of this approach is very broad, and most of the applications are beyond the scope of the thesis. One useful feature of this technique is the determination of the phase information of the oscillation signal. This information cannot be determined from the conversion matrix technique.

A schematic of the auxiliary generator applied to a power amplifier is shown in Figure 5.8. Unlike the small-signal current source in the conversion matrix approach, the AG is a large-signal signal source. Two important pieces of information contained in the large-signal source are the amplitude and the phase of the signal. This makes the AG approach more versatile than the conversion matrix approach. However, in some cases, the AG approach is much slower than the conversion matrix approach due to the large-signal nature of the AG.

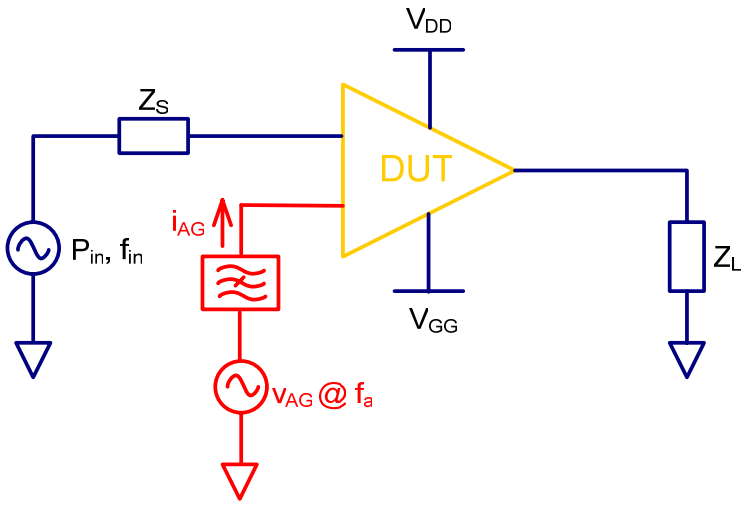

Figure 5.8. Schematic of auxiliary generator applied to a power amplifier.

Similar to the conversion matrix technique, the admittance function *Y* is calculated.

$$Y = \frac{I_{AG}}{V_{AG}} \tag{5.23}$$

The non-perturbation condition is solved to determine the amplitude and the phase of the oscillation. The result of the phase information is shown in the later part of the chapter. The phase information is used to determine whether the oscillation is even mode or odd mode.

$$\begin{aligned} \mathrm{Re}\{Y(f_a, V_{AG}, \phi_{AG})\} = 0 \\ \mathrm{Im}\{Y(f_a, V_{AG}, \phi_{AG})\} = 0 \end{aligned} \tag{5.24}$$

5.3 Application to L-Band Power Amplifier

Figure 5.9 shows the simplified schematic of our push-pull amplifier. The amplifier is optimized for a Class-E/$F_{odd,2}$ operation [52]. When backing off from deep nonlinear regions, it can also be operated in other modes, such as Class AB, and Class B. When operating in the Class-E/$F_{odd,2}$ mode, this amplifier has zero-voltage switching like a Class-E amplifier, while the odd harmonics and the 2nd harmonic are terminated like a Class-F^{-1} amplifier.

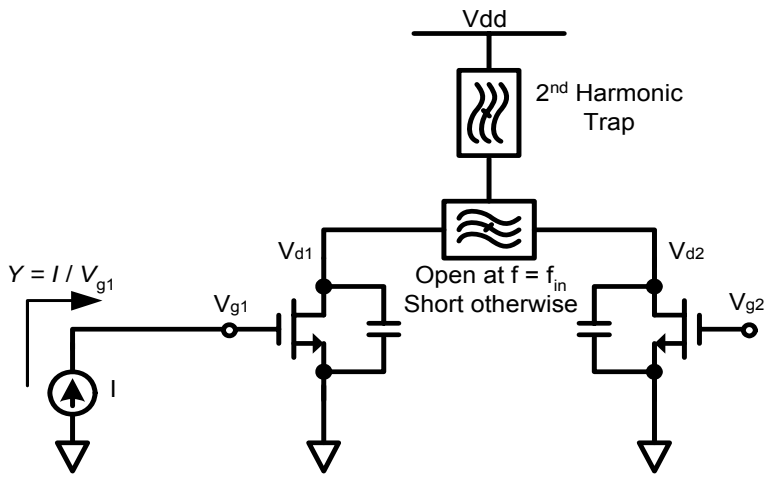

Figure 5.9. Simplified schematic of the Class-E/$F_{odd,2}$ amplifier.

During the operation of the Class-E/F amplifier, low-frequency oscillation is observed at around 200 MHz. This oscillation is only obtained at certain combination of input power, drive frequency, and drain and gate bias voltages. The oscillation frequency shifts slightly at different bias voltages and different input power. One example of the oscillation spectrum is shown in Figure 5.10. In this particular amplifier, no self-biasing oscillation is observed.

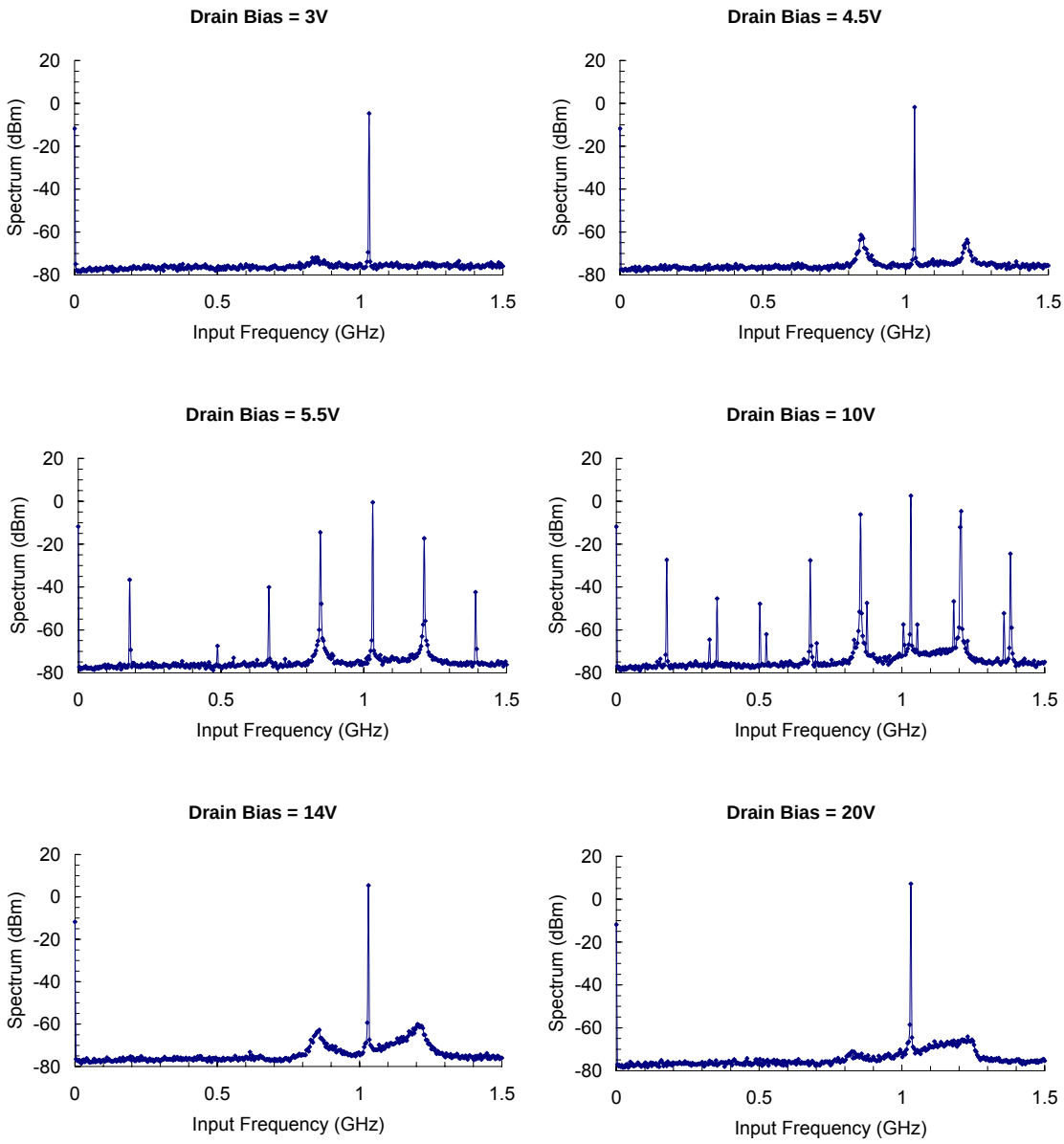

Figure 5.10. Oscillations in L-band power amplifier. The oscillation occurs at about 200 MHz. The oscillation is drive frequency is 1030 MHz, with the input power and gate bias voltage fixed. As the drain voltage increases, the low frequency oscillation is observed when drain bias is at 4.5 V. Mixer-type oscillation is observed, and vanishes when drain bias voltage reaches 20 V.

The above system is solved through error-minimization or optimization procedures, combining HB and the conversion-matrix approach. The analysis is performed for different V_D and constant $V_G = 3$ V, obtaining the loci of Figure 5.11. The frequency f_{in} is swept, calculating, at each step, P_{in} and the oscillation frequency f_a, which varies along the locus. As confirmed by pole-zero identification, the instability occurs at medium input power, where the gain is the highest. As the drain-bias voltage increases, the instability region shrinks due to reduced feedback through the gate-drain capacitance (C_{gd}). For $f_{in} > 1.14$ GHz, no instability is obtained at any of the considered bias voltages. Measurements are superimposed.

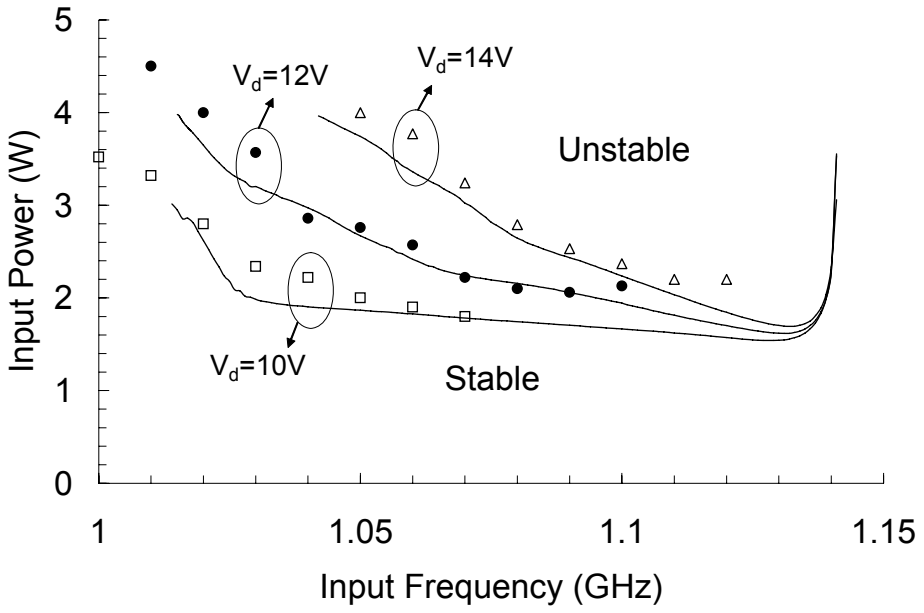

Figure 5.11. The boundaries between the stable and unstable regions based on global-stability analysis of the amplifier, for different operation conditions. Lines indicate simulation results, and markers indicate measurement points. In the plane defined by f_{in} and P_{in}.

The second analysis is carried out in the plane defined by V_G and V_D (Figure 5.12), solving:

$$\begin{aligned} \mathrm{Re}\{Y(f_a, V_G, V_D)\} &= 0 \\ \mathrm{Im}\{Y(f_a, V_G, V_D)\} &= 0 \end{aligned} \tag{5.25}$$

Constant $f_{in} = 1.03$ GHz and two typical operation P_{in} values have been considered, with the results of Figure 5.12. In agreement with the pole-zero identification technique, the

amplifier is unstable inside the different loci. The unstable behavior is observed in different operating modes: Class AB, Class B, and Class C. However, the instability region is smaller for the Class-C operation, which corresponds to lower V_G. At higher V_D, oscillation vanishes due to smaller feedback capacitance.

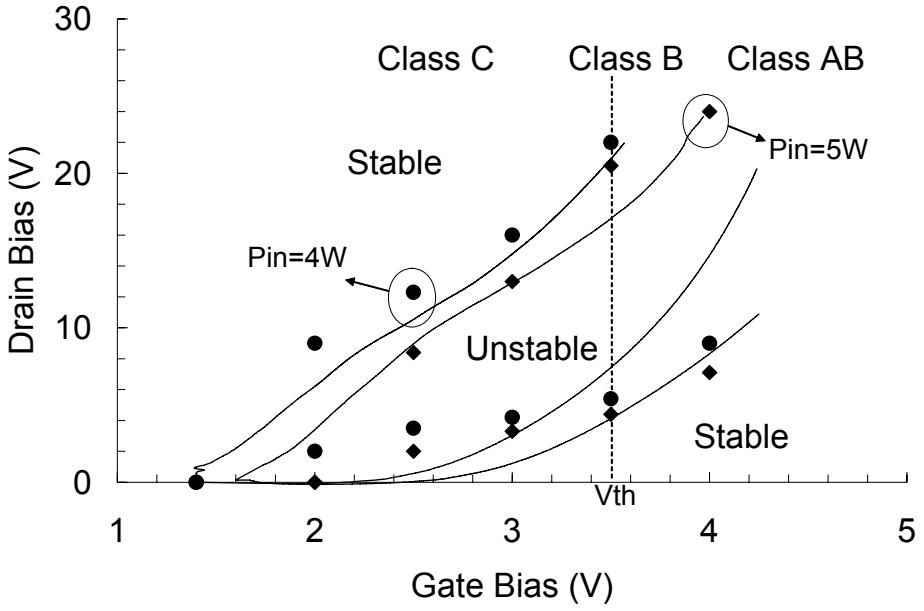

Figure 5.12. The boundaries between the stable and unstable regions based on global-stability analysis of the amplifier, for different operation conditions. Lines indicate simulation results, and markers indicate measurement points. In the plane defined by V_G and V_D.

5.4 Stabilization Techniques

The actual design goal will be the stabilization of the amplifier, and the knowledge of the instability regions in the parameter space, together with the analysis of the oscillation mode, will be helpful to devise a proper stabilization technique. Three different techniques will be considered here, based on the use of odd-mode stabilization resistor, neutralization capacitors, and feedback resistors. The use of bifurcation analysis enables efficient determination of the element values of each stabilization network. The performances of the resulting stabilized amplifiers will be compared, in terms of output power and efficiency.

The nature of the oscillation has been investigated obtaining the steady-state solution within the unstable regions, where the amplifier behaves as a self-oscillating mixer, at the two fundamental frequencies f_{in} and f_a. An auxiliary generator (AG) has been used, in order to avoid the HB convergence to the unstable periodic solution at f_{in} [44]. The transistor harmonic voltages at the input-drive and oscillation frequencies are compared in Table 5.3, for $V_G = 3.5$ V, $V_D = 7$ V, $P_{in} = 3$ W, $f_{in} = 1030$ MHz. The voltages exhibit a phase difference close to 180º at both f_{in} and f_a. Thus, there is an odd-mode oscillation. In the following, three different stabilization techniques will be considered.

Table 5.3 The phases of voltages at the gate and drain terminals

	V_{g1}	V_{g2}	V_{d1}	V_{d2}
f_a (200 MHz)	0°	180°	−98°	72°
f_{in} (1030 MHz)	−137°	43°	−84°	96°

5.4.1 Stabilization with an Odd-Mode Stabilization Resistor

Based on the result shown in Table 5.3, we see an odd-mode oscillation at 200 MHz. The odd-mode oscillation can be eliminated through the connection of a resistor between the gate terminals of the two transistors shown in Figure 5.13. Since the oscillation frequency (200 MHz) is sufficiently lower than the operating frequency of the amplifier, inductors may be used to block the signal at the operating frequency. Thus, the input power from the input drive will not be dissipated in the stabilization resistor. Using the half-circuit analysis for the odd-mode oscillation at 200 MHz, the stabilization resistor is in parallel with the gate of the transistors, thereby shunting the oscillation signal to ground.

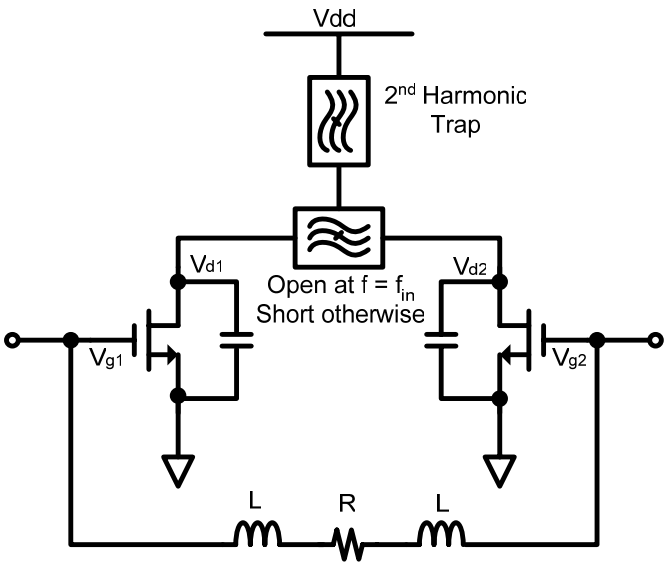

Figure 5.13. Schematic of stabilization circuit using odd-mode stabilization resistor.

The maximum allowed value for the stabilization resistor R is obtained by tracing the oscillation boundary in the plane defined by R and one of the four circuit parameters. In the analysis of Figure 5.14, the considered parameter is f_{in} and the oscillation boundary is determined for different P_{in} and bias values. The amplifier is unstable on the right-hand side of the represented loci. Note that the selected bias values correspond to the edges of the operation intervals. Due to the continuity of the system, this provides information about the required resistance for a general stabilization of the amplifier, for all the operation conditions. In order to avoid the instability, the amplifier must operate outside the instability regions for all the f_{in} values. Thus, the maximum allowed value for the stabilization resistance is 200 Ω.

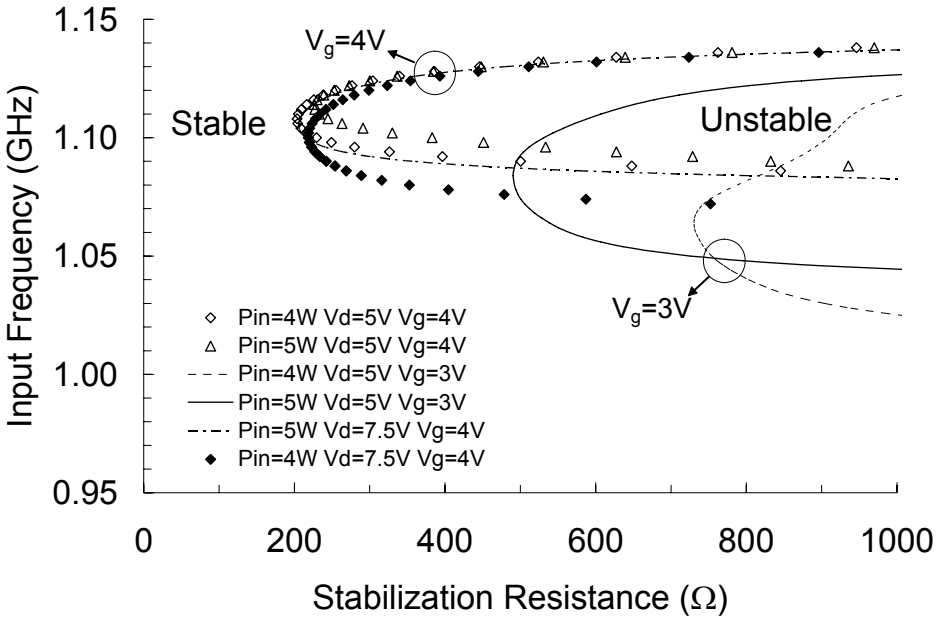

Figure 5.14. Stabilization with an odd-mode stabilization resistor. Typical operation conditions have been considered in these simulations.

The global stabilization is verified using the admittance plots (Figure 5.15). Different curves in the plots represent different operating conditions, sweeping the bias voltages, input power, and the input frequency. When no stabilization resistor is implemented, the amplifier is unstable at certain operating points, because the curves cross the real axis with negative conductance values. As stabilization resistors are implemented, the curves shift to the right-hand side of the complex plane. As the stabilization value reaches 200 Ω, the amplifier is globally stable for all operating conditions.

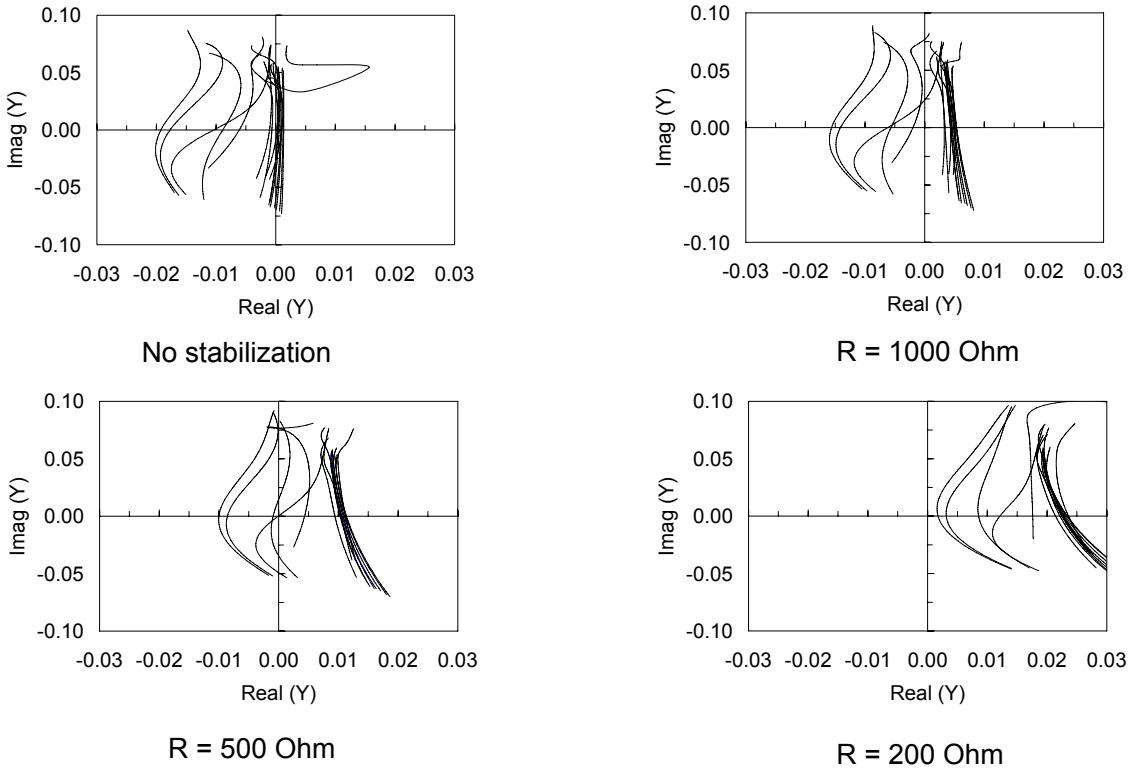

Figure 5.15. Admittance plot for various stabilization resistances. For clarity purposes, only a portion of the representative curves are shown.

5.4.2 Stabilization with Neutralization Capacitors

In push-pull configurations, neutralization capacitors can be connected between the gate and drain terminals of the opposite transistors to cancel undesired feedback through C_{gd} shown in Figure 5.16. Since the oscillation is odd-mode, it is clear that the feedback through the neutralization capacitor is 180^{o} out of phase with the feedback through C_{gd}. The two signals at 200 MHz therefore are cancelled to achieve stabilization. Effectively, a negative capacitance is added in parallel to C_{gd}.

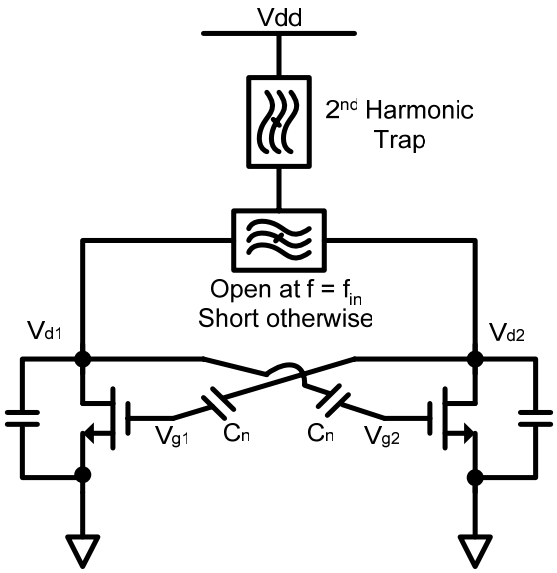

Figure 5.16. Schematic of stabilization circuit using neutralization capacitors.

To determine the minimum capacitance value required for stable operation, the oscillation boundary will be traced on the plane defined by C_n and f_{in}, considering different P_{in} values and bias conditions. For clarity, only two loci have been represented in Figure 5.17. To ensure stable behavior for all the operating conditions, the entire set of bifurcation loci must be taken into account. From this global analysis, the neutralization capacitance should be larger than 25 pF.

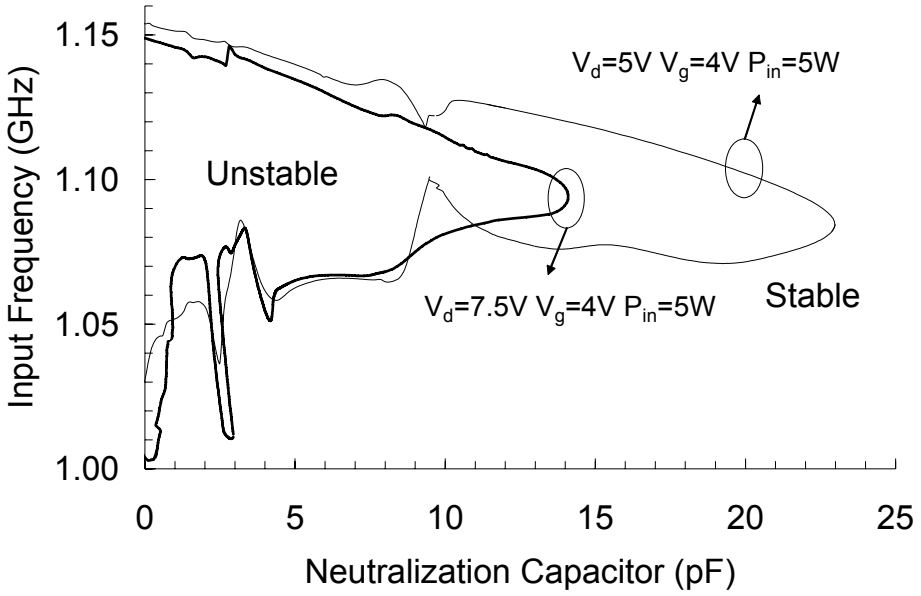

Figure 5.17. Stabilization with neutralization capacitors using bifurcation loci. For clarity reasons, only two representative sets of curves are shown.

5.4.3 Stabilization with Feedback Resistors

In order to reduce the positive feedback, a resistor and a DC-blocking capacitor are connected between the gate and the drain terminals of the same transistor, shown in Figure 5.18. Only limited power is dissipated, as parasitic inductances of the two elements provide high impedance at f_{in}, which is about five times the oscillation frequency. These parasitic inductances do not have a significant effect on the feedback resistance at f_a. The bifurcation-analysis technique indicates the maximum value of stabilization resistance of 90 Ω, shown in Figure 5.20.

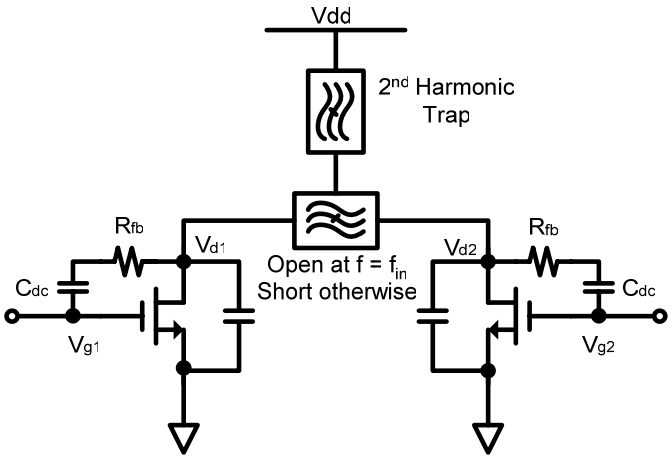

Figure 5.18. Stabilization circuit using feedback resistors and DC-blocking capacitors.

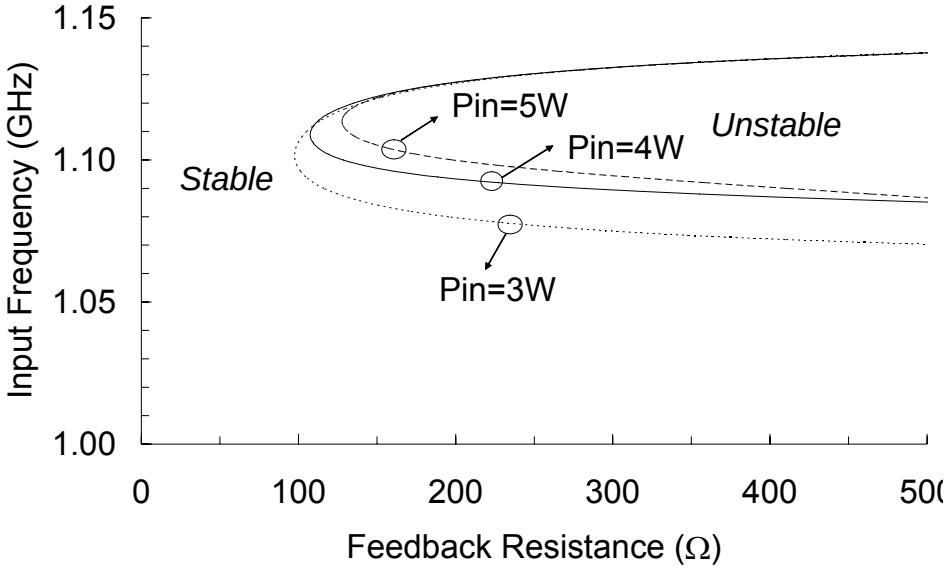

Figure 5.19. Stabilization with feedback resistors. Typical operation conditions have been considered in these simulations.

5.4.4 Comparison of Performance

Figure 5.20 shows the comparison of the stabilized-amplifier performance for the three different stabilization techniques. The resistive stabilization techniques show little change in performance. The neutralization capacitors improve the gain of the amplifier by about 2 dB, but the PAE is reduced by 6%. In this particular amplifier, neutralization is not easy to implement due to layout constraints. The odd-mode resistor is implemented in the

amplifier. Figure 5.21 shows the gain and the PAE at 1210 MHz before and after applying the odd-mode stabilization. The measured performances are almost identical.

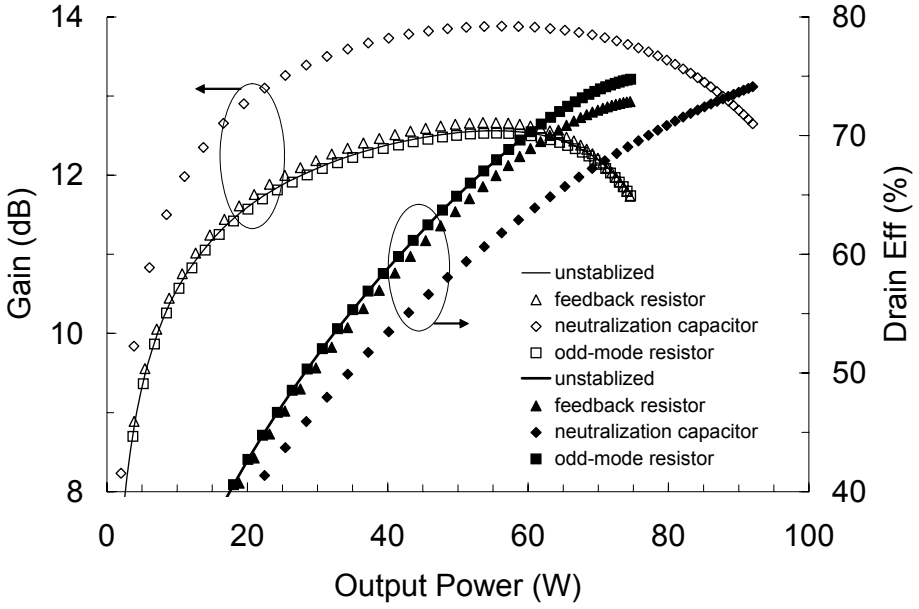

Figure 5.20. Simulated amplifier performance after applying three different stabilization techniques.

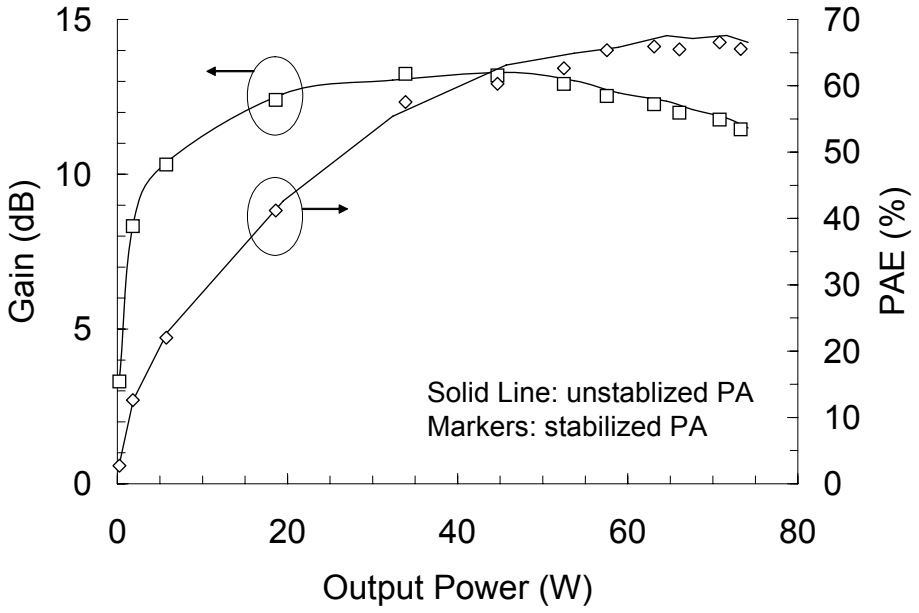

Figure 5.21. Measured amplifier performance before and after applying odd-mode stabilization resistor of 150 Ω.

5.5 Summary

In this chapter, the global stability analysis of an LDMOS amplifier has been presented. Four parameters—two bias voltages, the input power and the input frequency—have been considered. After determination of the oscillation mode, three different stabilization techniques have been compared. For each approach, the values of the stabilization elements ensuring stable behavior for all the operation conditions have been determined through bifurcation analysis.

Chapter 6

Future Opportunities

As discussed in Chapter 1, discrete high power amplifiers have many applications in the fields of wireless communications and space technologies. It is no surprise that improvements can always be made for the future applications and technologies. The development of new semiconductor devices, particularly SiC and GaN, has opened new horizons for better performing power amplifiers. At the same time, more efficient power combining techniques, such as DAT, as well as other transformers and baluns, can be used to achieve high output power at higher frequency.

6.1 New Transistor Technologies

In this section, current state-of-the-art power transistor technologies are reviewed. The new immerging devices, such as SiC and GaN, are discussed. The performance of these technologies is compared. A singled-ended Class-E amplifier based on the SiC MESFET is built, and the preliminary results are presented.

The table below compares the most popular semiconductor materials for discrete power amplifiers from HF frequency up to 3.5 GHz. It is clear that SiC and GaN wider bandgaps and higher breakdown field. Because of these properties, they achieve much higher power density than Si and GaAs.

Table 6.1. Key Properties Comparison for Microwave Power Transistors

Properties	*Si*	*GaAs*	*SiC*	*GaN*
Bandgap (eV)	1.12	1.42	2.86	3.45
Thermal conductivity (W/^{o}C cm)	1.5	0.54	4.9	1.3
Breakdown field (KV/cm)	3×10^{5}	4×10^{5}	2.5×10^{6}	2×10^{6}
Saturated electron velocity (cm/sec)	1×10^{7}	1×10^{7}	2×10^{7}	2.2×10^{7}
Relative permittivity	11.9	12.5	10	9

6.1.1 Si and GaAs Devices

There are many different choices of RF power devices between 1 and 2 GHz. The selection criteria for such devices include power density, power gain, efficiency, output capacitance, on-resistance, bias voltage, input and output impedances, thermal conductivity, availability, reliability, cost, etc.

Currently, the dominating technologies in L-Band high power amplifiers are Si LDMOS, VDMOS and GaAs based power devices including GaAs HBT's and GaAs MESFETS. Below 500 MHz, VDMOS achieves nice performance, while LDMOS has been the most widely used technology from 500 MHZ to 2 GHz. GaAs HBT's and MESFET's have shown superior performances beyond 2 GHz, but they are several times higher in cost.

Si VDMOS and LDMOS have the lowest cost of all RF power devices. They have lower power density than GaAs power devices. However, the operating voltage is around 28 V, which is higher than that of typical GaAs devices. High drain bias voltage is preferred in the class-E/F_{odd} power amplifiers.

The modeling of LDMOS power transistors is quite mature. Some manufacturers, such as Motorola, provide excellent large signal models, which are also compatible with circuit simulation software like Agilent ADS. Both the small signal and the large signal models are fairly accurate.

GaAs HBT and MESFET have the higher power densities than Si VDMOS and LDMOS. They operate at around 12V, but can handle more current than the Si devices. Recently, there is development of high-voltage GaAs devices, which are operated at 28V like LDMOS. The thermal conductivity of GaAs is not as good as Si. The performance of a GaAs power amplifier at 1 GHz is similar to LDMOS amplifiers, but at higher frequency above 2 GHz, GaAs amplifiers still hold some advantages.

6.1.2 SiC and GaN Devices

Another important development in the last several years is the emergence of wide bandgap semiconductors SiC and GaN for high power RF applications. These devices exhibit superior properties, such as high electric breakdown field, high power density, high saturated electron drift velocity, and in the case of SiC, high thermal conductivity.

The drawback of these devices is that they are still not as reliable and are not widely available commercially. The costs of these devices are several times higher than their Si and GaAs counterparts. Also, the modeling of these devices is not as mature as Si and GaAs devices. Designers have to use many crude models to estimate the performance of the amplifier. The lack of accurate large signal models significantly increases the difficulty and the length of time to do the power amplifier design.

One major consideration of power devices for switching power amplifiers is the output capacitance. Traditionally, the operating frequency of the switching power amplifier is limited by the output capacitance of the device. Even though new techniques have been developed in this work to exceed this limit, a lower output capacitance can be advantageous. However, power devices are typically large in size, thereby having very large input and output capacitances and low input and output impedances. Low input and output impedances increase the difficulty of the design of the amplifier. They also limit the bandwidth and increase the complexity and the size of the power amplifier.

SiC MESFETs are very promising power devices in RF frequencies. They have much higher power density than Si LDMOS and GaAs. Because of that, the SiC devices are significantly smaller than LDMOS devices and GaAs devices for the same output power. The output capacitance of the device is smaller than LDMOS and GaAs devices. Smaller SiC devices lead to high input and output impedances. This property greatly simplifies the input and the output circuits of the power amplifier. Figure 6.1 shows the comparison of L-band power devices: a Freescale Si LDMOS and a Cree SiC MESFET. Both devices have nominal output power of 10W. As we can see from the photo, both devices apparently have the same size package. As we take a closer look at the specifications in Table 6.1, we see that the output capacitance of the Freescale LDMOS transistor is 8 pF at the operating

voltage and the output capacitance of the Cree SiC MESFET is 1.9 pF at the operating voltage. The low output capacitance property can significantly simplify the output matching circuit, and improve the efficiency of the power amplifier. It is now possible to build a broadband 5W PA from 20 MHz to 2.5 GHz, using one SiC transistor.

Figure 6.1. Photos of two 10W L-band power transistors: Freescale MRF282S Si LDMOS (left) and Cree CRF 24010 SiC MESFET (right).

Table 6.2. Comparison of Key Specifications of LDMOS and SiC Devices

Properties	***Si LDMOS***	***SiC MESFET***
Maximum V_{DS}	65 V	120 V
1dB Output Power	10 W	10 W
Output Capacitance	8.0 pF at Vds = 26 V	1.9 pF at Vds = 48 V
Operating Voltage	26 V	48 V

The measured input and output impedance (provided by Cree) of the SiC MESFET are shown in Figure 6.2. The input resistance of the device is about 5.5 Ω. This impedance is about 5 times higher than the Si LDMOS counterpart, which has an input resistance about 1 Ω. This comparison shows that there is a great potential for broadband amplifiers using these SiC devices.

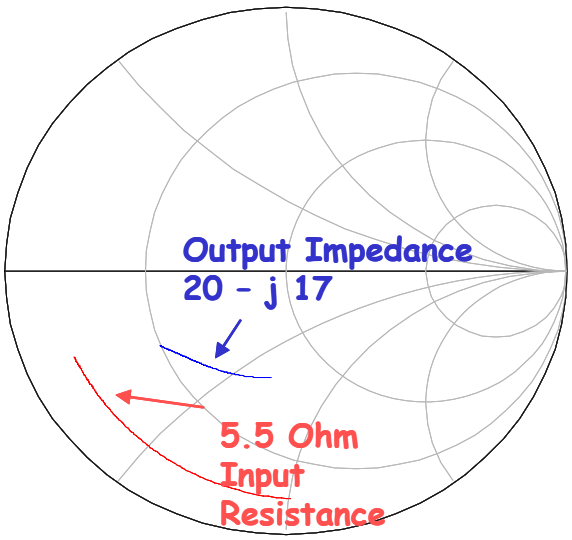

Figure 6.2. Measured input and output impedance of the SiC MESFET.

While both SiC and GaN have very high power density, SiC has an advantage over GaN in thermal conductivity. SiC has much higher thermal conductivity than Si LDMOS, GaAs devices, and GaN devices. This device is suitable for operating at relatively high temperature.

Currently, the only commercially available SiC power transistors are from Cree, Inc. The only power device outputs 60W per transistor. The output power capability is not nearly as high as the state of the art LDMOS and GaAs power devices, which can output over 200 W.

The modeling of the SiC is not mature. There is no high frequency large signal model available from the manufacturer. The only model provided is the S-parameter data at certain bias points. In order to design power amplifiers with SiC transistors, designers need to make their measurements of the devices in order to gain insights that are critical for power amplifier design. The design cycle may be longer due to the lack of accurate models.

The GaN HEMT has the highest power density among all devices. GaN HEMTs also have superior current handling capability. However, GaN devices suffer from low thermal handling capabilities. Therefore, they are grown on the SiC or Si substruates. Also, GaN

HEMT shares some of the problems with SiC devices, such as lack of large signal models and reliability problems. Recently, there are some commercially available GaN HEMT devices by Eudyna. Since the GaN devices have the highest power density in the group, we may expect to see great performance by these devices.

6.1.3 SiC Class-E Power Amplifier

The active device used in the Class-E amplifier is Cree CRF-24010. Due to the lack of nonlinear model of this device, it is difficult to optimize a push-pull design in a short period of time. In particular, the tuning of the second harmonic and third harmonic are difficult. DC measurement of the device is performed, and the on-resistance is extracted from the DC curves. The nonlinear output capacitance of the amplifier is approximated using a reverse-biased diode model. The Class-E amplifier is then built and tested. The layout and the photo of the amplifier are shown in Figure 6.3 and Figure 6.4.

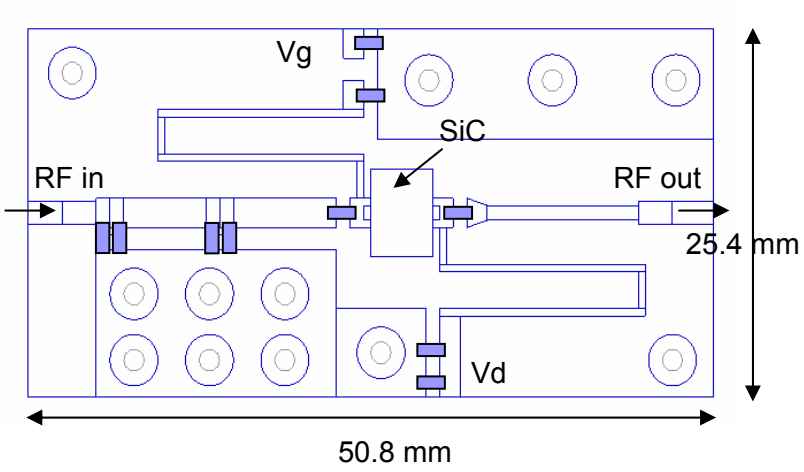

Figure 6.3. Layout of SiC Class-E power amplifier

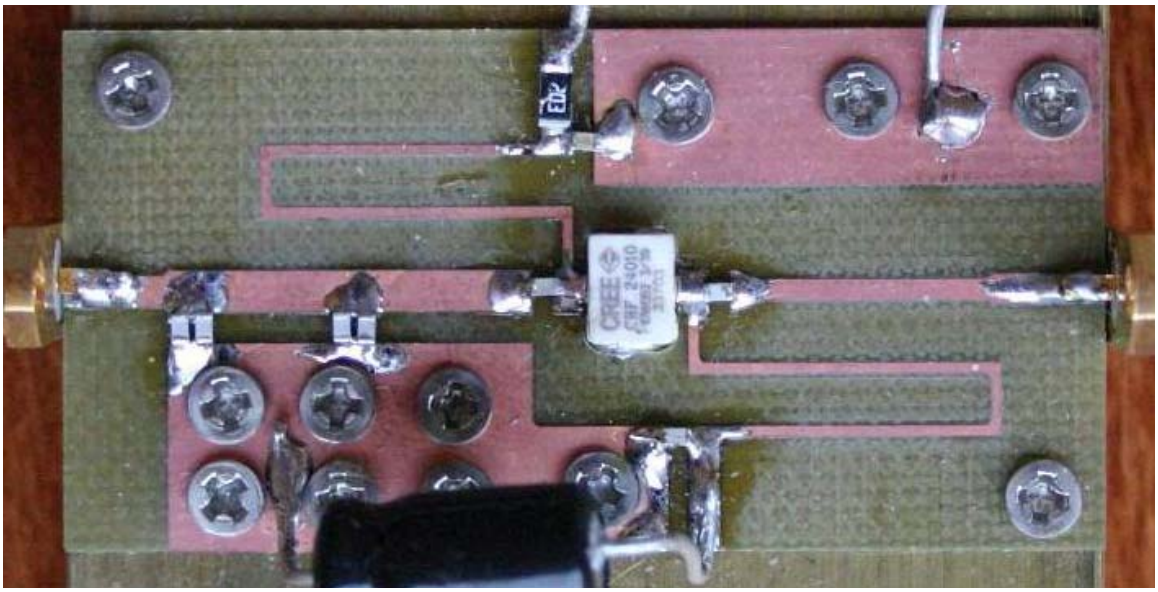

Figure 6.4. Photo of Class-E SiC power amplifier.

The preliminary performance of the Class-E amplifier is shown in Figure 6.5. The peak output power is 19W with a power gain of 9 dB. The peak PAE is 65%. It is worth noting the bandwidth of the amplifiers. Even without an accurate model, the gain remains very flat over a broad frequency band, from 980 MHz to 1200 MHz.

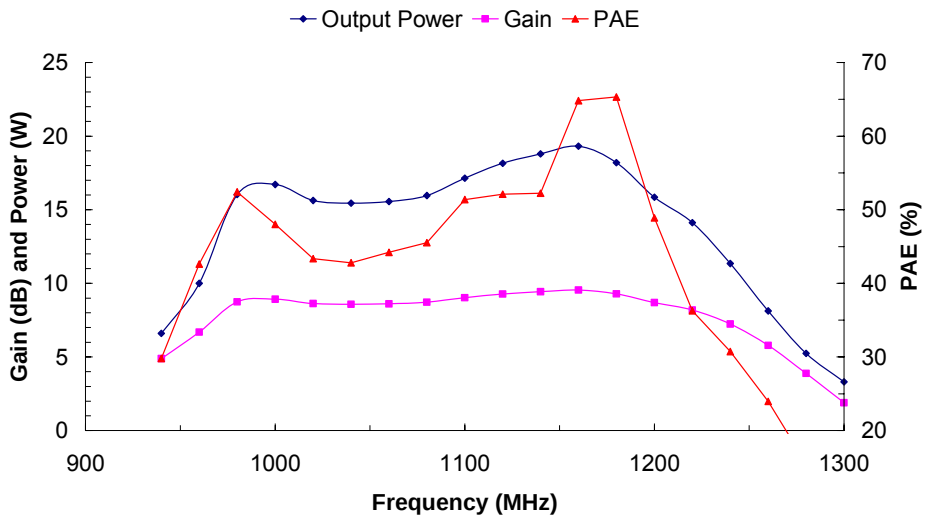

Figure 6.5. Measurement bandwidth performance of the SiC power amplifier.

6.2 Modeling for Switching-Mode Amplifiers

It may seem strange that almost no transistor modeling has been discussed up to this point in the dissertation on power amplifiers design. The simple answer to this is that there is no easy route to obtain an accurate nonlinear model at microwave frequency for harmonic balance simulation. Most of the L-band high-power amplifiers are based on one of the following models.

The simplest model is based on the assumption of a Class-AB design. One set of linear S-parameter is measured at one single bias point, and the input and output matching are designed based on the linear matching network. It is well known that the large-signal behavior of the transistor is very different from the small-signal behavior. This kind of the design is clearly not accurate. Extensive tuning has to be performed manually after the building the circuit, and many iterations of re-designs are typically required.

The second approach is the opposite extreme of the first approach. Expensive equipment, such as nonlinear vector network analyzers, is used. Also, the measurements are performed at an exhausting range of conditions. Then a complex system is used to collect all measurement data to provide an accurate, often table-based model. Some of the models used in designing the Class-E/F amplifiers described in the thesis are based on this approach. The advantage of the approach is that the model is accurate for a wide range of conditions. The disadvantage is the cost is high and the process is time consuming. Another problem with the approach is that the table-based model does not provide equivalent circuit model, which is needed for useful insights for the circuit design.

Another approach to switching-mode amplifiers is the simplified switch model shown in Figure 6.6. The transistor output characteristics are modeled using a simple switch in series with an ON resistance, and in parallel with the device output capacitance. At microwave frequencies, it is important to include the package inductance of the device. The advantage of this approach is that the nonlinear output capacitance can be modeled as a function of drain bias voltage, and the design of the output termination network is based on the

nonlinear output capacitance and the package inductance. The voltage and current waveforms can be simulated and optimized easily to achieve high efficiency. The difficulty with this approach is that the measurement of the output capacitance is difficult. At this frequency, it is difficult to separate the measurement of the output capacitance C_{ds} from the feedback capacitance C_{dg}.

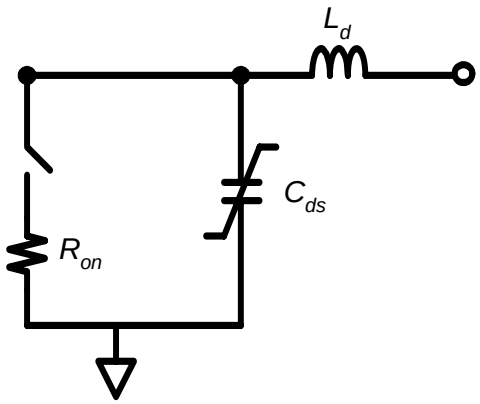

Figure 6.6. Switch model of the transistor output circuit.

It is necessary to come up with a set of simple measurements and extract the critical nonlinear elements in the transistor model and optimize the waveforms of the amplifier based on the equivalent circuit model shown in Figure 6.7.

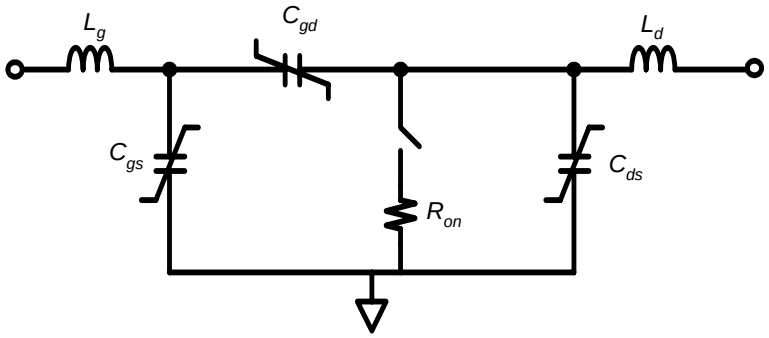

Figure 6.7. Simplified switch model for the input and the output circuit of the transistor.

The on-resistance of the power device is an important property of the switching power amplifiers. The resistive dissipation of the power amplifier is directly related to the on-resistance of the power amplifier. Lower on-resistance translates directly to lower resistive

loss in the amplifier and high efficiency. The on-resistance can be determined by measuring the DC IV characteristics of the device.

The input, output, and feedback capacitors can be extracted from S-parameter measurement using the network analyzer. The nonlinearity of the capacitance can be modeled by fitting a curve for a variety of bias conditions.

6.3 Discrete L-Band DAT[1]

As introduced in Chapter 3, the Distributed Active Transformer is a promising candidate for effective power combining and impedance transformation. Ichiro Aoki's original designs are integrated CMOS amplifiers at 2.4 GHz [4] and then 1.9 GHz. A discrete version of DAT in Class-E/F mode is implemented at 29 MHz to achieve 2.7 kW of output power with high efficiency [35]. A natural question is: can this discrete version of DAT be implemented at L-band? We will look at some of the challenges and possibilities in this section.

6.3.1 Challenges in Discrete L-band DAT

Perhaps the biggest challenge in designing an L-band discrete DAT is the layout problem. If we assume that theoretical designs indicate that it is possible to combine output power of eight transistors, the size of the DAT may be too large for an ideal operation. If we calculate the electrical length of the previous DAT amplifiers, we see that since the L-band power transistors are much larger in size, the layout with larger transistor packages like MRF 284 used in the amplifier is extremely difficult. However, since DAT structure combines the output power of eight transistors, we can afford to use smaller transistors with less power for the power combining, and still achieve higher total output power than the push-pull amplifiers designed in this thesis.

The second challenge to implement as a design is the high device output capacitance, discussed several times in the thesis. Using the typical DAT, the operating frequency of the amplifier is limited by the output capacitance of the transistors. One solution to this is

[1] This portion of the work is collaborated with Sébestien Lasfargus.

similar to the technique discussed in Chapter 3 by inserting an external capacitor at the output of the DAT as shown in Figure 6.8. We can use this external capacitor to increase the operating frequency of the amplifier.

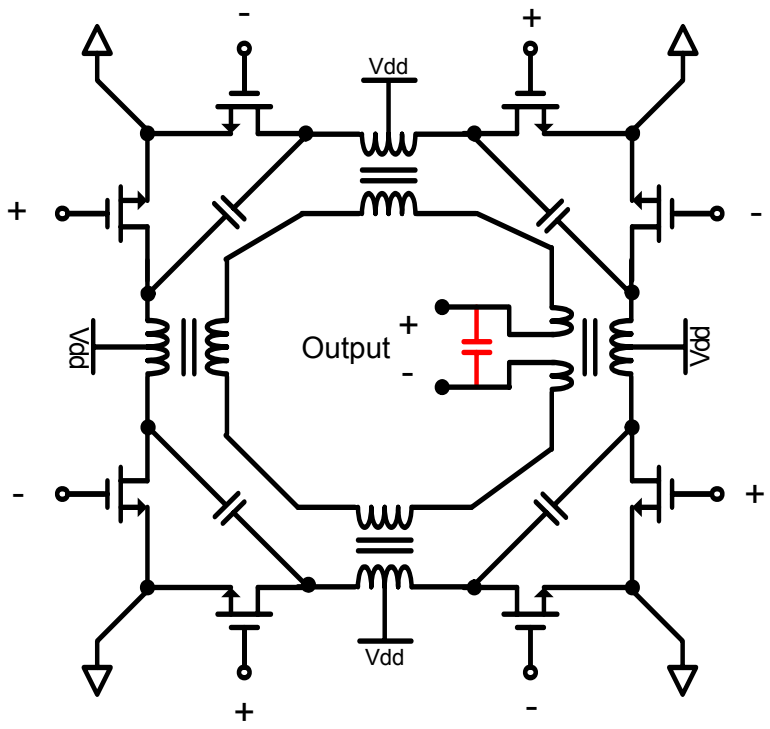

Figure 6.8. Output circuit of the PA with DAT and an external output tuning capacitor.

6.3.2 Layout and Simulation

Preliminary layout of the discrete L-band DAT using eight Freescale MRF 282 transistors was simulated in commercial microwave simulator. The simulated output power is over 120W, and the simulated PAE is about 65%. A Class-E driver stage may be added to improve the gain and the input matching of the amplifier. Future amplifiers may use the SiC and GaN devices for higher frequency operation.

References

[1] T. Kikkawa, T. Maniwa, H. Hayashi, M. Kanamura, S. Yokokawa, M. Nishi, N. Adachi, M. Yokoyama, Y. Tateno, K. Joshin, "An over 200-W output power GaN HEMT push-pull amplifier with high reliability," *IEEE MTT-S Int. Microwave Symp. Dig.*, vol 3, pp. 1347–1350, Jun., 2004.

[2] C. Dragon, W. Brakensiek, D. Burdeaux, W. Burger, G. Funk, M. Hurst, D. Rice, "200W push-pull & 110W single-ended high performance RF-LDMOS transistors for WCDMA basestation applications," *IEEE MTT-S Int. Microwave Symp. Dig.*, vol. 1, pp. 69–72, Jun., 2003

[3] K. Ebihara, K. Inoue, H, Haematsu; F. Yamaki, H. Takahashi, J. Fukaya, "An ultra broad band 300 W GaAs power FET for W-CDMA base stations," *IEEE MTT-S Int. Microwave Symp. Dig.*, vol. 2, pp. 649–652, May, 2001.

[4] I. Aoki, S. D. Kee, D. B. Rutledge, A. Hajimiri, "Fully integrated CMOS power amplifier design using the distributed active-transformer architecture," *IEEE J. Solid-State Circuits*, vol. 37, no. 3, pp. 371–383, Mar., 2002.

[5] I. Aoki, S. Kee, D. Rutledge, A. Hajimiri, "A fully-integrated 1.8-V, 2.8-W, 1.9-GHz, CMOS power amplifier," *Radio Frequency Integrated Circuits (RFIC) Symp.*, pp. 199–202, Jun., 2003.

[6] P. C. Dubois, J. van Zyl, and T. Engman, "Measuring soil moisture with imaging radars," *IEEE Trans. Geosci. Remote Sens.*, vol. 33, no. 4, pp. 915–926, Jul., 1995.

[7] J. Shi and J. Dozier, "Estimation of Snow Water Equivalence Using SIR-C/X-SAR, Part I: Inferring snow density and subsurface properties", *IEEE Trans. Geosci. Remote Sens.*, vol. 38, no. 6, pp. 2465–2474, Nov. 2000.

[8] F. H. Raab, "The class BD high-efficiency RF power amplifier," *IEEE J. Solid-State Circuits*, vol. 12, no. 3, pp. 291–298, Jun., 1977.

[9] M. K. Kazimierczuk, W. A. Tabisz, "Class C-E high-efficiency tuned power amplifiers," *IEEE Trans. Circuits Syst.*, vol. 36, no. 3, pp. 421–428, Mar., 1989.

[10] H. Koizumi, T. Suetsugu, M. Fujii, K. Shinoda, S. Mori, K. Iked, "Class DE high-efficiency tuned power amplifier," *IEEE Trans. Circuits Syst. – I, Fundam. Theory Appl.*, vol. 43, pp. 51–60, Jan., 1996.

[11] S. Kee, I. Aoki, A. Hajimiri, D. B. Rutledge, "The class-E/F family of ZVS switching amplifiers," *IEEE Trans. Microwave Theory Tech.*, vol 51, no. 6, pp.1677–1690, Jun., 2003.

[12] L. R. Khan, "Single Sideband Transmission by Envelope Elimination and Restoration," *Proc. IRE*, vol. 40, pp. 803–806, July 1952.

[13] F. H. Raab, "Efficeincy of Doherty RF Power Amplifier Systems," *IEEE Trans. Broadcast.*, vol. 33, no. 3, pp. 77–83, Sep., 1987.

[14] F. H. Raab, B. E. Sigmon, R. G. Myers, and R. M. Jackson, "L-band transmitter using Kahn EER technique," *IEEE Trans. Microwave Theory Tech.*, vol. 46, pt. 2, pp. 2220–2225, Dec. 1998.

[15] F. H. Raab, "Intermodulation distortion in Kahn-technique transmitters," *IEEE Trans. Microwave Theory Tech.*, vol. 44, pp. 2273–2278, Dec.1996.

[16] W. H. Doherty, "A New High Efficiency Power Amplifier for Modulated Waves," *Proc. IRE*, vol. 24, no. 9, pp.1163–1182, Sep., 1936.

[17] J. Cha, J. Kim, B. Kim, J. S. Lee, S. H. Kim, "Highly efficient power amplifier for CDMA base stations using Doherty configuration," *IEEE MTT-S Int. Microwave Symp. Dig.*, vol. 2, pp. 533–536, Jun., 2004.

[18] H. Chireix, "High Powoer Outphasing Modulation," *Proc. IRE*, vol. 23, no. 11, pp.1370–1392, Nov. 1935.

[19] F. H. Raab, "Efficiency of outphasing RF power-amplifier systems," *IEEE Trans. Commun.*, vol. 33, no. 10, pp. 1094–1099, Oct. 1985.

[20] I. Hakala, D. K. Choi, L. Gharavi, N. Kajakine, J. Koskela, R. Kaunisto, "A 2.14–GHz Chireix outphasing transmitter," *IEEE Trans. Microwave Theory Tech.*, vol. 53, no. 6, pt. 2, pp. 2129–2138, Jun., 2005.

[21] R. Sperlich, J. A. Sills, J. S. Kenney, "Closed-loop digital pre-distortion for power amplifier linearization using genetic algorithms," *IEEE MTT-S Int. Microwave Symp. Dig.*, vol. 1, pp. 347–350, Jun. 2003.

[22] K. Horiguchi, M. Miki, J. Nagano, H. Senda, K. Yamauchi, M. Nakayama, T. Takagi, "A UHF-band digital pre-distortion power amplifier using weight divided adaptive algorithm," *IEEE MTT-S Int. Microwave Symp. Dig.*, vol. 3, pp. 2019–2022, Jun., 2004.

[23] R. Sperlich, Y. Park, G. Copeland, J. S. Kenney, "Power amplifier linearization with digital pre-distortion and crest factor reduction," *IEEE MTT-S Int. Microwave Symp. Dig.*, vol. 2, pp. 669–672, Jun., 2004.

[24] H. L. Krauss, C. W. Bostian, and F. H. Raab, *Solid State Radio Engineering*. New York: Wiley, 1980.

[25] S. C. Cripps, *RF Power Amplifiers for Wireless Communication*, Norwood, MA, Artech House, 1999.

[26] Albulet, *RF Power Amplifiers*, Noble Publishing Corporation, Atlanta, GA, 2001

[27] K. Potter, M. Jian, D. Rutledge, "A 30-W 50-MHz Class-E Solid-State Amplifier," *Int. Symp. for Deepspace Commun. Navigation*, Sep. 1999.

[28] H. Zirath, D.B. Rutledge, "An LDMOS VHF Class E power amplifier using a high Q novel variable inductor," *IEEE Trans. Microwave Theory Tech.*, vol. 47, no. 12, pp. 2534–2538, Dec., 1999.

[29] S. D. Kee, I. Aoki, D. B. Rutledge, "7-MHz, 1.1-kW demonstration of the new E/$F_{2,odd}$ switching amplifier class." *IEEE MTT-S Int. Microwave Symp. Dig.*, vol. 3, pp. 1505–1508, May, 2001.

[30] N. O. Sokal, A. D. Sokal, "Class E - A new class of high-efficiency tuned single-ended switching power amplifiers," *IEEE J. Solid-State Circuits*, vol. 10, no. 3, Jun., 1975.

[31] N. O. Sokal, "Class E high-efficiency power amplifiers, from HF to microwave," *IEEE MTT-S Int. Microwave Symp. Dig.*, vol. 2, pp. 1109–1112, Jun., 1998.

[32] J. F. Davis and D. B. Rutledge, "A low-cost class-E power amplifier with sine-wave drive," *IEEE MTT-S Int. Microwave Symp. Dig.*, vol. 2, pp. 1113–1116, Jun., 1998.

[33] S. Kee, "The Class-E/F Family of Harmonic-Tuned Switching Power Amplifiers," Ph.D. Dissertation, California Institute of Technology, Pasadena, CA, 2002.

[34] I. Aoki, "Distributed Active Transformer for Integrated Power Amplification," Ph.D. Dissertation, California Institute of Technology, Pasadena, CA, 2002.

[35] Sanggeun Jeon, D. B. Rutledge, "A 2.7-kW, 29-MHz class-E/F_{odd} amplifier with a Distributed Active Transformer," *IEEE MTT-S Int. Microwave Symp.*, pp. 1927–1930, Jun., 2005.

[36] J. Sevick, *Transmission Line Transformers*, 2nd ed., American Radio Relay League, Newington, CT, 1990.

[37] R. Mongia, I. Bahl, P. Bhartia, *RF and Microwave Coupled-Line Circuits*, Artech House, Norwood, MA, 1999.

[38] K.-C. Tsai, P. R. Gray, "A 1.9-GHz, 1-W CMOS Class-E Power Amplifier for Wireless Communications," *IEEE J. Solid-State Circuits*, vol. 34, no.7, pp 962–970, Jul., 1999.

[39] G. Matthaei, L. Young, E. M. T. Jones, *Microwave Filters, Impedance-Matching Networks, and Coupling Structures*, Artech House, Norwood, MA, 1980.

[40] W.L. Gore & Associates Inc., "A Low Loss Dielectric for High Frequency HDI Substrates and PCBs," *Microwave Journal*, Dec., 2000.

[41] A. Long, J. Yao, S. Long, "A 13W Current Mode Class D High Efficiency 1 GHz Power Amplifier," 2002 45th Midwest Symposium on Circuits and Systems, 2002.

[42] N. Le Gallou, J. F. Villemazet, B. Cogo, J. L. Cazaux, A. Mallet, L. Lapierre, "10 W High Efficiency 14V HBT Power Amplifier for Space Applications," 11th GaAs Symp.,2003.

[43] A. Adahl, H. Zirath, "A 1 GHz Class E LDMOS Power Amplifier," 33rd European Microwave Conf., 2003.

[44] A. Suárez and R. Queré, *Global Stability Analysis of Microwave Circuits*, Artech House, Boston, 2003.

[45] S. Jeon, A. Suárez, D. B. Rutledge, "Analysis and Elimination of Hysteresis and Noisy Precursors in Power Amplifiers," accepted to *IEEE Trans. on Microwave Theory Tech*.

[46] A. Anakabe, J. M. Collantes, J. Portilla, J. Jugo, S. Mons, A. Mallet, and L. Lapierre, "Analysis of odd-mode parametric oscillations in HBT multi-stage power amplifiers," EuMW – 11th GAAS Symposium, Munich, October 2003, pp.533–536.

[47] S. Jeon, A. Suárez, D. B. Rutledge, "Global stability analysis and stabilization of a Class-E/F Amplifier," *IEEE Trans. Microwave Theory Tech.*, vol. 53, no. 12, pp. 3712–3722, Dec., 2005.

[48] K. Kurokawa, "Power Waves and the Scattering Matrix," *IEEE Trans. Microwave Theory Tech.*, vol. 13, no. 2, pp. 194–202, Mar., 1965.

[49] G. Gonzalez. *Microwave Transistor Amplifiers: Analysis and Design*, 2nd ed., Prentice Hall, New Jersey, 1997.

[50] S. A. Maas, *Nonlinear Microwave and RF Circuits*, 2nd ed., Artech House, Norwood, MA, 2003.

[51] K. Kurokawa, "Some basic characteristics of broadband negative resistance oscillator circuits," *Bell Syst. Tech. J.*, vol. 48, pp. 1937–1955, Jul.–Aug., 1969.

[52] Feiyu Wang and David B. Rutledge, "A 60-W L-Band Class-E/$F_{odd,2}$ LDMOS Power Amplifier Using Compact Multilayered Baluns," *Proc. IEEE Topical Workshop on Power Amplifiers for Wireless Commun.*, San Diego, CA, Sep., 2004.